Characterization of Mild Oxidative Stress Response in Human IMR-90 Fibroblasts by Subcellular Quantitative Proteomics

Noor Othman Baqader

A thesis submitted to the University College of London for the Degree of Doctoral of Philosophy

December 2014

University College of London
UCL

DECLARATION

I Noor Othman Baqader confirm that the work presented in this thesis is my own work, except where indicated and that I have:

I) Clearly referenced/ listed all sources as appropriate.

II) Given the sources of all pictures, data etc. That are not my own.

III) Not made any use of report (s) or essay (s) by any other student (s), either past or present.

IV) Not sought or used the help of any external professional agencies for the work reported in the thesis.

Signature: ..... Date: .....

Abstract

Oxidative stress is a biological state that occurs due to imbalance between reactive oxygen species (ROS) and the antioxidant system leading to subcellular disturbance. The purpose of this thesis was to determine changes in protein abundance/distribution between nuclear and cytoplasmic cell compartments in the normal human IMR90 fibroblasts subjected to mild oxidative stress. The experimental design was to exert *tert*-butyl hydrogen peroxide upon the IMR90 cell lines to induce mild oxidative stress followed by fractionation of the cells into nucleus and cytoplasm. Cellular response was measured by the use of subcellular spatial razor approach based on quantitative shotgun LC-MS/MS-based proteomics with SILAC isotope labeling. It has been found that, in response to the treatment, proteins were redistributed between nucleus and cytoplasm including numerous proteins that were not previously known to associate with oxidative stress. We found 121 most significant proteins with known function at unexpected subcellular location. These proteins were known to contribute to different cellular processes such as, transcription, iron/haem metabolism, TCA cycle, glycolysis, autophagy, signal transduction and ATP synthesis, and are consistent with functional networks that are spatially distributed across the cell. Specific metabolic pathways of NRF2 and proline regulatory axis were found to play an important part on the cellular response to mild oxidative stress. Iron metabolism with iron/haem as a cofactor and mitochondrial proteins were prominent into the response as well. By initial comparison of the oxidative stress fibroblasts with Cdc7 depleted fibroblasts after induction of origin activation checkpoint, it was found that both responses affect proteins related to glycolysis, TCA cycle and proline regulatory axis. Evidence suggested nuclear import/export of proteins induced by the treatment. Subcellular spatial razor results for response of fibroblasts to oxidative stress clearly suggested that, to obtain comprehensive pictures of cellular function, measurements of global changes in total

protein abundance need to be combined with measurement of the dynamic subcellular spatial redistribution of proteins.

Contents

List of Figures

List of Tables

List of Supplementary Materials and Tables

Supplementary Table 1. All Detected Proteins for Cells Subjected to Oxidative Stress.	CD-xlsx.1
Supplementary Table 2. Summary of Significant Changes for Cells Under Oxidative Stress.	CD-xlsx.2
Supplementary Table 3. Enrichment of GO Biological Process Terms	CD-xlsx.3
Supplementary Table 4. Proteins were Quantified for both Oxidative Stress and Cell Cycle arrest at the Origin Activation Checkpoint.	CD-xlsx.4
Supplementary Table 5. Summary of SILAC ratios for the 305-joint Network Search Set.	CD-xlsx.5
Supplementary Table 6. GO Biological Process annotation related to Nucleo-Cytoplasmic Trafficking and MS data for 133 Proteins with One or More of S_n, S_c, S_t *or* S_n/S_c Quantified in both OxS and OAC	CD-xlsx.6

List of Abbreviations

ABC	Ammonium Bicarbonate
ARE	Antioxidant Responsive Element
Arg10	Arginie10
BSA	Bovine Serum Albumin
CAT	Catalase
CID	Collision-Induced Dissociation
Cdc7	Cell division cycle7
CdK	Cyclin-dependent Kinases
CdkI	Cdks Inhibitor
CIP/KIP	Cdk Interacting Protein/ Kinase Inhibitory Protein
1D	1Dimension
Da	Dalton
DMEM	Dulbecco's Modified Eagle's Medium
DMSO	Dimethyl Sulfoxide
DNA	Deoxyribonucleic Acid
DTT	Dithiothreitol
EGF	Epidermal Growth Factor
EDTA	Ethylenediaminetetraacetic Acid
ETC	Electron Transport Chain of the Mitochondria
FA	Formic Acid
FACS	Fluorescence-Activated Cell Sorting
FDR	False Discovery Rate
FoxO3a	Fork head box protein type3a

FSA	Foetal Serum Albumin
G1	Gap 1 phase
G2	Gap 2 phase
GPX1	Glutathione Peroxidase1
H_2O_2	Hydrogen Peroxide
HEPS	4-(2-hydroxyethyl)-1-piperazineethanesulfonic acid
IMR90	Human Foetal Lung Fibroblast cell line
IODO	Iodoacetamide
IS	Buffer Isotonic Sucrose Buffer
KCl	Potassium Chloride
KDa	Kilo Dalton
Keap1	Kelch-like ECH-associated protein 1
LC-MS/MS	Liquid Chromatography-MS/MS
Lys6	Lysine6
M	Mitotic phase
MCM	Mini-Chromosome Maintenance protein
$MgCl_2$	Magnesium Chloride
MS	Mass Spectrometry
MS/MS	Tandem Mass Spectrometry
Myc	Myelocytomatosis
NaCl	Sodium Chloride
NADPH	Nicotinamide Adenine Dinucleotide Phosphate Hydrogen
NP-40	Nonyl phenoxypolyethoxylethanol
Nrf2	Nuclear factor-erythroid 2-related factor 2
NO	Reactive Nitrogen Species
NOX	NADPH oxidases

eNOS	Enzyme Nitric Oxide Synthase
O_2^-	Superoxide Anion
OH·	Hydroxyl Radicals
ORC	Origin Recognition Complex
PBS	Phosphate Buffered Saline
PD	Population Doubling
Pi	Propidium Iodide
PI3K	Phosphoinositide 3 Kinase
PRX	Peroxiredoxins
Pre-RC	Pre-Replicative Complexes
ppm	Part Per Millions
ppp	Part Per Billions
Rb	Retinoblastoma protein
RIPA	Radio Immuno Precipitation buffer
ROS	Reactive Oxygen Species
rpm	Revolutions Per Minute
RTKs	Protein Tyrosine Kinases Receptors
S	Synthesis phase
SDS-PAGE	Sodium Dodecyl Sulfate-Polyacrylamide Gel Electrophoresis
SOD1	Superoxide Dismutase 1
SOD2	Superoxide Dismutase 2
SILAC	Stable Isotope Labeling with Amino acids in Cell Culture
siRNA	Small Interference RNA
SMI	Small Molecule Inhibitor
TBP	Tert-Butyl- hydrogen Peroxide
TBS	Tris-Buffered Saline

TBST	Tris-Buffered Saline and Tween 20
Trx	Thioredoxin
Uniprot	Universal Protein Resource
X-gal	5-bromo-4-chloro-3-indolyl-beta-D-galacto-pyranoside

Acknowledgment

I am most grateful to my primary supervisor Professor Jasminka Godovac-Zimmermann, the head of the proteomics group (Center for Nephrology, Division of Medicine, UCL, UK). It was my pleasure to work under her supervision during the studying years of my PhD. I have learnt a lot during my work with her starting from learning how to do science, the way of thinking, designing the experiment, solving problems and how to be confident about myself as future scientist. I would also like to thank her for all wisdom and knowledge I learnt from her that is important and will be valuable for my life and not only for doing science.

I would also like to thank my secondary supervisor Dr Kai Stoeber (Department of Pathology, UCL. UK) for his great support throughput this work and for his review and constructive criticism of the results.

I would like to thank Dr Marko Radulovic (Institute of Oncology and Radiology, Pasterova, Belgrade, Serbia) for his generosity and great support at all stages of my PhD work. I believe without him and Prof JGZ support I would not have been able to achieve what I achieved here.

I would like to thank the proteomics great laboratory manger, Mr Mark Crawford (Center for Nephrology, Division of Medicine, UCL, UK) for his help in operating mass spectrometry instruments and protein database searches. Without his technical support I am sure I could not have been able to obtain my data and finish my work.

I would like to thank Mr Tomas Adejumo (Wolfson Institute for Biomedical Research and the UCL Cancer Institute, UCL, UK) for helping me to acquire nice and clear confocal microscopy pictures.

I would like to thank all doctors and colleagues in JGZ group from past and present and I would like to thank Dr Slavica Tudzarova (WIBR, UCL, UK) for her valuable help and discussion at early stage of my PhD.

Special thanks also to Dr Jill Norman, my postgraduate tutor and to all helpful staff I met at UCL.

I would gratefully like to dedicate this thesis to my family, especially to my mother and brother and to my very close friends. I am sure without their great help, advice and support during my studying years I would not have been able to come and study in UK.

Finally, I would like to thank our Saudi Arabia King the Custodian of the Two Holy Mosques King Abdullah Al Saud government for offering me the opportunity to come to UK for postgraduate studies, which includes my master and PhD degrees. I would like to thank the Saudi embassy and Saudi Cultural Bureau (London, UK) for their help and support during these years.

My postgraduate and PhD study was supported by King Abdullah Al Saud Foreign Scholarship for studying abroad Program and the Saudi Ministry of Higher Education (Riyadh, Saudi Arabia).

Thanks to you all,

Noor Baqader, December 2014

Talks and Publications

- Paper (2014), **Noor Baqader**, Marko Radulovic, Mark Crawford, Kai Stoeber, and Jasminka Godovac-Zimmermann; ***Nuclear-Cytoplasmic Trafficking of Proteins is a Major Response of Human Fibroblasts to Oxidative Stress***, Journal of Proteome Research 13 (10), page 4398–4423.

- Paper (2015), Marko Radulovic, **Noor Baqader**, Claire Mulvey, Kai Stoeber, and Jasminka Godovac-Zimmermann; ***Spatial Cross- Talk Between Oxidative Stress and DNA replication in Human Fibroblasts*** (in preparation).

- Departmental talk (2013), **Noor Baqader**; ***Subcellular Quantitative Proteomics after Induction of Origin Activation Checkpoint in Normal Human Fibroblasts IMR90.*** Centre for Nephrology, UCL, UK.

- Poster presentation (2012), S. Tudzarova, C. Mulvey, **N. Baqader**, K. Stoeber, G. H. Williams, J. Godovac-Zimmermann; ***Quantitative subcellular proteomics at the novel DNA replication origin activation checkpoint***, 9th Siena meeting, from Genomics to Proteomics, Siena, Italy.

Copyright Permission

Chapter 1: Introduction

Oxidative stress is a biological state that occurs due to imbalance between reactive oxygen species (ROS) and cell antioxidant components (Halliwell, 2007, Halliwell and Gutteridge, 2007). Alternatively, it can be defined as the damage caused by ROS to proteins, lipids and DNA leading to cellular pathology (Jenkins, 2000, Cross et al., 1987).

The term ROS was first used in 1945. Later on, more than 140,000 English language articles and more than 15,000 reviews were written about this subject. Most of the articles were predominately connecting ROS either with physiological states such as cell division cycle, immune defence system, signal transduction, apoptosis and antibacterial action or to pathological conditions such as aging, cancer, diabetes and cardiovascular diseases. ROS need to be under control by antioxidant defence systems (Alfadda and Sallam, 2012, Burhans and Heintz, 2009b).

It is obvious that an excessive oxidative stress may harm the cells and cause macromolecular damaging, protein aggregation (Sohal, 2002) and protein dysfunction leading to cell death. However, the low level of stress is needed for balancing of protein expression (Vogel et al., 2011). Moreover, distribution of proteins over subcellular organelles is highly dynamic and affected by different conditions (Hansen et al., 2006, Henke et al., 2011, Jung et al., 2013, Mulvey et al., 2013, Qattan et al., 2012, Pinto et al., 2014). This thesis investigated the influence of mild oxidative stress, by the use of spatial razor subcellular quantitative proteomics approach, with an aim to determine changes in protein abundances and distribution between the nucleus and cytoplasm of human IMR90 fibroblasts. The results obtained were compared to the results previously obtained in Cdc7-depleted human IMR90 fibroblasts (Mulvey et al., 2013).

In the following sections of the introduction, the literature relative to this work is

reviewed focussing in ROS, oxidative stress and their roles under both physiological and pathological conditions, while the second section is about the application of quantitative proteomics to study proteins spatial dynamic changes under oxidative stress.

1.1 General ROS Physiology

ROS are active molecules that are produced mainly from the electron transport chain of the mitochondria (ETC) by the conversion of oxygen molecules into superoxide anion (O_2^-) by univalent reduction process. It can also be generated in other cellular locations such as phagocytes. ROS can be by-products by different enzymes such as NADPH oxidases (Nox) or nitric oxide synthase (eNOS) and related proteins (Droge, 2002, Babior et al., 2002, Chen et al., 2008, Gough and Cotter, 2011, Block and Gorin, 2012, Bedard and Krause, 2007). ROS molecules include hydrogen peroxide (H_2O_2), reactive nitrogen species (NO), superoxide anion (O_2^-) and hydroxyl radicals (OH^-). All these molecules play important physiological roles in healthy cells (Cross et al., 1987, Fridovich, 1984, Orient et al., 2007, Pacher et al., 2007), such as regulation of redox signaling pathways (Figure 1-1), which includes mediating H_2O_2 oxidation to the protein's cysteine residues (Rhee, 2006). At physiological pH, cysteine residues exist as thiolate anion (Cys-S^-) that is more sensitive to oxidation compared to the protonated cysteine thiolate (Cys-SH) (Finkel, 2012). Redox signaling may be mediated by Cys-S^- H_2O_2 oxidation to the sulfenic form (Cys-SOH) thus altering protein function. However, this reaction is mostly reversible in case of moderate oxidation and protein function may be retrieved back to Cys-S by reduction process in the presence of reductase enzymes thioredoxin (Trx) and glutaredoxin (Grx) (Winterbourn and Hampton, 2008, Schieber and Chandel, 2014). On the other hand, high exposure to H_2O_2 oxidation converts proteins thiolate anion into sulfonic (SO_3H^-) or sulfinic (SO_2H^-) anions which are irreversible forms leading to permanent protein damage.

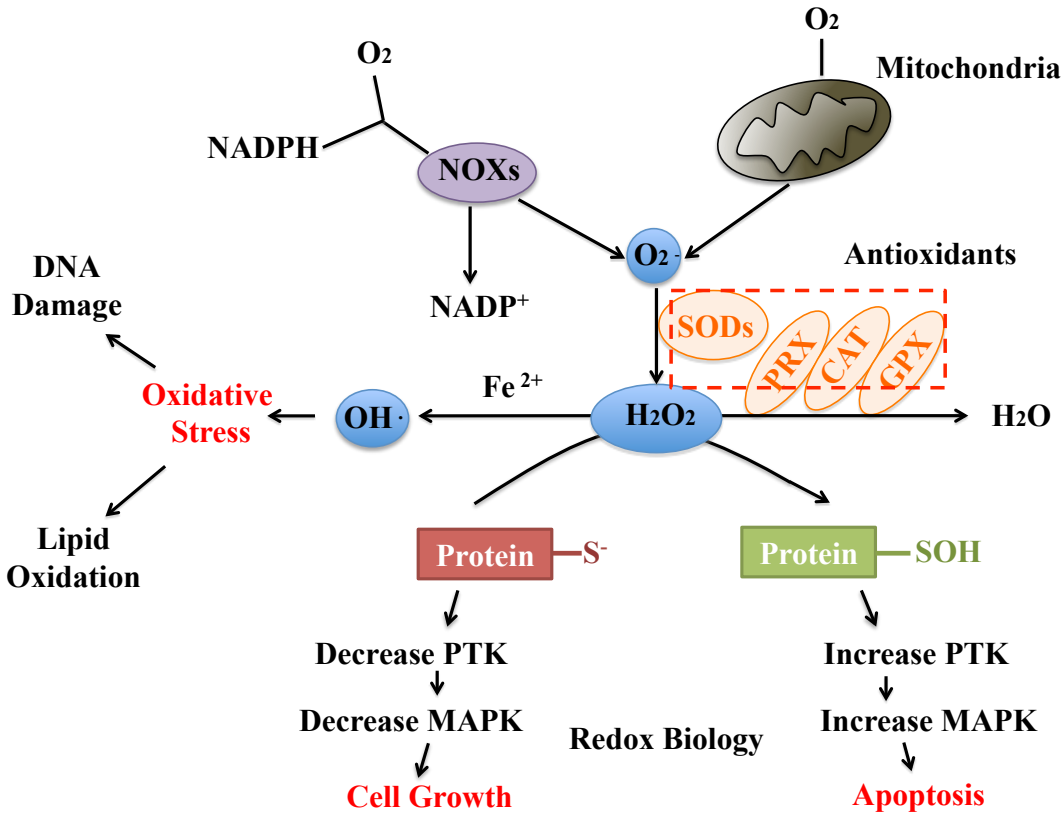

Figure 1-1. ROS Biology. Intercellular superoxide (O_2^-) is produced either by mitochondrial aerobic respiration due to leaking of electrons or via the NADPH and NOX enzymes. In the presence of antioxidant superoxide dismutases (SODs) enzymes, superoxide is quickly converted into hydrogen peroxide (H_2O_2). H_2O_2 may in turn oxidize the cysteine residues of proteins, forming thiolate anion (Cys-S-), and thus initiating redox signaling. Alternatively, antioxidant proteins such as glutathione peroxidase (GPX), peroxiredoxins (PRX) and catalase (CAT) can convert H_2O_2 into water. If the levels of H_2O_2 dramatically increase, hydroxyl radicals (OH^-) are generated from reaction with iron cations (Fe_2^+) that may permanently inactivate the cellular macromolecules. Figure adapted and modified according to figure in (Schieber and Chandel, 2014).

Therefore, in order to reduce the risk of intracellular build up of H_2O_2, cells produce protective antioxidant enzymes such as glutathione peroxidases (GPX), catalase (CAT) and peroxiredoxins (PRX), which act to convert H_2O_2 into water (Schieber and Chandel, 2014). For proteins that contain iron-sulfur clusters, enzymes like superoxide dismutase SOD1 (Cu/Zn SOD), located in the internal mitochondria membrane space and cytoplasm and SOD2 (Mn SOD), located in the mitochondrial matrix, prevent superoxide accumulation by converting O_2^- into H_2O_2 (Fridovich, 1997). Accumulation of superoxide is more connected to oxidative stress than redox signaling particularly with autophagy mechanism. Superoxide only affects some proteins, thus leading either to adaptation to oxidative stress, or starting a cellular death program (i.e. apoptosis) (Chen et al., 2009b, Murphy, 2012). Active hydroxyl radical (OH^-) is one of the ROS molecules, that is generated by reaction of H_2O_2 with ferrous ions in the Fenton's reaction. It randomly oxidizes lipids, DNA and proteins, thus causing chemical modifications and genomic instability (Dizdaroglu and Jaruga, 2012, Schieber and Chandel, 2014).

Eukaryotic cells often need growth factors for cell proliferation, nutrient uptake, and survival (Cooper and Hausman, 2004, Thompson, 2011). These growth factors such as epidermal growth factor (EGF), and platelet-derived growth factor (PDGF) induce protein tyrosine kinases receptors (PTKs) and their tyrosine kinase activity to phosphorylate the receptor cytoplasmic tails at specific tyrosine residues (Lemmon and Schlessinger, 2010). The receptor activation leads to down regulation and stimulation of important signal transduction pathways such as RAS-MEK-ERK MAP kinase cascade and phosphatidylinositol 3-kinase (PI3K)-AKT signaling pathway. PI3K pathway and RTKs can be inhibited by, for example, tumour suppresser PTEN and tyrosine phosphatases (PTPs) leading to a weaken mitogenic signaling (Tonks, 2006). For that reason, it is very important for these phosphatases to be under control to assure

sustaining signal transduction pathways (Schieber and Chandel, 2014). Growth factor such as EGF quickly and transiently increases ROS formation from NADPH oxidases to stimulate PTKs which in turn leads H_2O_2 to inactivation of protein tyrosine phosphatase PTP type 1B by oxidation of its cysteine residues to sulfonic acid (Bae et al., 1997). PTP B1 generally dephosphorylates EGF receptor in tyrosine residues and inactivation of it by H_2O_2 leads to increasing the EGF receptor phosphorylation and its downstream signaling (Adachi et al., 1996). However, PTP B1 can be reactivated by thioredoxin (Lee et al., 1998). Moreover, antioxidant PRX has been found to govern and reduce H_2O_2 generation upon the EGF stimulation depending on the molecular localization (Woo et al., 2010). The compartmentalization of ROS production is crucial for differentiation of their origin, as ROS can be elevated due to redox signaling or oxidative damage. For example, in redox biology for the efficient signals, proteins that depend on H_2O_2 are likely to be presented near the H_2O_2 sources. The proteins that control the H_2O_2 production from NADH in the plasma membrane are as well compartmentalized accordingly. In addition, mitochondria are known to have the ability to move toward their target due to cellular state such as hypoxia (Al-Mehdi et al., 2012). Moreover, the accumulation of superoxide in cytosol has a different outcome than accumulation in the mitochondrial matrix due to the high abundance of iron-sulfur proteins in the mitochondrial matrix. These differences have been found between cytosolic SOD1 and mitochondrial SOD2. Knockdown of SOD2 in mice and neuronal cells showed to be far more severe pathogenic comparing to SOD1 knockdown (Schieber and Chandel, 2014, Fukui and Zhu, 2010). Thus, the role of ROS and their subcellular location are generally very important for the regulation of different cellular functions.

1.1.1 Role of ROS in Cell Division and Cell Cycle Regulation

ROS are important for the activation of checkpoints and thus the cell cycle regulation (Burhans and Heintz, 2009b). Cell division cycle is a vital process whose mechanism is tightly regulated and rigorously checked by checkpoints, which are placed in between the cell cycle phases to avoid any damage to cellular genomic materials (Hartwell and Weinert, 1989). The division cycle for most of the eukaryotic cells passes through four stages: cell growth, DNA copying, chromosome distribution and cell division. These stages encompass two main phases that regulate the division process of cells: interphase and mitotic phase. Interphase is the longest phase with approximately 95% of the duration and is divided into: G1 (Gap 1), S (synthesis) and G2 (Gap2) phases (Figure 1-2A). Each phase plays an important role and is regulated by different groups of proteins. In addition, at the G1 phase, cells can abandon cellular division by entering the G0 phase (quiescent) and stay metabolically highly active but away from proliferation. Mitosis (M phase) consists of four stages: prophase, metaphase, anaphase and telophase, followed by cytokinesis, which includes cytoplasm segregation to form the two daughter cells. Most of the critical events during the cell division occur in S phase with the DNA synthesis and replication and in M phase when the parental cell separates into two daughter cells. Movement of cells through the cycle phases is promoted by a family of proteins known as cyclin-dependent kinases (CDKs) and cyclins as their regulatory activators (Figure 1-2B) (Cooper and Hausman, 2004, Blow and Gillespie, 2008, Garrett, 2001, Morgan, 2006, Williams and Stoeber, 2012). CDKs are usually regulated via phosphorylation but also can be negatively regulated by CDK inhibitors (CDKIs), which promote cell cycle withdrawal. CDKIs consist of two inhibitor families: Ink4 that includes $p16^{Ink4A}$, $p15^{Ink4B}$, $p18^{Ink4C}$ and $p19^{InK4D}$, which inhibit CDK4 and CDK6 leading to G1 arrest. Cip/Kip family includes p21, p27 and p57 which

inhibit CDK2 and most of CDKs (Williams and Stoeber, 2012, Morgan, 1997, Orzaez et al., 2009, Sherr and Roberts, 1999).

Elevation of cellular ROS level has been found to control the key cell cycle proteins (Havens et al., 2006). The CDKs inhibitor, p21 inhibits G1/S CDKs by many stressors such as oxidant agents (Gartel and Radhakrishnan, 2005).

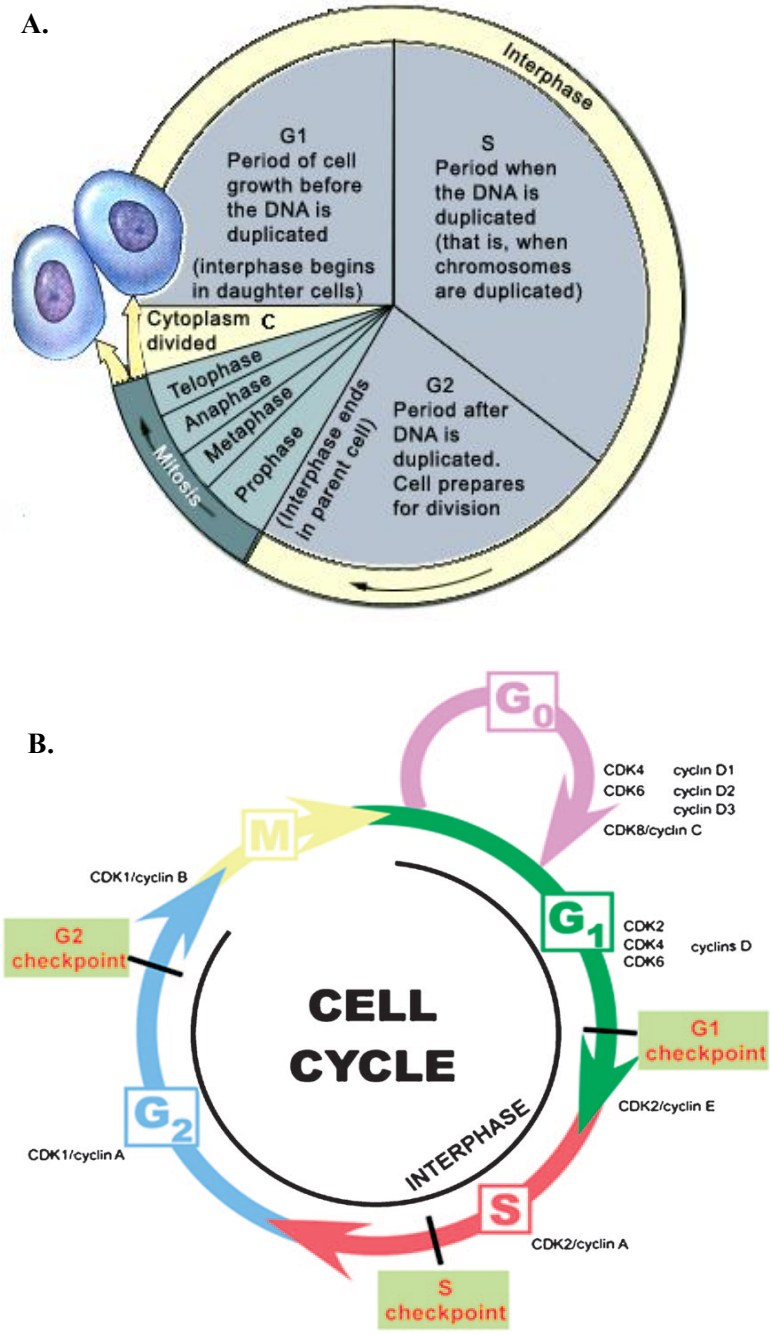

Figure 1-2. The Cell Division Cycle. **A.** Two main phases that control the cell cycle division process are Interphase and Mitosis. Interphase includes G1, S and G2. M phase includes prophase, metaphase, anaphase, telophase and cytokinesis (http://www.tutorvista.com/content/biology/biology-iii/cell-reproduction/cell-cycle.php Data accessed on 30-11-2014). **B.** The figure illustrates stages of the cell cycle with positions of regulatory cyclins/Cdcks and the main checkpoints. Figure originally adapted from (Orzaez et al., 2009).

In G1, ROS control mitogenic pathways that are important for activation of CDKs and phosphorylation of retinoblastoma protein (pRB) for S phase entry. Under oxidative stress, nuclear factor erythroid 2-related factor 2 protein (Nrf2) and forkhead box protein 3a (FoxO3a) control cell survival and lead to cell cycle arrest via specific factors such as CDKs inhibitor, p27 activation and stimulation of antioxidant enzymes. In S phase, ROS can induce S phase arrest via pRB dephosphorylation by phosphatase 2A (PP2A) protein, which negatively regulates signaling pathways initiated by protein kinases (Burhans and Heintz, 2009a). The stress transcriptional factors forkhead box Foxo proteins activate the p27CDK inhibitor, up regulate SOD1, and withdraw cells out of the cycle without apoptosis, as a response to the oxidative stress, thus leading to G1 arrest (Fu and Tindall, 2008, Sedding, 2008, Kops et al., 2002b). This results in reduction of ROS levels and activation of AMPK pathway, tumour suppressor p53 and activation of cell cycle checkpoints.

In fact, most of the cells stay out of the division cell cycle and remain at G0 phase, unless there are specific circumstances requiring them to enter the division cycle again (Jones et al., 2005). FoxO3a with Nrf2 are always functional in G0 phase in order to prevent the damage occurring from ROS accumulation, which might cause malignant transformation of cells (Kops et al., 2002a, Burhans and Heintz, 2009b, Osburn and Kensler, 2008, Kobayashi and Yamamoto, 2005).

It is noteworthy that re-entry to the cycle is not regulated by cyclin/CDKs but by the redox dependent signaling pathways. Redox signaling triggers the core cell cycle genes and cyclins D even in the absence of growth factors and active PTKs (Latella et al., 2001). Sarsour et al. proposed that O_2^- is more linked to proliferation while H_2O_2 is more linked to quiescence (Sarsour et al., 2008).

1.1.1.1 Oxidative Stress and Origin DNA Activation Checkpoint

The purpose of checkpoints is to detect any abnormal changes arising during the division process such as DNA damage (Garrett, 2001). If unfavourable conditions are detected, checkpoints halt the cycle by inducing cell cycle arrest until the problem is resolved. Checkpoints are located at specific sites of the cell cycle and each one has their well-defined function (Garrett, 2001, Hartwell and Weinert, 1989, Bartek et al., 2004, Musacchio and Salmon, 2007). In addition to such well-defined checkpoints a novel checkpoint monitoring DNA replication origin activation in G1/S phase has been recently revealed, which was the subject of our interest. Montagnoli et al. have found that S phase entry can be prevented in normal fibroblasts by inactivation of minichromosome maintenance complex Mcm helicase using small interference RNA (RNAi) against cell division cycle 7 (Cdc7) protein, which is an important kinase for phosphorylation of MCM complex and initiation of DNA replication. Cells are thus arrested in G1 phase by activating the novel checkpoint called the origin activation checkpoint (Montagnoli et al., 2004).

Briefly, cell division cycle 7 protein (Cdc7) has an important role during origins activation and breaking of DNA double strand but not in formation of replication forks (Montagnoli et al., 2004). It is estimated that 30,000 replication origins are scattered along the human DNA (Mechali, 2001, Biamonti et al., 2003). Initiation of DNA replication occurs between G1 and S phases and consist of two steps: licensing and firing (Yekezare et al., 2013). In early G1 the origin replication complex (ORC) binds to DNA and recruits Cdc6 and Cdt1, which in turn loads mini-chromosome maintenance replicative helicase Mcm2-7 onto the DNA. Together, they form pre-replicative complex (pre-RC). In late G1 phase, the origins are “fired” by phosphorylation of pre-RC through specific Cdk/Cyclins and Cdc7/ASK (Bell and Dutta, 2002, Blow and

Gillespie, 2008, Sclafani and Holzen, 2007). Cdc7 phosphorylates subunits of Mcm2, 4, and 6 leading to conformational changes and activation of Mcm helicase. This activation allows recruiting of other accessories such as Cdc45 and GINS complex, which is important for the establishment of DNA replication fork. In the S phase, DNA synthesis is started by forming bidirectional replication fork and loading their accessories (Figure 1-3) (Swords et al., 2010, Williams and Stoeber, 2012).

In contrast to normal cells, it has been shown that types of malignant cells lack this novel checkpoint and proceed to an abortive S phase which lead to cell death (Montagnoli et al., 2004, Rodriguez-Acebes et al., 2010, Kulkarni et al., 2009). In order to clarify this possibly novel mechanism Gillespie and Blow 2008 have argued that perturbation of replication initiation could delay progression of the cycle from G1 into S (Blow and Gillespie, 2008). Motagnoli et al. (Montagnoli et al., 2004) have found that it is possible to prevent S phase entry in fibroblasts by tendering Cdc7 RNAi and thus arresting cells in G1 phase.

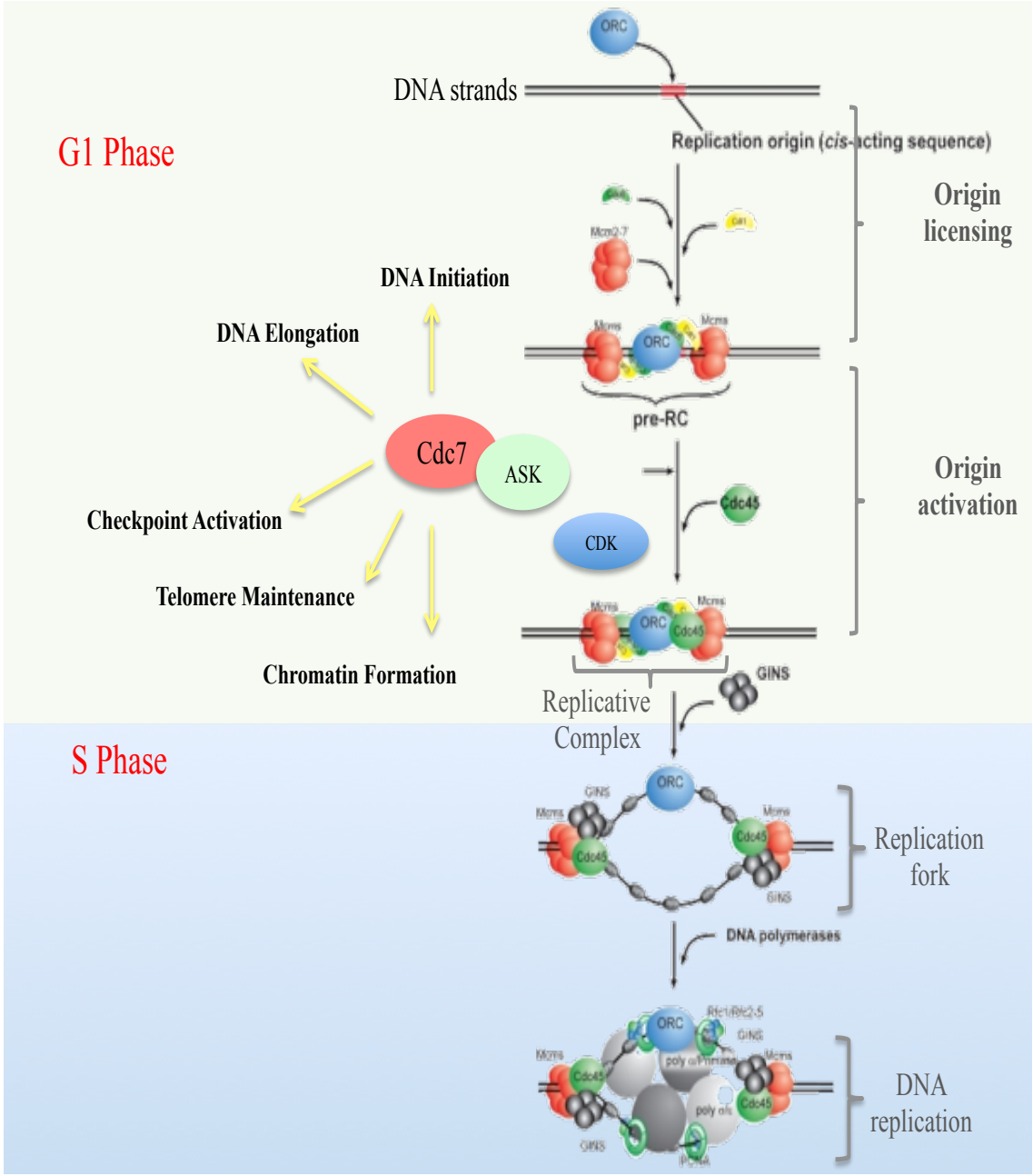

Figure 1-3. DNA Replication Initiation Pathway and the Function of Cdc7. After mitosis and in early G1, DNA replication pathway is initiated by origin replication complex (ORC) that recognizes and binds to replication origins. ORC recruits other proteins Cdc6 and Cdt1which in tern load the Mcm2-7 complex to the origins to form a pre-RC (pre- replicative complex). For origin activation, in late G1, both Cdc7/ASK and Cdk2/Cyclin become active and phosphorylate Mcm2-7 complex to trigger a conformational change that is required for unwinding of DNA which in turn leads to loading of other accessory factors such as Cdc45 and the GINS complex and generating a replication fork. Figure modified according to figure in (Sawa and Masai, 2009).

This finding allowed Stoeber and his colleagues to investigate and reveal the molecular architecture of this enigmatic checkpoint in normal human diploid fibroblasts (Figure 1-4) (Tudzarova et al., 2010). They revealed that depletion of Cdc7 triggers a fully reversible arrest of the cell cycle via activation of groups of proto-oncogenes and tumour suppressors as follows: FoxO3a boosts the activation of p14/ARF followed by loss of Hdm2. This destabilizes Mdm2 while stabilizing p53, activating p21and up-regulating the CDK inhibitor $p15^{INK4B}$. P53 in turn activates Dkk3, which is a Wnt/beta-catenin antagonist to down regulate Myc and cyclin D1. As a result, loss of CDK activity inactivates Rb-E2F pathway and prevents G1-S transition causing G1/S cell cycle arrest (Tudzarova et al., 2010).

Large-scale proteomics analysis has revealed that the main response to Cdc7 knockdown was a mild oxidative stress response followed by down regulation of DNA synthesis and retinoblastoma (Rb) dephosphorylation, followed by sequential stimulation of cell cycle-regulated proteins p53, p21 and p16 in normal somatic cells (Mulvey et al., 2010). Also the nucleus and cytoplasm subcellular quantitative proteomics revealed the alterations in some significant proteins that are essential for DNA replication and cell cycle, which included the tricarboxylic acid cycle (TCA) cycle, iron metabolism and protein translation (Mulvey et al., 2013). These results indicate that redox signaling pathways are strongly influencing the cell cycle (Mulvey et al., 2010, Burhans and Heintz, 2009b).

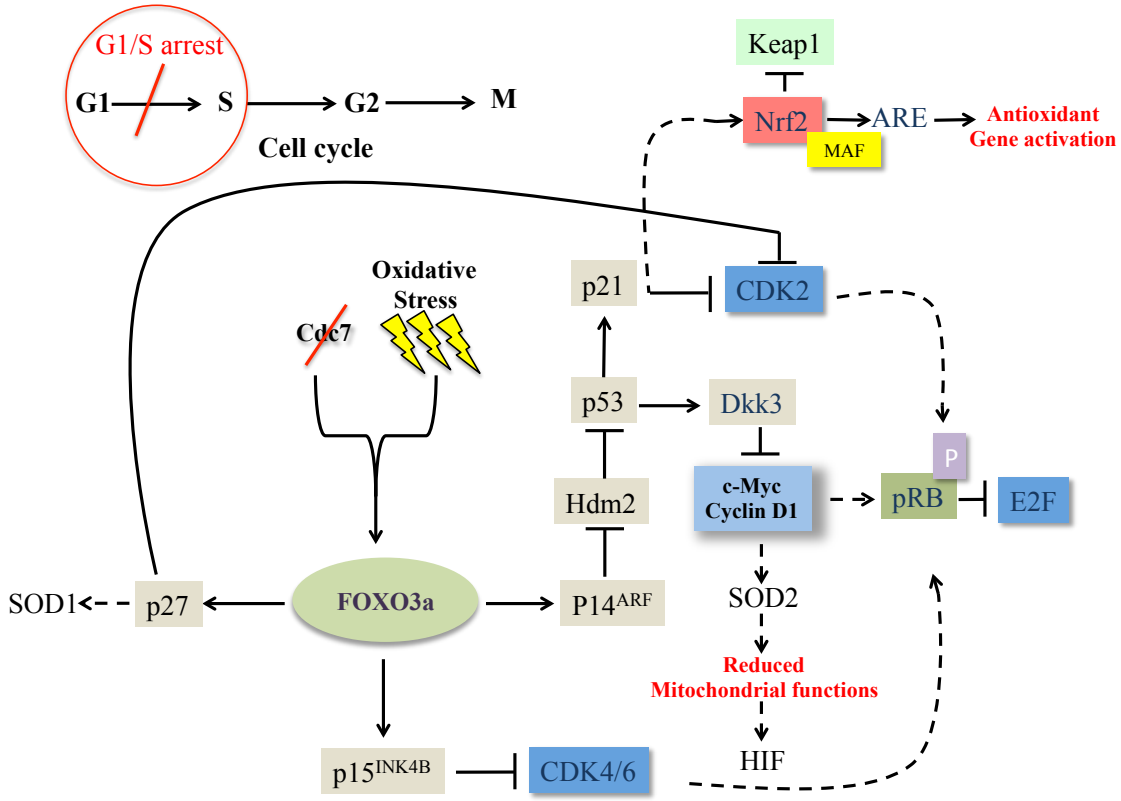

Figure 1-4. The Molecular Architecture of the DNA Origin Activation Checkpoint.

Inhibition of Cdc7 kinase activity activates a cellular response that is dependent on three checkpoint axes coordinated via the cell stress transcription factor FoxO3a. Activation of FoxO3a arrests the cell cycle in G1 through activation of the ARF–Hdm2–p53–21 pathways which in turn lead to up-regulation of CDKIs: p15 (INK4B) and p27 (CDKN1B). P53 in turn activates expression of the Wnt/β-catenin signaling antagonists Dkk3, leading to Myc and cyclin D1 down-regulation. The loss of CDK activity inactivates the Rb–E2F pathway and prevents the G1–S transcriptional programme. Under oxidative stress, p21 activates the transcription factor Nrf2, which detaches from Keap 1 protein and translocates to the nucleus to interact with antioxidant response element ARE to trigger antioxidant genes. The loss of Cdc7 kinase leading to checkpoint activation depends on tumour suppressors that are generally known to be inactivated in human tumours and this may explain why cancer cell enter lethal S phase leading to specific cancer cell death. Figure originally adapted and modified according to figure in (Williams and Stoeber, 2012).

1.1.2 ROS Regulation of Mitochondrial Activity

Mitochondria are important organelles that participate in the cell fate. The mitochondrial structure consists of inner and outer membrane separated by inter-membrane space. The inner-membrane surrounds the mitochondrial matrix as numerous folds called crista. Notably, this organelle is the main source of energy that is generated within the eukaryotic cells from catabolism of carbohydrates (i.e. glycolysis) and fatty acids leading to the production of ATPs via oxidative phosphorylation process. In addition these organelles are considered to be a main producer of superoxide O_2^- and participating in ROS activation (Schieber and Chandel, 2014). Most of ROS are produced in mitochondrial electron transport chain (ETC) and recently suggested complex III (Chandel, 2010). The outcomes of the accumulated superoxide O_2^- in mitochondrial matrix are different than the outcome in the cytoplasm due to the redundancy of iron cluster proteins, which are important for oxidation reduction reactions of mitochondria ion transport (Schieber and Chandel, 2014).

Mitochondria contain their own DNA (mDNA), which encodes ribosomal, transcriptional RNAs, and some proteins. There are two types of the mitochondrial proteins depending on their source: proteins that are encoded by the mitochondrial genome and translated inside mitochondria and proteins encoded by the nuclear genome imported to mitochondria from the nucleus. Among 1000 mitochondrial proteins, 15 are encoded by mitochondrial DNA and the rest by nuclear DNA (Wallace, 2012).

The mitochondrial energy metabolism is a process occurring in the matrix by the conversion (i.e. oxidation) of cytosolic pyruvate, which is the outcome of glycolysis; and fatty acids into acetyl CoA, which in turn is converted to CO_2, flavin adenine dinucleotide hydrogenase 2 (FADH2) and nicotine adenine dinucleotide hydrogenase (NADH) by the citric acid cycle (TCA). In the case of oxidative phosphorylation

process, the inner-membrane contains more than 70% of oxidative phosphorylation proteins that are responsible for the transport of pyruvate and fatty acids between the mitochondria and the cytoplasm. The NADH and FADH2 high energy electrons transfer to the inner-membrane and after a series of reactions they are converted into molecular oxygen and release energy for ATP synthesis (Cooper and Hausman, 2004).

In cancer cells, Otto Warburg (a Nobel prize laureate in physiology in 1931s) observed that tumour cells shift their energy metabolism from oxidative phosphorylation to aerobic glycolysis in the presence of oxygen, which is known as the Warburg effect, thus producing a large amount of lactate. Several hypotheses have been postulated for the Warburg effect such as; cancer cells adapting to a low oxygen environment (i.e. hypoxia) for survival, oncogenes reducing the amount of mitochondria in order to avoid apoptosis by shutting them down, or because the glycolysis process is the main event in the normal cell proliferation (Lopez-Lazaro, 2008). Mitochondrial disorders are a cause of a number of diseases including cancer, neurodegenerative diseases and type 2 diabetes (Patti and Corvera, 2010). There is no definitive evidence to support that the Warburg effect occurs due to the mitochondrial defect. For instance, in cancer cells, enzymes such as phosphoglycerate mutase 1 (step 8 in glycolysis pathway) have been found to alter their expression and shift the metabolism to different biosynthetic pathways, such as pentose phosphate and serine biosynthesis pathways to promote cancer growth due to the loss of p53 (Vander Heiden et al., 2009, Hitosugi et al., 2012).

Wallace, 2012 discussed in his review paper (Wallace, 2012) that, functional mitochondria are important for cancer cell and that the mutation in mDNA is essential for remoulding the bioenergetics and biogenesis mitochondrial states to allow the survival of cancer cells.

Redox regulation of cytochrome c to prevent apoptosis has been found to occur due to the increase of glucose metabolism and the Warburg effect leading to tumour survival in

cancer and neuron cells (Vaughn and Deshmukh, 2008, Boland et al., 2013). Increased levels of ROS change mitochondrial function, leading to disturbance in ETC and change of metabolism. Oncogenes that induce ROS support tumorigenesis via increasing the stability of HIFα hypoxic factor, increased oxidative DNA damage, increased calcium flux levels, inactivating the growth factor inhibitors the phosphatases, and activating the transcription factors Nrf2 and NF-κB (Hamanaka and Chandel, 2010, Schumacker, 2006, Sena and Chandel, 2012, Wheaton and Chandel, 2011).

Mitochondria are normally regulated by mechanisms which include mitophagy, fusion, fission and biogenesis (Boland et al., 2013). Fusion helps mitigate stress by mixing the contents of partially damaged mitochondria as a form of complementation. Fission is needed to create new mitochondria, but it also contributes to quality control by enabling the removal of damaged mitochondria and can facilitate apoptosis during high levels of cellular stress. Disruptions in these processes affect normal development, and they have been implicated in neurodegenerative diseases, such as Parkinson's, Alzheimer's, and Huntington's diseases (Detmer and Chan, 2007, Boland et al., 2013, Hales, 2004).

Endoplasmic reticulum (ER) plays a key role in fission and fusion regulation. For example, in fission, ER regulates division of mitochondria sites (Friedman et al., 2011). Mfn2 protein, which is a fusion protein, works as a connector between mitochondria and ER in the aim to absorb calcium from ER (de Brito and Scorrano, 2008). It has been found that, in yeast, mitochondria may bind to the ER and the cellular cortex for changing organelle cellular location (Lackner et al., 2013). The rates of fission and fusion are also coordinated with the cell cycle (Boland et al., 2013). Mitochondrial fusion has been reported to be required for G1/S transition and S phase entry in the presence of cyclin E (Mitra et al., 2009).

Markedly, the signaling pathways regulating fission and fusion are also involved in types of cellular stress that are associated with cancer such as the changes in energy

levels, cell cycle signals and hypoxia (Boland et al., 2013). For example, UV light activates OPA1 fusion protein to increase fusion (hyper-fusion), produce ATP and prevent apoptosis (Tondera et al., 2009). In contrast, fission leads to mitochondrial membrane depolarization, disturbance in H^+ flow around the inner-membrane leading to membrane loss and reduction in Ca^+ mitochondrial uptake. The depolarization of mitochondria in turn leads to prevention of cytochrome c being released in the cytoplasm as well as to apoptosis. Moreover, in HeLa cells, ROS induce mitochondrial depolarization and degradation by autophagy (i.e. mitophagy) depending on mitochondrial morphology (Wang et al., 2012).

Surprisingly, mitophagy is not only important for cancer cells but also for the stromal cells nearby to these cells. For example, Bonuccelli and his collages (Bonuccelli et al., 2010) have detected that, the stromal fibroblasts that are neighbouring to the breast cancer epithelial cells shift their metabolism to glycolysis due to the absorption of H_2O_2 generated from the neighbouring transformed cells. As a result, the mitophagy in the normal fibroblast cells is induced switching their metabolism to produce lactate that is important to feed cancer cells. This process is called 'the reverse Warburg effect' (Wallace, 2012).

1.2 Intracellular Signaling Pathways of Nrf2, FoxO3a, HIFs and Arginine/Proline are regulated by ROS

1.2.1 Nrf2 Signaling: Under oxidative stress, the activation of the transcription factor nuclear factor erythroid 2-related factor 2 protein (Nrf2) via disassociation from its inhibitor protein Kelch-like ECH-associated protein 1(Keap1) leads to increase in production of cancer cells antioxidant proteins (Sporn and Liby, 2012, Guo et al., 2014, Chun et al., 2014).

Normally, Nrf2 is located in the cytoplasm and is detected from degradation by interaction with Keap1. However, increased ROS oxidize Keap1 at its cysteine residues leading to dissociation and preventing degradation of NRF2. As a result, Nrf2 translocate to the nucleus and form heterodimers with the transcription factor MAF protein, and interact with the antioxidant responsive element (ARE) at the regulatory regions of antioxidant genes (Chun et al., 2014, Schieber and Chandel, 2014, Dinkova-Kostova et al., 2002, Nguyen et al., 2000, McMahon et al., 2003, Numazawa et al., 2003, Itoh et al., 1997). This leads to activation of stress response genes such as haem oxygenase 1 (HMOX1), which is a vital enzyme for haem catabolism (Frezza et al., 2011, Adam et al., 2011).

High levels of ROS are an activator for Nrf2. It has been found that mutated Keap1, PI3 and ERK MAP kinase signaling pathways may be involved in Nrf2 activation as well (Jaramillo and Zhang, 2013, Je et al., 2012, Wang et al., 2008a). Recently, in mice, oncogenes involving Myc, Kras and Braf were shown to enhance Nrf2 expression in order to control the ROS antioxidant production and detoxification (DeNicola et al., 2011). On the contrary, the Nrf2 defect in cancer cells may lead to increased oxidative stress, and cellular damage (DeNicola et al., 2011, Schieber and Chandel, 2014).

It is estimated that Nrf2 has the ability to activate more than 100 antioxidant genes (Itoh et al., 1997, Rushworth et al., 2012). However, it has been observed that deletion of specific antioxidants such as peroxiredoxins Prdx1 may not elevate ROS to the level that causes the damage in cancer cells and instead may enhance tumorigenesis (Neumann et al., 2003, Cao et al., 2009). Under normal conditions, Nrf2 can play a crucial role as a cyto-protective agent against the cellular injury and oxidative damage due to its ability to stimulate the cellular antioxidants (Rushworth et al., 2012). Nrf2 proteins also adapt their localization according to the cellular redox situation.

1.2.2 P53 and ROS: There are massive groups of proteins coordinating with ROS for cells growing and differentiation. For example, a tumour suppressor such as p53 can act as an antioxidant to prevent ROS formation above the levels that encourage the signals of proliferation (Sablina et al., 2005). P53 also has been found to up-regulate a set of genes that generate antioxidant products such as the mitochondrial superoxide dismutase 2 (SOD2), glutathione peroxidase 1 (GPX1) and aldehyde dehydrogenase 4 family member A1 (ALDH4A1) (Tan et al., 1999, Hussain et al., 2004, Yoon et al., 2004).

1.2.3 FoxO3a Signaling: Previous work from our group (Tudzarova et al., 2010) revealed a particular importance of FoxO3a protein in signaling leading to cell cycle arrest following Cdc7-depletion of human fibroblasts. Fork head box O (FOXO) is a tumour suppressor and a transcription factor has been found to be regulated by oxidative stress by SOD2, upon which it translocates to the nucleus (Furukawa-Hibi et al., 2005) and controls the antioxidant expression genes.

It‘s role in cell cycle arrest via checkpoint activation, DNA repair and apoptosis (Figure 1-4) has been described in details by Tudzarova and Stoeber (Tudzarova et al., 2010). In addition, FoxO3a has been found to participate in negative regulation of hypoxia-inducible factor 1 (HIF1) (Dansen and Burgering, 2008, Ferber et al., 2012). Thus, FOXO and p53 negatively regulate the ROS production.

1.2.4 HIFs Signaling: ROS normally support the metabolic stress in order to maintain mitogenic signals when tumour cells exceed their blood supply. As a result, tissue response to hypoxia leads to stabilization of HIFs (Semenza, 2012). HIFs mediate the effect of ROS on angiogenesis, which is very important for tumour growth (Krock et al., 2011). These proteins are heterodimers consisting of two alpha (HIFα) and beta subunits (HIFβ). Under normal conditions, the oxygen sensitive subunit alpha (HIFα) is hydroxylated by prolyl hydroxylases (PHDs) at the proline residues to be recognized by

E3 ubiquitin ligase, pVHL and targeted for proteasomedegradation. Under hypoxia, high ROS levels, proline residues of HIFα are not targeted by PHDs for degradation, resulting in HIFα translocation to the nucleus and dimerizes with HIFβ to regulate the cellular adaptation to hypoxia and activation of the pro-angiogenic genes (Miyata et al., 2011, Semenza, 2012, Kaelin and Ratcliffe, 2008). Thus, tumorigenesis of certain cancers can be promoted via stabilization of HIFs due to increase levels of ROS (Gao et al., 2007, Ma et al., 2009).

1.2.5 Arginine/Proline Metabolism: Besides their role as tumour suppressors Arginine/proline metabolism, have been found to influence ROS regulation (Phang et al., 2012). Mitochondrial ROS translocate to the cytosol and target proline cycle catalytic enzyme proline oxidase (POX)/proline dehydrogenase (PRODH) to initiate ROS-responsive signaling pathways (Donald et al., 2001, Maxwell and Rivera, 2003, Kim et al., 2007, Liu et al., 2005). Interestingly, POX/PRODH were reported to significantly inhibit tumour growth in immunodeficient mice, and this enzyme may thus be considered as a tumour suppressor (Liu et al., 2010, Liu et al., 2009). This also explains why ROS-dependent POX/PRDH pathways regulate pathways such as p53, AMPK and PPARγ and its importantance for mitochondrial mitophagy and apoptosis in response to oxygen deprivation (Phang et al., 2012). Proline can also be incorporated in many cancers as collagen (Priest and Davies, 1969, Kao et al., 1986).

1.3 ROS in Pathology

Pathways responsive to ROS are very important for cellular function and thus cellular ROS levels are involved in pathogenesis of a number of diseases.

1.3.1 Role of ROS with Cancer

Cancer refers to a large group of different diseases resulting in uncontrolled cell growth. The origin of the word cancer is credited to the Greek physician Hippocrates (460-370 BC) (Mukherjee, 2010). In cancer cell, the growth mechanisms are permanently activated even in the absence of mitogens, thus sustaining persistent proliferation (Harbour and Dean, 2000, Hanahan and Weinberg, 2011). Markedly, cancer cells induce elevated ROS generation from the endoplasmic reticulum, mitochondria and the cytoplasm from NADPH oxidase (Cairns et al., 2011). High level of ROS may cause genomic instability and lead to tumorigenesis (Figure 1-5) (Szatrowski and Nathan, 1991). However, tumorigenesis requires the avoidance of cell death and therefore cancer cells usually produce an equal amount of antioxidant to keep redox balance (Gorrini et al., 2013, Trachootham et al., 2006, Nogueira et al., 2008). Moreover, regardless of the high levels of antioxidants within cancer cells the ROS responsive signaling pathways are activated presumably due to their physical proximity to ROS production sources (Schieber and Chandel, 2014). Inhibition of NF-kB prevents accumulation of Nrf2 and prevents chemotherapy resistance in acute myeloid leukaemia (Rushworth et al., 2012).

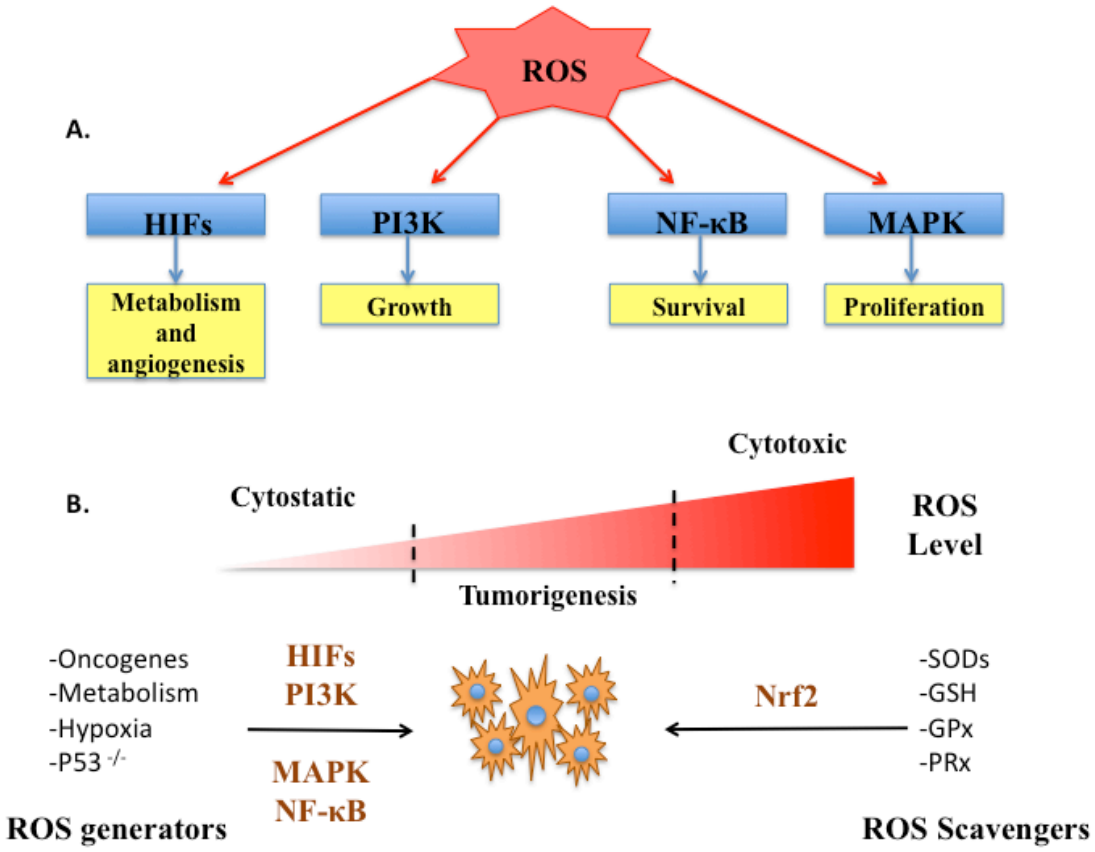

Figure 1-5. ROS in Normal and Cancer Cell Regulation. **A.** ROS affects important pathways that participate in cellular metabolism, angiogenesis, growth, survival and proliferation. **B.** Cancer cells produce high level of ROS and promote tumorigenesis. Oncogenic proteins such as HIFs, PI3K, MAP kinases and NF-κB under hypoxia and in the absence of p53 lead to increased redox levels and rapidly enlarging tumours. At the main time, Nrf2 participates in the elimination of high level of oxidative stress that lead to establishment of cell apoptosis via controling sets of important cellular antioxidants including SODs, GSH, GPXs and PRXs (Schieber and Chandel, 2014).

1.3.2 Role of ROS in Diabetes, Insulin Resistance and Neurodegeneration

Diabetes is mainly characterized by excessive amounts of glucose and fatty acids in the cells leading to several physiological damages. High glucose levels lead to increased oxidative stress via activation of several processes such as the hexosamine pathway, oxidative phosphorylation, glyceraldehyde autooxidation and sorbitol production (Robertson, 2004). In addition, accumulation of fatty acids might cause lipotoxicity leading to failure of several organs (Brookheart et al., 2009, Alfadda and Sallam, 2012). In adipocytes, saturated fatty acids, generation of ROS and NF-κB activation can result in inflammation (Yeop Han et al., 2010). ROS play a central role in insulin resistance as it has been found that pharmacological inhibition of ROS can affect insulin resistance state (Houstis et al., 2006). This effect has been suggested to occur by the regulation and translocation of Forkhead transcriptional factor 1 (FOXO1) from cytoplasm to the nucleus enhancing insulin resistance via gluconeogenesis (Kaneto et al., 2010).

It is clear that ROS and oxidative stress are of major physiological and pathological relevance to the cells. The role of ROS in neurodegenerative disease such as Alzheimer and Parkinson's is of a particular and increasing interest (Dumont and Beal, 2011, Campos et al., 2014).

Thus any new information on the cellular processes during oxidative stress is potentially of high clinical relevance based on the ROS involvement in pathology and aetiology of a number of diseases. It is thus clear that there is an urgent need for exhaustive analysis of changes in the cellular proteome under oxidative stress.

1.4 The Use of Subcellular Quantitative Proteomics to Study ROS and Oxidative Stress: Bottom-up and Top-down Strategies

Proteomics is a science that describes the characterization of all protein phenotypes in a living system including protein amount, form, modification and location (Godovac-Zimmermann and Brown, 2001). The proteomics methodology in study of a cellular system involves parallel investigation of proteome phenotype alterations with an ultimate attempt to explain the cause of these changes (Godovac-Zimmermann and Brown, 2003). Mapping of all cellular proteins is not sufficient to understand the dynamics of proteins *in vivo* as it basically catalogues the proteins without giving a functional explanation. Thus, emergence of the awareness of functional proteomics in order to describe and quantify the spatial and temporal distribution and interaction between different protein networks (Godovac-Zimmermann and Brown, 2001) is seen as a paradigm shift in protein science.

Determination of protein abundance, localization and modification are amongst the most interesting goals in post-genomic biology. Classical methods of protein chemistry such as western blot or immunoprecipitation helped to reveal a large number of cellular protein interactions but they are not sufficient for the study of the molecular mechanics of the entire proteome. In addition, the correlation between mRNA and protein abundances in the cell has been reported to be notoriously poor (Anderson and Seilhamer, 1997, Gygi et al., 1999b) stressing the need for the investigation at protein level. Finally, the crucial protein regulation processes, post-translational modifications such us phosphorylation, acetylation and glycosylation can only be studied at the protein level.

Methodologically, current proteomics is driven by the extensive development of mass spectrometry (Walther and Mann, 2010). There are two fundamental strategies currently

used for protein identification and characterization by the use of MS-based proteomics: the first one is called bottom-up or 'peptide levels' proteomics, which depends on the specific mass of the tryptic peptides and top-down 'protein levels' proteomics, where protein characterization relies on the unique molecular mass of the whole protein followed by "*in-situ*" MS fragmentation. Both of these approaches have advantages and disadvantages as described in Table 1-1. Although bottom-up proteomics uses peptide as surrogates for proteins, it is more popular and encompasses around 90% of all recent proteomics experiments due to current technical developments in the hybrid mass spectrometry field. Among the disadvantages of top-down proteomics is the fact that insoluble proteins such as membrane proteins are difficult to handle and require the use of detergents which in turn interferes with MS analysis. Other limitations, such as often huge masses of the intact proteins as well as different post-translational modifications that the proteins normally undergo can eliminate the MS ability to correctly identify those proteins. These reasons make bottom-up method more suitable for the analysis of complex protein samples (Wehr, 2006).

Bottom-up proteomics can also refer to the shotgun proteomics. This approach ensures a high-throughput, on-line and highly confident protein identification (Walther and Mann, 2010) making it often a method of choice for large scale proteomics experiments.

With this strategy, which uses peptides as protein surrogates, protease enzymes such as trypsin and chymotrypsin are used for protein digestion. The high specificity of trypsin and tryptic peptide length is a crucial factor for MS detection ability and the use of trypsin has great advantages for bottom up proteomics. Trypsin cleaves the peptides at C-terminus of arginine (Arg) and lysine (Lys) and most of tryptic peptides are 4 to 40 amino acids long. These cleavage method has a huge commercial advantages as trypsin is cheap, easy to produce, peptide mass is easy to predict due to trypsin high specificity and tolerance of different concentrations and conditions. Trypsin can work well with

either native or denatured proteins. However, there are several limitations with trypsin such as, the endogenous ability to cut a peptide sequence at Arg or Lys at the consecutive positions and incomplete digestion especially at the side close to peptide C-terminus. Tryptic peptides that are outside the MS size range cannot be detected which can result on the loss of the information for some proteins. The biological nature of trypsin is known to require slightly basic and mildly denaturing experimental conditions (Lovric, 2011). The most common form that is used in proteomics sample preparation is so-called trypsin gold from Promega, which has been modified to be more stable and resistant to autolysis.

Peptide sample generation for MS driven proteomics analysis using trypsin can be achieved either by in-gel or in-solution digestion at an optimal temperature for trypsin of 37^{o}C. In fact, the use of trypsin with any of these approaches (i.e. in solution or in gel) can be varying according to experimental design, amounts, concentrations and nature of the sample (Lovric, 2011, Beynon and Bond, 1989, Mann et al., 2001, Rosenfeld et al., 1992, Shevchenko et al., 1996, Rice et al., 1977). The gel approach, which was the most popular at the early beginning of proteomics, such as two-dimensional gel (2-D) gel was widely used (O'Farrell, 1975). However, disadvantages such as low resolution, protein dynamic range, long separation time, insufficient protein separation and inability to separate membrane proteins limited the use of 2D gel in proteomics laboratories today (Ong and Mann, 2005, Wilkins et al., 1996, Corthals et al., 2000, Anderson and Anderson, 1998). 1D SDS-PAGE (Shevchenko et al., 1996) has overtaken 2D (Au et al., 2007) gels and is wildly used today to reduce sample complexity prior to LC-MS/MS experiment.

	Bottom-up	Top-down
Advantages	• Widely used for identification and characterization of proteins at their peptides level. • Can be applied with very complex samples. • It uses HPLC that has reversed phase that uses solvents are compatible with ESI. • Can be used with online fully automated nano-LC-MS/MS. • Compatible with most labeling methods. • Software and bioinformatics analysis tools are available.	• Complete access to intact proteins sequence. • Ability to locate post-translational modifications. • Less time for sample preparation as there is no need for digestion step.
Disadvantages	• Identified fraction of total peptide population of given protein which give information relay on part of the proteins sequence. • Sometime limited sequence coverage can lead to the loss of much information about PTMs and protein isoforms. • Limited information about low abundant peptide in mass spectra dominated by high abundant spectra. • Long running time within chromatography for very complex mixtures. • Need to narrow chromatographic peak widths to get adequate amount of information and that can be achieved by the use of nano-LC.	• Sometime it is a challenge to determine ions masses and analyse the very complex spectra with multiply charge ions. • Not widely used compared to bottom-up. • Limitation in terms of instrument. Only coupled with relatively expensive MS such as FT-ICR. • It has not worked with any protein larger than 50KDa. • Coupled with electron-transfer dissociation fragmentation method (EDT) that needs long time for ion accumulation, activation and detection. • Protein dissociation behaviour is less understood. • Bioinformatics analysis tools for top down just recently improved.

Table 1-1. Advantages and Disadvantages Bottom-up and Top-down Proteomics Approaches (Wehr, 2006).

1.4.1 Quantitative Proteomics and Labeling Strategies

MS-based quantitative proteomics is a crucial approach that allows us to differentiate and quantify between protein levels under different conditions. However, the MS intensity peak remains a bad indicator of protein amounts within the sample. MS-based protein quantification can be absolute or relative. Absolute quantification means that samples are determined directly in absolute values in the presence of internal proteins labeling standard for each protein while relative quantifications rely on recognition of the changes in protein levels relative to another protein abundance (Ong and Mann, 2005); Yet, the ultimate goal of quantitative proteomics is to achieve absolute quantification of the protein abundance (Kito and Ito, 2008). Also, it is clear that absolute quantification requires more time and is a costly undertaking with complex samples.

The relative quantification of a proteome can be achieved by two methods: label-free and isotopic labeling (Figure 1-6). Currently, the use of SILAC or stable isotope labeling of amino acids in cell culture is considered as one of the most popular nonradioactive labeling approaches in the quantitative proteomics field. For the SILAC method, the proteins of two cellular states (i.e. treated and non-treated) are fully labeled by incorporation of essential amino acids such as arginine (Arg) and/or lysine (Lys) with heavy ^{13}C or ^{15}N or both and light ^{12}C or ^{14}N followed by digestion with trypsin of mixed cell samples. The mixture of heavy and light labeled cells remains indistinguishable until analysed by MS and by a suitable software package such as MaxQuant (Cox et al., 2009, Cox and Mann, 2008). The double charge intensity peak of the isotopic peptide for heavy lysine (Lys 6) is shifted by 6 Da from the light one (Lys 0), which is easy to distinguish by MS (Walther and Mann, 2010, Ong et al., 2002).

The most common advantages of using SILAC in quantitative proteomics are time saving, low contamination levels (i.e. keratin), reduced false negative results and quantification errors as sample combining is achieved at the early stage of the experiment.

There are other often used labeling strategies such as ICAT and iTRAQ. ICAT (isotope code affinity tag) is a chemical labeling for relative quantification developed in 1999 in the Aebersold's laboratory (Gygi et al., 1999a). The labeling includes introduction of a chemical tag (biotin) to particular residue (cysteine) to all proteins of the target population and mixing of the samples is carried out at the peptide level. However, non-specific binding to the tag and incomplete proteome coverage has limited the wider use of this technique (Zhou et al., 2002). iTRAQ is another type of chemical labeling that can be applied for relative and absolute quantifications with the tag normally introduced to the N-terminus and the side-chain of the peptides. Tag differentiations are carried out at MS analysis level (Ross et al., 2004).

The choice between different labeling types depends on the sample itself. SILAC use has been extended from cell lines to microorganisms and vertebrates (Kirchner and Selbach, 2012). However, some cell types are not metabolically stable with introduction of the labels or cannot tolerate the effect of the treatment. In these cases the alternative labeling types or label free quantitation are better choices.

1.4.2 Subcellular Organelle Proteomics

In order to obtain better understanding of the cellular organization and function the proteomics field recently concentrated on subcellular organelles. Since the dynamic entities of organelles such as proteins move from one compartment to another to accomplish their specific function, it is important to try to understand the role of

proteins at various cellular locations (Cox and Mann, 2011). Organelle separation methods such as density-based methods already used since the 50s are often used today in addition to various methods for organelle enrichment.

Following organelle separation or enrichment the major experimental step of sub-cellular proteomics is to quantify enriched organelle fractions of interest and compare it to non-enriched fractions. The crucial task is to differentiate between true permanent or temporary organelle resident proteins and to identify "background proteins" that in turn can indicate the secondary localizations of each protein.

Various methods and strategies for control of the process are described in details by Qattan and Pinto work (Qattan et al., 2010, Qattan et al., 2012, Pinto et al., 2014).

Databases such as Gene Ontology helps to classify proteins according to their biological process, localization and molecular function giving useful overall but not definitive estimate of the data (Cox and Mann, 2011, Gauthier and Lazure, 2008, Brunet et al., 2003).

There is increased evidence that many proteins (at least 50%) are not exclusive to one organelle and are present in several locations (Drissi et al., 2013, Cox and Mann, 2011, Qattan et al., 2010). Recent investigations using a SILAC strategy for spatial proteomics quantitative changes in protein localization under diverse conditions showed that multiple distribution of proteins could be crucial for cellular function (Drissi et al., 2013, Mulvey et al., 2013, Pinto et al., 2014). Surprisingly, SILAC labeling of MCF7 breast cancer cells exposed to the estradiol showed that there were significant changes of the proteins distribution between nucleus and cytoplasm compared to the total cell lysate, concluding that the spatial proteins distribution is an important feature of cancer (Pinto et al., 2014).

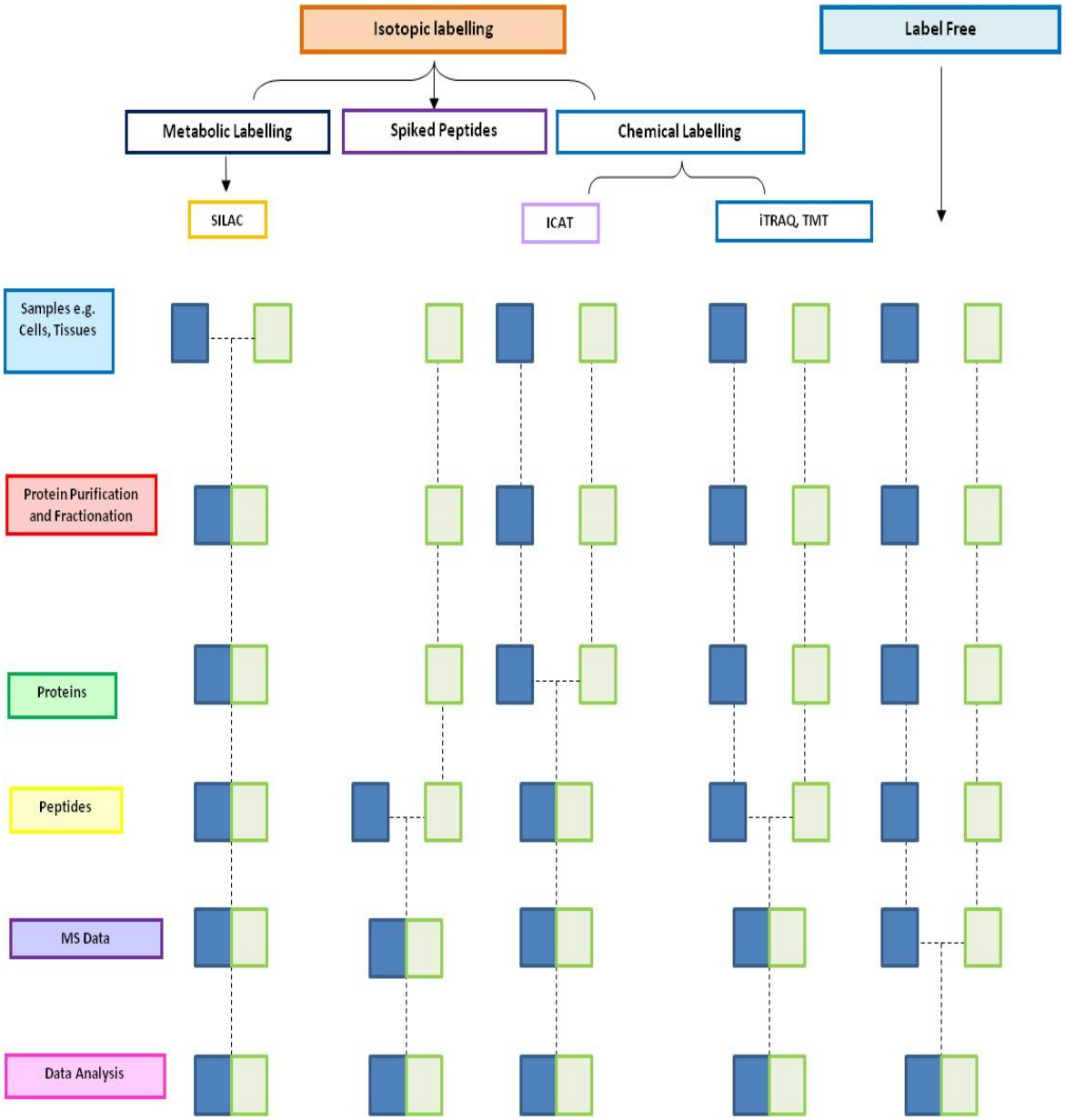

Figure 1-6. Work Flow of the Comparison among the Different Labeling Strategies in Quantification Proteomics. There are two main labeling approaches: isobaric labeling and label free. Isobaric labeling consists of metabolic labeling such as SILAC and chemical labeling such as iCAT and iTRAQ. Green and blue boxes represent an example of two states that are compared. In the SILAC approach the isotopic labels are initiated in the cell culture, samples are combined at the protein extraction stage and they continue together through all the steps of the analysis. In the iCAT method, proteins are extracted in parallel and combined at the peptide level. In iTRAQ the tag is introduced once the samples are digested into peptides. For label free method data can be combined at any stage and the data are obtained from MS spectral counts or ion current information. Modified according to figure in (Ong and Mann, 2005).

1.4.3 Overview of Mass Spectrometry based Proteomics

Mass spectrometry is a powerful tool for measuring the mass of a molecule by measuring the mass-to-charge ratio (*m/z)* of ions. Mass spectrometry is widely used in biology, chemistry and physics. It is an attractive analytical method used in proteomics for studying protein roles, functions and modifications. Mass spectrometer (MS) relies on accelerating the ionized charged-molecules in vacuum with high energy under high atmospheric pressure encouraging them to go through a electric and magnetic field that allows them to be detected and the generated information appears as spectral data on the computer screen.

MS consists of three crucial parts and each part plays an important role within the instrument: ionisation source, mass analyser and detector (Figure 1-7A). The most popular ionization sources that are widely used in proteomics laboratories are electrospray ionization (ESI) and matrix assisted laser desorption ionization (MALDI) (Figure 7B and 7C) (Aebersold and Mann, 2003). MALDI and ESI are considered to be "soft" ionization techniques. Soft ionization is especially useful for generation of ions from proteins since it overcomes the tendency of these molecules to fragment when ionized. (Guerrera and Kleiner, 2005). MALDI generally ionizes the samples out of dry solid phase using laser pulses and it is extensively applied with relatively limited peptide mixtures whereas ESI ionizes the samples out of solution. ESI is often coupled with liquid chromatography making this method highly efficient for analysis of complex samples and high throughput proteomics.

The exact desorption/ionization mechanism for MALDI is not known but it is generally believed that MALDI causes the ionization and transfer of a sample from the condensed phase to the gas phase via laser excitation and ablation of the sample and matrix. MALDI (Figure 1-7C) analysis includes the co-crystalization of the sample with an

organic matrix such as sinapinic acid that coats a metal board. The matrix is then stimulated through the pulsed laser light such as, UV light, leading to vaporization and desorption of the sample from the surface (Lovric, 2011, Guerrera and Kleiner, 2005, Yates, 2004). As the consequence of using laser pulses in MALDI the ions are generated as packages rather than a continuous beam and that might require a specific analyser that is able to measure all ions without considering their mass range or trap them for subsequent analyser, usually time of flight analyser (TOF).

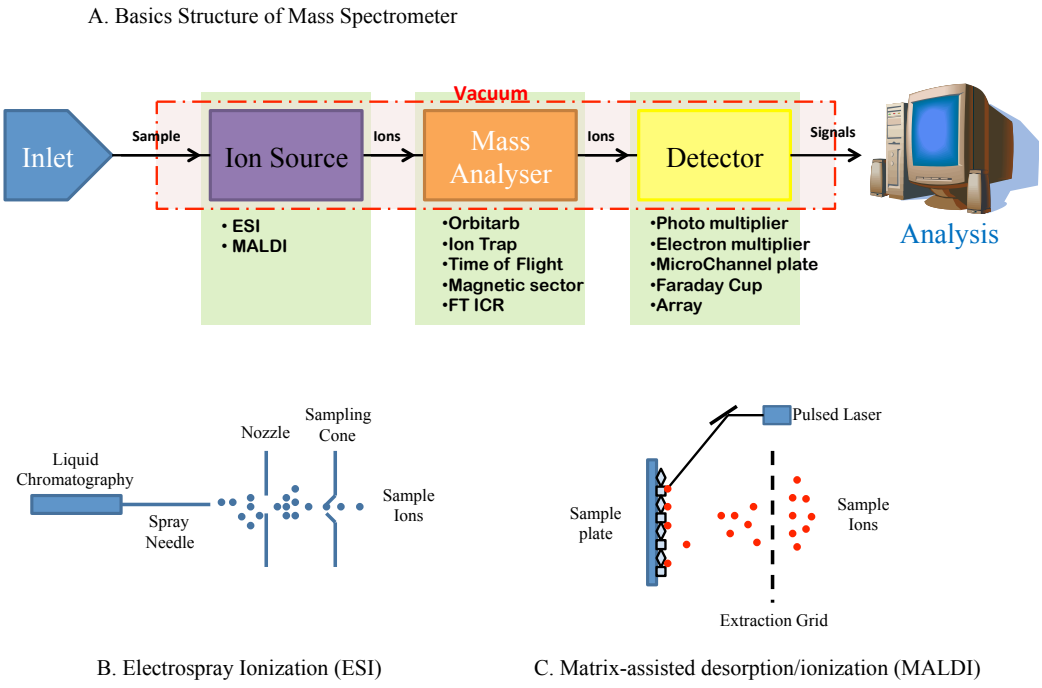

Figure 1-7. The Anatomy of the Internal Parts of a Mass spectrometer. A. Shows the basic structure of a mass spectrometer, while B. and C. represent the sample introduction process to the MS via electrospray ionization (ESI) and matrix-assisted laser desorption (MALDI). Modified according to figure in (Aebersold and Mann, 2003).

In ESI (figure 1-7B) the ionization procedure is normally accomplished by spraying the electrically fine vapored ions under atmospheric pressure with a low flow rate. Samples are introduced to ESI through a charged needle held at high electric potential (2.5-4kV). This allows sample molecules to diffuse from charged droplets. Then, between needle and sampling cone, the evaporation of the solvent reduces the droplets size and increases the charge density, which in turn increases charges collision. This collisions lead to desorption of sample ions and the reduction of the droplets size until it becomes almost one ion. The protein ions normally accept positive charge, which allows them to be easily dragged and accelerated by negatively charged ion magnetic source. Coupling the ESI with special analysers can lead to fragmentation of the selected precursor ion via a method called collision-induced dissociation (CID). Particular improvement in ESI mass spectrometry occurred with Nano spray technology developed by Mann and Wilm where the ESI needle is connected to a Nano-flow reverse phase liquid chromatographic system (RP-HPLC) allowing the initial fractionation of the peptide samples with low flow rates (50nl/min) in order to perform better MS analysis (Ho et al., 2003, Fenn et al., 1989, Pitt, 2009, Mann and Wilm, 1995).

In mass spectrometry different analysers have been used such as, ion trap, time-of-flight (TOF), quadrupole, and Fourier transform ion cyclotron (FT-ICR) analysers. Each analyser depends on special theory and principles with specific advantages and disadvantages. For example, an ion trap analyser traps and centres the ions for a certain period of time (time interval) at cylindrical volume storage to allow easily insertion of the ions for further processing. There are many different ion traps such as, linear, two or three-dimensional trap. The ion trap is a robust analyser, reliable, sensitive, and not expensive. FT (Fourier transform) analyser traps the ions under a high vacuum and magnetic field. It is an accurate, sensitive tool and gives a high resolution with the dynamic range of quantitation of at least 5 orders of magnitude. TOF (time-of-flight)

analyser separates the ions depending on there flying time that is affected by the m/z of the molecules (m/z).

Linear quadruple ion trap (LTQ) is a mass analyser (Figure 1-8) that can be used as collision cell for peptide ions fragmentation. It consists of four rods that restrain ions radially and electro-static potential on the end of the electrodes that restrains ions axially (Douglas et al., 2005).

Each analyser can be standing alone or together in tandem increasing the productivity of the MS. In MALDI the ion source can be coupled with a TOF analyzer or TOF-TOF instrument, which is able to fragment the ions via a collision cell. Usually, ESI is connected with an analyser such as, ion trap, triple quadrupole (linear) trap, quadrupole TOF and FT-MS.

Recently, a FT-MS instrument has been rapidly developed and notably employed in the proteomics field due to the machine's ability to provide a wide mass range analysis, its high resolution and sensitivity. The advantages of these instruments are accuracy and maximum mass resolution that are accomplished even for a small amount of ions. These privileges allow FT-MS and Orbitarp to outperform other mass spectrometers in the large scale proteomics field (Perry et al., 2008).

Two major characteristics of the MS analysis are mass accuracy and mass resolution. The mass accuracy is the ratio between false *m/z* to the true *m/z* in part per million (ppm). While resolution means ability to segregate differences between two peaks with highly similar *m/z*. High accuracy can remarkably determine an element's formula, which can be used as filters to define the identity of the compounds. This is important because it is impossible to achieve mass quantitation of a peak accurately if the target molecules are not sufficiently determined (Perry et al., 2008).

The most of mass spectrometric experiments currently used in proteomics are consisting of two or more MS experiments, called tandem experiment (MS/MS). The first MS

usually determine the mass/charge for the initial molecules known as parent or precursor ions while the second MS experiment fragments these parent ions producing new daughter ions (Walther and Mann, 2010). The advantage of a tandem experiment is that it allows protein quantification and subsequently the reliable identification based on peptide sequence information.

In this study, we have used a classic 'LTQ-Orbitrap hybrid' mass spectrometer (figure 1-8) that has been developed by Thermo-Fisher scientific (for further information about the Orbitarp, see the references (Scigelova et al., 2011, Perry et al., 2008) and related references).

Orbitrap is an ion trap analyser that consists of a vacuumed chamber that contains inner and outer spindle electrode, with high electrostatic field. The electrostatic field leads to trapped ions and makes them move in spiral motion around the spindle with different frequencies. The image current of the trapped ions can be detected and converted into a spectrum by Fourier transform (FT). The Orbitrap has the ability to offer high mass accuracy with high resolving power (Makarov, 2000, Hardman and Makarov, 2003, Scigelova and Makarov, 2006). The detected mass accuracy of the Orbitrap from complex peptide mixtures is normally less than 2 ppm. However, this mass accuracy has been subsequently improved to be less than 1 ppm (Olsen et al., 2005). Moreover, the Orbitrap outer electrode can work as a detector making the Orbitrap more practical and faster for ion fragmentation. Coupling an Orbitrap with a linear trap increased the LTQ-Orbitrap's sensitivity (figure 1-8).

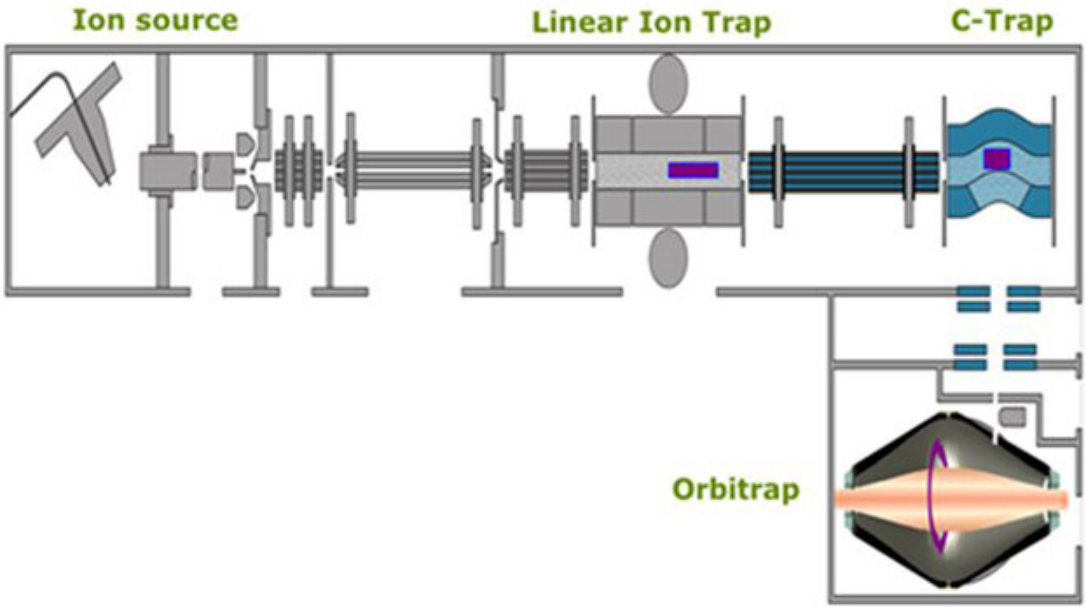

Figure 1-8. The Anatomy of the Internal Parts of 'LTQ-Orbitrap Hybrid' Mass Spectrometry. Samples are injected tangentially via charged needle to the electrospray ionization source (ESI). The charged ions go through a quadruple ion trap, which increases the ion's speed in the presence of different pressure from atmospheric conditions and accelerates them toward the linear ion trap. |The Liner ion trap reduces the speed of the ions and stores them until enough ions are accumulated. This is followed by injection to the C-trap, which is the last quadruple that compresses the ions and dampens their energy before sending them to the Orbitrap with constant speed with an accurate direction (Scigelova and Makarov, 2006, Perry et al., 2008).

1.4.4 Interpretation of the Quantitative Proteomics data and Spatial Razor Peptide Approach

Shotgun-proteomics is based on tandem MS/MS experiment or parent ion fragmentation by collision induced dissociation (CID) in the presence of inert gas (i.e. nitrogen, argon or helium).

The information of the peptide sequence generated from the tandem MS spectra consists of the fragments *x, y or z* if the charge is maintained on the C-terminus or by *a, b, or c* if the charge is retained on the N-terminus. By determination of the mass difference between C- and N- ion peaks the peptide sequence can be generated. Then, the obtained peptide sequences are compared to protein database that is mostly generated from genomic/protein sequence database using a computer algorithm to match peptides to their target protein and control the false discovery rate. The most popular peptide search engines that uses database matching for peptides and the assembling of proteins are Mascot (Perkins et al., 1999), SEQUEST (Eng et al., 1994) or X!Tandem (Craig and Beavis, 2003, Craig and Beavis, 2004). The software generates a list of detected proteins within the sample, as it is impossible to check the predictability of huge amount of data set manually. Software such as MaxQuant can be used coupled with its own search engine such as Andromeda followed by the evaluation of the analysis to assemble the protein groups and quantify them between the different conditions (Cox and Mann, 2008, Cox et al., 2009, Cox et al., 2011).

The spatial distribution of the proteins between organelles can be detected by the use of mathematical formulation of the subcellular spatial razor. The major need for the development of this approach is the fact that under a specific cellular perturbation protein response may show both change in total abundance and in their compartmental spatial distribution such as between nucleus and cytoplasm. The spatial razor model

(figure 1-9) assumes that a given protein can be present in the nucleus (n) and cytoplasm (c) for both stimulated (s) and unstimulated cells (u) (Baqader et al., 2014, Pinto et al., 2014, Mulvey et al., 2013). Correspondence abundance of each protein is scattered between protein abundance in nucleus stimulated ($A_{n,s}$), protein abundance in nucleus unstimulated ($A_{n,u}$), protein abundance in cytoplasm stimulated ($A_{c,s}$) and protein abundance in cytoplasm unstimulated ($A_{c,u}$). This gives the value of SILAC ratios as the following:

$S_n = A_{n,s} / A_{n,u}$

$S_c = A_{c,s} / A_{c,u}$

$S_t = (A_{n,s} + A_{c,s}) / (A_{n,u} + A_{c,u})$

As results it has been found that the values of the nucleus fraction unstimulated f_u and fraction stimulated f_s are closely related to SILAC ratios as following:

$f_u = A_{n,u} / (A_{n,u} + A_{c,u}) = (S_t - S_c) / (S_n - S_c)$,

$f_s = A_{n,s} / (A_{n,s} + A_{c,s}) = S_n (S_t - S_c) / S_t (S_n - S_c)$.

As results ratios for the distribution plan will be as following:

$S_n / S_t = f_s / f_u$ and, $S_c / S_t = (1 - f_s) / (1 - f_u)$.

The advantage of subcellular spatial razor formulation is that it can distinguish between changes in total protein abundance (S_t) and redistribution (S_n / S_c) to/from a target organelle (e.g. the nucleus).

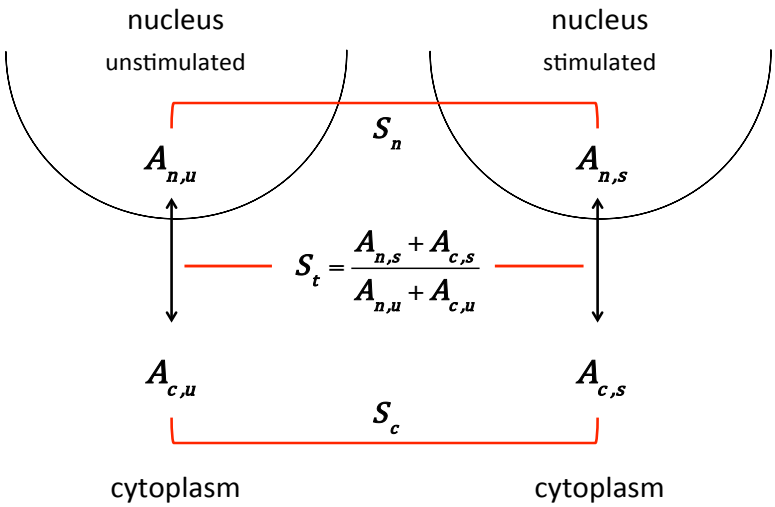

Figure 1-9. Mathematical Formulation of the Spatial Razor Model. Letter (A) represent the correspondence appendance and letter (S) represent SILAC ratio H/L. The razor model postulated that proteins could be presented in the nucleus (n), cytoplasm (c), and total (t) fractions under stimulated (s) and unstimulated (u) conditions; when S_n is $A_{n,s}/A_{n,u}$, S_c is $A_{c,s}/A_{c,u}$ and S_t is $(A_{n,s}+A_{c,s})/(A_{n,u}+A_{c,u})$ (Pinto et al., 2014, Mulvey et al., 2013, Baqader et al., 2014).

1.5 Aim of Study

The novel DNA replication origin activation checkpoint and its architecture has been recently described (Tudzarova et al., 2010) and the large scale shot gun quantitative proteomics study of Cdc7-depleted IMR90 fibroblasts (Mulvey et al., 2010, Mulvey et al., 2013) revealed that cells maintain reversible cellular arrest by initiating a dynamic quiescence-like response, and that the complexities of this phenotype will have important implications for the continuing development of promising Cdc7-targeted chemotherapeutics. This development is based on the fact that several cancer cells bypass G1/S arrest and progress to an abortive S phase triggering cell death. Targeting of Cdc7 with RNAi results in cancer cell specific killing in numerous tumours (Blow and Gillespie, 2008); but, at the same time may protect non transformed cells by reversibly arresting them in G1/S phase (Rodriguez-Acebes et al., 2010).

Our quantitative large scale proteome analysis of Cdc7 depleted IMR90 fibroblasts revealed that an extensive range of biological changes such as altered cellular energy flux, mild oxidative stress response, lower proliferative capacity are spatially distributed over various subcellular locations inducing a dynamic quiescence-like response (Mulvey et al., 2010).

The global and subcellular proteome analysis of Cdc7 depleted IMR90 fibroblasts generated considerable interest due to its implications for the development of promising Cdc7-targeted cancer therapies.

In order to understand the mechanism of DNA origin activation checkpoint in normal human fibroblasts under oxidative stress we undertook the present study. The strategy to achieved the study aims are summarised in Figure 1-10.

The aims of this study are to:

1. Investigate oxidative response of normal IMR90 fibroblasts by use of tert-butyl-hydrogen peroxide TB-H_2O_2 and large-scale quantitative SILAC LC-MS/MS proteome analysis.
2. Investigate and compare quantitative dynamical changes in nucleus and cytoplasm of IMR90 cells under oxidative stress.
3. Evaluate proteome data sets of IMR90 fibroblasts under oxidative stress.
4. Investigate resulting protein pathways involved in IMR90 response to oxidative stress.

Following detailed bioinformatics analysis of identified pathways we hope to understand the cellular changes at G1/S arrest under oxidative stress. In addition, these results will provide the reference point for Cdc7 targeted drug development.

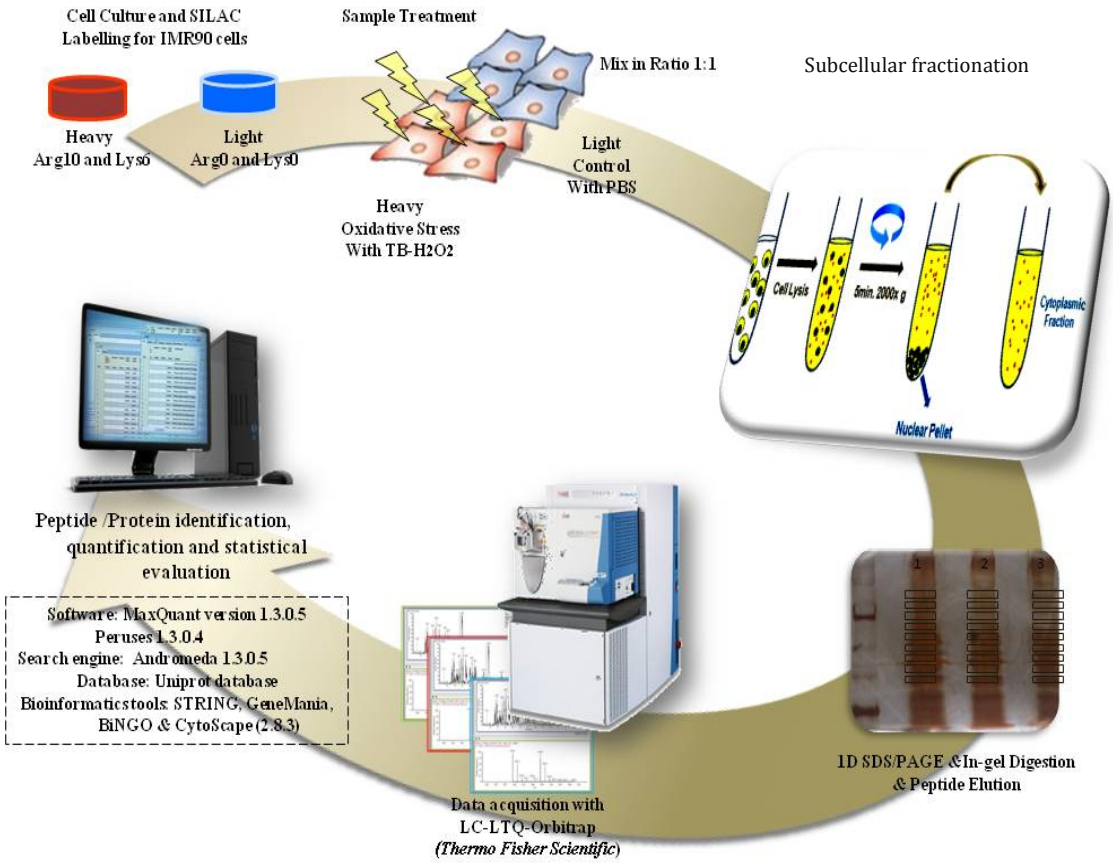

Figure 1-10. The Schematic of SILAC Experiment for the Use of Quantitative Proteomics to Study the IMR90 Human Fibroblast Cells under Mild Oxidative Stress. A combined strategy involving oxidative stress, protein subcellular fractionation, 1D SDS-PAGE, LC-MS/MS data acquisition with LTQ-Orbitrap, and downstream bioinformatics for identification, quantification, statistical evaluation and network analysis was applied in this study.

Chapter 2: Materials and Methods

2.1 Materials

2.1.1 Chemicals and Reagents

Most of the chemicals that were used in the preparing of buffers and washing solutions were purchased from ***SIGMA Aldrich Company Ltd, Poole, UK***.

Other purchases were obtained from different companies as following:

- **Martials for Cell Cultures:**

  LGC Standards, Middlesex, UK:

  IMR-90 (#ATCC CCL-186), a human diploid fibroblast cell line from foetal lung tissue.

  Gibco, life technologies, Invitrogen, Manchester, UK:

  D-MEM (#31966-021), a Dulbecco's Modified Eagle Medium with high glucose, GlutaMAX™ and pyruvate.

  FBS (#26400-044), a dialyzed foetal bovine serum.

  Thermo Scientific, Rockford, USA:

  SILAC kit (#89983), stable isotope labeling by amino acids in cell culture (SILAC).

  The kit contains:

  D-MEM, heavy $13C_{6}$- (Lys6), light L-Lysine (Lys0) and dialyzed FBS.

  The Heavy $13C_{6}$ $15N_{4}$-L- Arginine (Arg10) (#89990) was purchased separately from the same provider.

  Sigma, Gillingham, UK:

Trypsin-EDTA (#T4049).

DMSO (#472301), dimethyl sulfoxide.

SIGMA Aldrich Company Ltd, Poole, UK:

TB-H_2O_2 70% wt. (#458139), tert-butyl- hydrogen peroxide (TBP).

TEMED (#T9281), tetra-methylethylenediamine.

APS (#A3678), Ammonium pre-sulfate.

- **Martials for Proteomics Laboratory:**

  Bio-rad, Hemel Hempstead, UK

  Bio-Rad protein assay (#500-0006).

  Merck Millipore, Darmstadt, Germany

  Acetone (#100020.100).

  National Diagnostics; Hessle, Yorkshire, UK

  The ultra pure acrylamide proto-Gel 30% (w/v) arcylamide: 0.8% (w/v) Bis acryl-amid stock (37.5:1) (#EC-890).

  Millipore Corporation, Billerica, MA:

  β–galactoaidase senescence kit (KAA002).

- **For mass spectrometry:**

  ARISTAR, VWR international, UK:

  Formic acid.

  Merck, Darmstadt, Germany:

  Acetonitrile (MS grad).

- **Martials and Antibodies for Western Blotting:**

  Abcam, Cambridge, UK:

Catalase (#ab76110); Superoxide Dismutase 1 (#ab79390); Glutathione Peroxidase 1(#ab108429), Nrf2 (ab89443), Keap1 (ab66620) and β-Actin (#ab75186).

The Secondary antibodie (#ab 97245), Anti-goat for anti-mouse IgG2a HRP-linked Antibody.

Cell Signalling, New England Bio-lab, Hitchin, Hertfordshire, UK:

Anti-Cdc7 (#3603S).

Secondary anti-rabbit IgG HRP-linked Antibody (#7074S).

Merck Millipore, Darmstadt, Germany:

Anti-p53 (#Merck Ab-6-100).

GE health care life science, Buckinghamshire, UK:

Western Blotting Detection kit Amersham ECL Plus (#RPN2132).

Bio-Rad, Hertfordshire, UK:

Kaleidoscope Standards (#161-0375), Precision plus Protein with detection range from 10-250kD.

GE Healthcare limited, Buckinghamshire, UK:

Whatman Nitrocellulose Transfer Membrane (#10401396 & lot: D146795).

WB films Amersham HyperFilm ECL (#28906837).

Whatman Gel Blotting paper (#10426994 & lot: D109105).

SIGMA Aldrich Company Ltd, Poole, UK:

Sliver stain kit (#PROTSIL1).

Promega, Southampton, UK:

Trypsin Gold for mass spectrometry (#V528A).

Roche Products Limited, Welwyn, UK:

Roche completes protease inhibitor cocktail tablets (#11836145001).

Phospho-stop (#04906845001).

- **For Immune-Cyto-Chemistry:**

  Thermo Fisher Scientific Inc; Rockford, USA:

  Anti-ATP5A1 antibody produced in rabbit (#PA5-27504).

  Atlas antibodies, Sigma, Gillingham, UK:

  Anti-ALDH18A1 antibody produced in rabbit (#HPA008333).

  Sigma, Gillingham, UK:

  Anti-Rabbit IgG (whole molecule)–FITC antibody produced in goat (#F0382).

  Formaldehyde for molecular biology 36.5% (#F8775).

  Triton X-100 (#033K0605).

  Molecular Probes-life technologies, Invitrogen, Manchester, UK:

  Mitotracker Green FM (#M-7514).

  Mitotraker Deep reed FM (#M22426).

  Hoechst 33342- readymade (#R37605).

  VECTOR LABORATORIES LTD, Peterborough, UK:

  VECTASHIELD Mounting Medium (#H-1000).

  VECTASHIELD with DAPI (#H-1200).

  SIGMA Aldrich Company Ltd, Poole, UK:

Glycerol (#G6279).

- **For FACS Analysis:**

  SIGMA Aldrich Company Ltd, Poole, UK:

  Propidium Iodide (PI) dye (#P4864).

  Ribonuclease A from bovine pancreas (#R4875).

2.1.2 Equipment and Software

SIGMA Aldrich Company Ltd, Poole, UK:

Siliconized micro-centrifuge tubes (#T3406-250EA).

NUNC-immuno-flat bottom plates (#M9410).

Corning, NY, USA; Cell star, Greiner Bio-One Ltd; UK and Falcon BD, Erembodegem, Belgium:

175, 75 and 25cm^2 flasks.

BD biosciences discovery lab ware, Bedford, USA:

8 and 4 wells BD Falcon culture slides (#354108; 354104).

Willcowells, Amsterdam, Netherland:

Glass bottom culture dishes with deiameter12 mm and glass thickness 1.5 (#GWSt-3512).

Total laboratory services, Dorset, UK:

Eppendrof centrifuge (#5804R).

Biofuge, Heraeus instrument, Kendro laboratory products, Germany:

Bench-top micro centrifuge.

MSE, London, UK:

Sonicator Soniprop150.

Millipore, Consett, Durham, UK:

Water purification system MilliQ for distilled and deionized the water with a Quantum EX (Organex Resin) cartridge.

Millex-GS Filter Unit (#SLGS033SB).

Digilab, Genomics Solutions, Huntingdon, UK:

ProGest Investigator, blue and red 96 well Microtiter plates tht used for alkaline-reduction process (#PRO10005, 10004 and 10006).

Qmax Lab., Chaomcol, Welwyn Garden city, Hertz, UK:

Chromatography vials (#V1504) with a black cap (#V0698).

Laboking, Paris, French:

2ml Cryotube, Ext-Thread (#COR-CT-01).

Bio-Rad, Herts, UK:

Mini-Protean III electrophoresis cell system tanks, 1.0mm glass plates, semidry electroblotting and electrophoresis power supplier.

GE health care life science, Buckinghamshire, UK:

Hyper film ECL (#28-9068-35), film cast and Whatman's nitrocellulose blotting membrane (#Protran BA85).

Beckman Coulter Inc., Orange County, CA:

Flow cytometer DAKO/Beckman Coulter MoFlo High speed sorter.

Speedvac plus SC110A, Savent, instrument Inc., Holbrook:

Vacuum evaporator centrifuge.

Anthos htll, Slazburg:

Standard spectrophotometer for calorimetric assays.

Olympus KeyMed Ltd., Essex, UK:

Olympous-CK2 inverted light microscope, attached to Axio Cam MRM ZEISS camera and the picture visualizer software Axio-Vision released at 4.5 SP (3/2006).

PerkinElmer, Cambridge, UK:

Perkin Elmer spinning-disk confocal laser microscope.

Thermo Fisher Scientific, Fremont, Canada:

LTQ-Orbitrap Classic mass spectrometer (XL), Surveyor MS pump and liquid chromatography Micro AS auto sampler.

Reprosil, Nikkyo Technos CO, Tokyo, Japan:

MiChrom C18 cap trap for desalting and nanoelectrospray ion source that consisted of a fused silica capillary column (i.d. 100 μm; o.d.360 μm; length 20 cm; 5 μm C18).

Matrix Science, London, UK:

Protein and peptide identification software tools, Mascot software (version 2.2).

Max Planck Institute of Biochemistry, Martinsried, Germany:

The quantitation software for SILAC labeling quantitation, MaxQuant coupled with Andromeda Configuration (versions 1.3.0.5); and Perseus (versions 1.3.0.4) were downloaded from http://maxquant.org/faq.htm; and from MaxQuant help http://groups.google.com/group/maxquant-list

Uniprot website (http://www.uniprot.org):

Human fasta file: (ftp://ftp.uniprot.org/pub/databases/uniprot/current_release/knowledgebase/proteomes/) accessed and download at 31-10-2012.

2.1.3 Buffers and Stock Solutions

10X TBS buffer

500mM Tris-Cl pH 7.5 and 1.5M NaCl in 1L of distilled H_2O.

TBST buffer

1X TBS with 0.2% Tween

10X PBS buffer

1.37M NaCl, 27mM KCl, 100mM Na_2HPO_4 and 18mM KH2PO_4 in 1L of H_2O.

PBS^+ buffer

1X PBS, 1mM $CaCl_2$ and 0.5mM $MgCl_2$.

Fractionation buffer

Buffer A: 10mM HEPES pH 7.9, 10mM KCl, 0.1% Triton X-100, 2mM EDTA, 2mM DTT, 0.34M sucrose and complete protease inhibitor cocktail tablets.

Buffer B (Isotonic sucrose IS buffer): 100mM NaCl and 200mM sucrose.

RIPA buffer

50mM Tris-HCl pH 7.4, 300mM NaCl, 1% sodium deoxycholate, 1% NP-40, 1mM EDTA, 0.1% SDS.

2X Sample buffer

4% of 10% (w/v) SDS, 2% Glycerol, 120mM of 1M Tris-HCl (pH 6.8) and 0.02% of bromophenol blue dissolved in distilled H_2O.

Transfer buffer

48mM Tris-HCl, 39mM Glysine and 20% methanol dissolved in distilled water.

2.2 Methods

2.2.1 Methods used in Cell Culture Laboratory

2.2.1.1 Cell Culture and Growth Conditions and SILAC Labeling

IMR-90, a human primary diploid fibroblast adherent cell line was obtained from the provider at population doubling (PD) 12, and was cultured with PD of less than 22 and tested for senescence by the measure of β–galactosaidase activity within the cells. Cells were cultured under normal growth conditions 37°C and 5% CO_2 in D-MEM medium that contained high glucose, Glutamax and pyruvate plus 10% FBS.

Cells were initially plated at T25 flask with capacity 500,000 cells per flask and incubated from overnight to three days. After cells recovered, they were washed with 37°C warmed up PBS p.H 7.4, detached from surface by the use of trypsin-EDTA and moved to T75 flasks that contained SILAC-DMEM media supplemented with 10% of SILAC dialyzed foetal bovine serum FBS. The SILAC medium was prepared by following the manufacturer's instructions (Thermo Scientific, UK).

For SILAC quantitative analysis, cells were divided into two populations and were cultured in either light medium containing amino acids $^{12}C_6$, $^{14}N_4$-Arginine and $^{12}C_6$-lysine (Arg0, Lys0) or heavy medium containing amino acids $^{13}C_6$, $^{15}N_4$-Arginine (Arg10) and $^{13}C_6$-lysine (Lys6) by at least 7 passages in parallel in order to achieve a full incorporation of SILAC amino acids. The full incorporation of heavy isotope was checked by mass spectrometry of samples of heavy/or light lysed cells (Mulvey et al., 2010, Mulvey et al., 2013, Ong and Mann, 2006).

2.2.1.2 Cell Counting

Small amount of the suspended cells in growth medium were mixed gently with trypan blue in ratio (1:1) by the use of serological pipette in cleaned *Eppendrof* tube. The mixture was drawn out gently to the edge of the chamber of a cleaned haemocytometer with 70% ethanol and affixed with coverslip. Suspension was diffuse into the chamber groove by capillary actions. The hemacytometer was viewed under the light microscope by the use of the 10x objective lens, and the cell numbers were counted only inside the four corners that consisted of 16 square and the central square of the slide manually.

Calculations normally done to determine the total number of cells per ml by applying the following equation:

Total cells /ml= total cells counted x (#dilution factor / #number of squares) x 10^4

Total cell numbers in the flask= Total cells/ml x Total sample volume in the flask

For cells viability= (Live cell count (shiny rounded cells)/ Total cell numbers) x 100

2.2.1.3 Preparation of Cryoprotective Medium for Storing of the IMR90 cells and Thawing Process

The harvested cells were spun down at 125g for 5 minutes combined with 2x wash with PBS to remove the excessive amount of the old medium. Cells were re-suspended in a fresh complete growth medium that was supplemented with 10% (v/v) DMSO at room temperature. The re-suspended cells were transferred into cryotube and kept at -80^{o}C overnight then transferred to liquid nitrogen for long term storing.

For thawing the cells, the cryotube was taken form liquid nitrogen and placed immediately at 37^{o}C water path; sprayed with 70% ethanol. The sample was diluted with 10ml of fresh and 37^{o}C in a warmed DMEM and spun down at 125g for 10 minutes to prevent toxicity of DEMSO on the cells. Old medium was discarded and cells were re-suspended in new fresh DMEM medium.

2.2.3 Cell Treatment

2.2.3.1 Oxidative Stress

Mild oxidative stress was exerted upon IMR90 cells according to a published protocol (Tudzarova et al., 2010, Chen et al., 2004) with minor modifications. Heavy cells were treated with 50μM tert-butyl hydrogen peroxide TBP in cell culture media for 2h, while the light cells were treated with 50μM PBS and used as control. The treatment was stopped by replacing the cell culture medium with fresh medium without peroxide. On the next day, the heavy cells were again treated with TBP for 1h. Four hours after the removal of media containing peroxide, heavy or light cells were detached from the surface of tissue culture flasks by use of Trypsin-EDTA, washed three times with PBS p.H 7.4 and recovered by centrifugation at 60g. For sample preparation, a total of 4 flasks each of heavy and light cells were used.

2.3 Methods used in Proteomics Laboratory

2.3.1 Sample Preparation

Protein concentration was measured by the use of the Bio-Rad protein assay kit. Heavy and light cells were mixed in a 1:1 ratio based on protein concentrations and the amount of cell pellet (Ong and Mann, 2006, Walther and Mann, 2010). Cell lysis and subcellular fractionation were performed in order to obtain cytoplasmic (C, nuclear-depleted fraction) and nuclear fractions (N). Cells were lysed as described in Mulvey et al. (Mulvey et al., 2010) in hypotonic buffer A. After 10 minutes of lysis, the salt concentration and viscosity of the buffer was adjusted by addition of (isotonic sucrose buffer B; IS buffer). Following a 5 minutes centrifugation at 2000g, the supernatant was collected as the crude cytoplasmic fraction. The nuclear fraction in the pellet was washed twice in IS buffer by an additional two centrifugation steps for 5 minutes at 2000g, with the washings restored to the crude cytoplasmic fraction. The crude cytoplasmic (nucleus-depleted) fraction was cleared by centrifugation at 13000g for 15 minutes and the supernatant used as the cytoplasmic fraction.

The cytoplasmic fraction was concentrated using the Aston precipitation method by adding 4:1 volumes of chilled acetone to the sample, which was kept overnight at -20 $^{\circ}$C. On the next day the sample was centrifuged and washed three times with chilled acetone at 13 000g for 10 minutes at 4 $^{\circ}$C. The pellet was air dried for 5 minutes at room temperature to eliminate any acetone residue and then dissolved in modified RIPA buffer.

2.3.2 Protein Separations and In-Gel Digestion

For each of the nuclear (N) and cytoplasmic (C) samples 60µg of total protein was separately resolved by 10% SDS-PAGE under reducing conditions. Proteins were visualized by silver staining with ProteoSilver Plus kit (Shevchenko et al., 1996). At least 30 horizontal bands were excised from each gel lane and processed on a 96-well Progest plate. Gel bands were processed with the Progest Investigator using established protocols for reduction and alkylation (Shevchenko et al., 2006). Finally, gel plugs were rehydrated in 20µg/ml sequencing grade modified trypsin (trypsin-Gold) that was prepared by adding (1:50 v/v) trypsin/25mM ammonium bicarbonate, and incubated overnight at 37 °C. Fifty microliters of 0.1% formic acid was added in order to stop the tryptic digestion, the extracted tryptic peptides were collected in siliconized Eppendorf tubes and vacuum-dried to about 20µl, the volume adjusted to approximately 30µl with 0.1% formic acid, and the sample analysed by Orbitap LC-MS/MS.

2.4 Immunoblotting

Treated heavy (T) or untreated light cells (UT) were lysed in SDS-sample buffer for 3 minutes at 90 ˚C and 60µg protein/lane resolved by 10-12% SDS-PAGE under reducing conditions. Proteins were transferred from gels onto Nitrocellulose membranes by semi-dry electroblotting (15 V for 1hr). For oxidative stress markers, the membrane was blocked with 5% semi–fat milk powder TBS-tween20 for 1hr followed by 3X washing with TBST; the antibodies were blocked in 5% semi–fat milk powder TBS-tween20 over night at 4 ˚C. The antibody concentrations were: 1:10000 of superoxide dismutase 1 **(**SOD1), 1:1000 of Glutathione peroxidase 1 **(**GPX1) and 1:500 of catalase. For the proteins Cdc7, p53, Nrf2 and Keap 1, the membrane was blocked with 10% semi–fat milk powder PBS for 1hr or overnight at 4 ˚C followed by 3X washing with PBS prior

to the use of the antibodies. The antibody concentrations were: 1:1000 Cdc7, 1:1000 p53, 1:300 Nrf2 and 1:500 Keap 1.

The next day the membranes were washed 3-5 times either with TBS-tween20 or PBS for 10 minutes each and incubated for an hour and half at RT with the appropriate secondary antibodies dissolved in 5% semi-fat milk powder TBS-tween20 or 10% semi–fat milk powder PBS. Secondary antibody concentrations were 1:2000 anti-rabbit IgG HRP-linked Antibody and 1:2500 Goat for anti-mouse IgG2a HRP-linked Antibody. Finally, the membranes were washed as described above. However, the last washing step for TBS was without tween20 to avoid interference with the ECL detection reagent. WB bands were visualised using ECL developing reagents kit by following of the manufacturer's instructions (GE healthcare, Buckinghamshire, UK).

2.5 Cell Cycle Analysis

Flow cytometery or FACS for cell cycle analysis followed the procedure described by Tudzarova et al., 2010 (Tudzarova et al., 2010). Heavy and light cells were collected and fixed overnight at -20 $^{\circ}$C in 80% methanol in PBS. Cells were precipitated by centrifugation at 50g for 10 minutes, the supernatant was discarded and the cells suspended in a Propidium Iodide master mix in PBS containing 50µg/ml RNase A, 50µg/ml Propidium iodide solution and protease inhibitors with a final cell density of $1x10^6$ cells/ml. Cells were incubated at 37 $^{\circ}$C for 30 minutes in darkness. Cells were sorted by use of a DAKO/Beckman Coulter MoFlo High speed sorter. The forward scatter signal was used for detection of cells and the propidium iodide signal fluorescence was linearly quantified to rationalize DNA content after excitation at 488 nm in the orange/red channel (613/20 nm band-pass filter) (Tudzarova et al., 2010).

2.6 Immunofluorescence and Confocal Microscopy

To validate that nuclei and mitochondria remained structurally intact before and after oxidative stress, immunofluorescence and confocal microscopy were used. The IMR90 cells were grown in glass bottom *Petri* dishes 12 mm, 1.5 thicknesses. Control and TBP-treated IMR90 cells were washed three times with PBS^{+}. Mitochondria were stained with 100nM of MitoTracker green M-7514 in the cell culture growth medium for 30 minutes at 37 ºC, followed by two washes for 5 minutes with medium at normal growth condition. The nuclear staining was performed by adding 1.5 drops of Hoechst-readymade to the medium for 15 minutes in the dark at room temperature.

Alternatively, prior to imunocytochemistry, cells were stained with 200nM MitoTracker deep red FM as before, directly fixed and permeablized for 5 minutes at -20^{o}C with ice-cold 1:1 methanol-acetone; and washed 3X with PBS for 2-5 minutes each. Primary antibodies for ALDH18A1 and ATP5A1 were respectively diluted 1:50 and 1:25 in 4% PBS/FBS and incubated with the fixed cells at 4 ºC overnight. Cells were subsequently washed 4X for 10 minutes with PBS and incubated for an hour and half in the dark with 1:1000 fluorescent secondary FITC antibody diluted in 4% FBS/PBS. Nuclei were stained and cells were covered with VECTASHIELD mounting media with DAPI. Image acquisition was performed with a Perkin Elmer spinning-disk confocal laser microscope and a 63×/1.4 numerical aperture oil immersion lens. The excitation maximum (nm) and emission maximum (nm) was the following: for DAPI, 358 and 461; for Hoechst 3342, 352 and 461; for Mitotracker Green FM, 490 and 516; for Mitotracker Deep red FM, 644 and 665; for FITC, 490 and 525 respectively. 3D images were taken with help from Mr. Thomas Adejumo from the Wolfson Institute for Biomedical Research and the UCL Cancer Institute (UCL, London, UK).

2.7 Mass Spectrometry

LC-MS/MS analysis was performed on a classic LTQ-Orbitrap equipped with a SURVEYOR-MS pump and Thermo Micro AS-autosampler. Peptides were resolved or loaded using a fused silica capillary column, which is a part of the nanoelectrospray ion source with an initial desalting step using a MiChrom C18 Captrap for peptides. Liquid chromatography was carried out at ambient temperature at a flow rate of 500nl/min using a dual gradient of Buffer A: 0.1% formic acid and Buffer B: 100% acetonitrile (ACN) with 0.1% formic acid. Separation was achieved by a 5-23% buffer B gradient (95-77% Buffer A) for 65 minutes, followed by 23-40% Buffer B (77- 60% Buffer A) gradient for 30 minutes, and a step gradient to 60% Buffer B for 5 minutes. Full Profile data was acquired on the LTQ-Orbitrap.

The measurements were done under positive ion mode. The tuning parameters were as follows: spray voltage 1.40kV, capillary temperature of 200°C. A full scan was collected for eluted peptides in the range 450-1600 m/z with the Orbitrap portion of the instrument at a resolution of 60,000 followed by MS/MS using CID (Collision Induced Dissociation) with dynamic exclusion of 40s and a maximum number in the dynamic exclusion list of 500 in the LTQ portion of the instrument with a minimum count threshold of 500. An activation q value of 0.25 and activation time of 30ms was applied for MS2 acquisitions. X!Calibur software version 2.0.7 was used for data acquisition as in Mulvey et al., 2010. Homo sapiens species restriction with the number of protein entries searched: 218,357.

2.8 Data Analysis, Protein Identification and Quantification

Raw MS files from all replicate SILAC experiments were uploaded into the MaxQuant software platform (version 1.3.0.3) for peak list generation, quantification of SILAC pairs, identification of individual peptides, protein identification and assembly into protein groups. XCalibur raw files were processed and searched against a UniProt fasta file. Selected MaxQuant analysis parameters included trypsin enzyme specificity, SILAC doublet measurements of Lys6 and Arg10, 2 missed cleavages, minimum peptide length of 7 amino acids, minimum of 2 peptides (1 of which is unique), top 6 MS/MS peaks per 100 Da, peptide mass tolerance of 10 ppm for precursor ions, and MS/MS tolerance of 0.5 Da. Oxidation of methionine and N-terminal protein acetylation were selected as variable modifications, and cysteine carbamidomethylation was selected as a fixed modification. All proteins were filtered according to a false discovery rate (FDR) of 1% applied at both peptide and protein levels. Proteins were automatically quantified by the MaxQuant software: a minimum of 2 peptide ratio counts from razor and unique peptides were necessary for protein quantification, and the "requantification" option was enabled. An Experimental Design template was used to specify individual experiments and reverse labeling conditions within the analysis. The final Protein Groups and peptide text files were processed with Perseus (versions 1.3.0.4). Peptides with a normalized Significance B score of $p < 0.05$ were included for downstream analysis (Cox and Mann, 2008, Cox et al., 2009, Mulvey et al., 2010)

2.9 Correlation of Proteins across Different Samples

The MaxQuant software package (Cox and Mann, 2008, Cox et al., 2009) was used to identify proteins for 12 data analysis sets: (a) each nucleus (N) sample replicate and the

union of the three N samples, (b) each cytoplasm (C) sample replicate and the union of the three C samples, (c) each C&N replicate and the union of the three C&N samples. C&N denotes that for each individual biological replicate, the MS data for the C and N samples were jointly processed with MaxQuant to estimate changes in total protein abundance. For this data, a correction for enrichment of nuclear proteins in the MS data analyses was applied during estimation of total protein abundance. Across these samples, a total of 4429 protein sequence groups were found. For the same underlying gene, slightly different protein sequence groups were sometimes observed depending on the exact set of peptides detected in each sample. Using the principle that sequence groups in different samples that correspond to the same underlying protein(s) must have protein sequences in common, the union of the unique peptides for protein sequence groups with shared protein sequences was formed and used to re-query the full UniProt human sequence data set to identify "consensus" sequence groups across the three sample types. This gave 3589 independent proteins (sequence groups) for which the MS data, including the individual replicates, is given in Supplementary Table 1.external CD All of the consensus sequence groups contained at least one consensus protein sequence that contained all unique peptides in the group and all were independent, i.e. there were no protein sequences shared between different consensus protein sequence groups (Pinto et al., 2014, Mulvey et al., 2013, Baqader et al., 2014).

2.10 Selection of Significantly Changed Proteins

To select a set of proteins showing the most significant changes in SILAC ratios for the oxidative stress experiments we used the MaxQuant Significance B score (Cox and Mann, 2008) (SigB hereafter) and procedures analogous to those applied previously for cell cycle arrest (Mulvey et al., 2010, Mulvey et al., 2013). A minimum of at least 3

ratio counts were required for inclusion of a SILAC ratio in the selection procedures. For SILAC ratios measuring changes in the nuclear (S_n), cytoplasmic (S_c) and total (S_t) abundances, we used the cutoff limits $SigB^{union} < 0.002$ and $SigB^{replicate} < 0.006$, where $SigB^{union}$ refers to the union over the three replicates (e.g. the 3 nuclear replicates) and $SigB^{replicate}$ refers to the individual replicates (e.g. each nuclear replicate). Proteins showing the most significant changes in S_n, S_c and S_t were selected with the joint requirement $SigB^{union} < 0.002$ and $SigB^{replicate} < 0.006$ for at least two replicates. For the redistribution parameter S_n/S_c, which detects nucleus-cytoplasmic redistribution even in the absence of changes in total protein abundance (Mulvey et al., 2013, Pinto et al., 2014), we used the joint limits $|\log_2(S_n/S_c)|^{union} > 0.9$ ($0.54 > S_n/S_c > 1.87$) and $|\log_2(S_n/S_c)|^{replicate} > 0.8$ for at least two replicates. This led to selection of 121 proteins (the 121-OxS set, see text) for subsequent network analyses. A summary for these proteins and the selection procedures is given in Supplementary Table 2, external CD. As described previously,(Mulvey et al., 2013) the concomitant use of limits on the union and on individual replicates tended to select proteins with substantial numbers of ratio counts, i.e., a minimum of 9 ratio counts (in a single sample) and a median of 120 ratio counts per protein were used in classifying the proteins in the 121-OxS set (Mulvey et al., 2013, Pinto et al., 2014, Baqader et al., 2014).

2.11 Bioinformatics Analysis of Functional Networks

For the identification of functional annotations, associations, interactions and networks within the dataset, combinations of several data analysis tools were used. The consensus Gene Name identifiers for the 121-OxS set of most significantly changed proteins were uploaded into STRING version 9.1 (Search Tool for the Retrieval of Interacting Genes/Proteins), to create a protein interaction network based on known and predicted

protein-protein interactions (Franceschini et al., 2013, Szklarczyk et al., 2011). A threshold confidence score of 0.7 was used to ensure that only highly confident protein interactions were considered for inclusion in the network. Seven types of protein interaction information were used for network generation, including neighbourhood, gene fusion, co-occurrence, co-expression, experimental, database knowledge and text mining. Three networks from STRING were further analysed: the 121-OxS set, a 240-OxS set containing an additional 119 "white nodes" densely connected to 121-OxS that were suggested by STRING, and a 180-OxS set containing the 121-OxS set and 59 of the 119 "white nodes" quantified in our experiments, but not amongst the proteins showing the most significant changes (see text). Densely connected clusters in these networks were identified with MCODE 1.32. (Bader and Hogue, 2003) BiNGO 2.44 (Maere et al., 2005) was used to obtain enriched GO BP (biological process) terms. DAVID (Huang da et al., 2008) was used to scan for other types of annotations. The combined STRING, BINGO and DAVID results were used to select a set of 32 GO biological process terms to describe the cellular response (Table 3-2). These terms corresponded to groups of proteins with enriched GO BP terms, but we also included additional terns to cover other proteins selected as significant in the 121-OxS set. The networks were imported into Cytoscape version 2.8.2 for further analysis and visualisation (Shannon et al., 2003, Smoot et al., 2011). Other groups of proteins, e.g., proteins annotated to glycolysis (see text), were selected for comparison using the QuickGO (Binns et al., 2009) facility at the European Bioinformatics Institute (http://www.ebi.ac.uk/QuickGO/) with appropriate sets of GO identifiers.

Chapter 3: Results: Nuclear-Cytoplasmic Trafficking of Proteins is a Major Response of Human Fibroblasts to Oxidative Stress[1]

3.1 Introduction

The cellular oxidative state has been known to contribute to different disease processes. Recently there has been huge interest in the roles of ROS and mitochondria in diseases such as diabetes, inflammatory diseases, neurodegenerative disease such as Parkinson's and Alzheimer diseases and also cancer (Brownlee, 2001, Finkel et al., 2007, Lin and Beal, 2006, Nathan, 2002, Naik and Dixit, 2011).

As there is interest in the protein damage caused by ROS, one of the active research branches is currently aimed at understanding the processes responsible for the protein damage and biological quality control process such as mitophagy and autophagy (Ryter and Choi, 2013, Lee et al., 2012). As a result, this led to the finding that, under specific physiological conditions, ROS tend to act as strong signaling systems (Droge, 2002, Ray et al., 2012). The intimate participation of ROS on the mitochondrial oxidative environment, where mitochondria are the origin of most of the ROS production and most mitochondrial proteins depend on ROS response (Park et al., 2011), recently became more attractive, especially for cysteine-related protein systems (Mailloux et al., 2013). However, ROS can also be generated by other processes in other locations such as by the NOX family of enzymes (Gough and Cotter, 2011, Babior et al., 2002, Chen et al., 2008, Block and Gorin, 2012, Bedard and Krause, 2007) and the roles of ROS signaling may be exclusive to certain cellular locations. The redox spatial localisation

[1] The results of this chapter have been published on the journal of proteome research (on 18-08-2014) under the same title. Authors' contribution to that scientific paper was as following; KS, MR and JGZ generated the hypothesis; MR, KS and JGZ designed the experiments; NB, MC and MR performed the experiments; NB did the Maxquant analysis and the obtained tables were reviewed and checked by JGZ; JGZ and MR wrote the scientific paper manuscript.

within the eukaryotic cellular compartments may participate in the control of ROS-related signaling (Go and Jones, 2008, Hansen et al., 2006).

The proteome of cellular organelles and their subcellular protein distribution are highly dynamic and affected by different conditions (Henke et al., 2011, Jung et al., 2013, Mulvey et al., 2013, Pinto et al., 2014, Qattan et al., 2012). Therefore, it is not surprising that the response of cells to ROS and oxidative stress may also influence the dynamics of the cell proteome. For example, under oxidative stress and ROS signaling, the Nrf2 protein becomes detached from the cytoplasmic-associated protein Keap1 and translocates to the nucleus to interact with the antioxidant response element (ARE) in the presence of phosphorylation signals and lipid peroxidation proteins (McMahon et al., 2003, McMahon et al., 2010, Zhu et al., 2008, Numazawa et al., 2003, Lee et al., 2014, Itoh et al., 1997). Nrf2 usually regulates antioxidants to control ROS levels, and Nrf2 activation depends on the oxidation state of cysteine residues (Kaspar et al., 2009, Bloom et al., 2002, Zhang and Hannink, 2003).

The need for a global, spatially-resolved monitoring system to address the changes in functional protein processes between various subcellular locations might help to understand cellular responses to specific conditions such as stress simulations caused by the use of mild tert-butyl peroxide (TBP) treatment. Thus, it was postulated that protein trafficking between subcellular compartments might be sensitive to oxidative stress.

3.2 Results

In this study, the intracellular protein translocation/abundance oxidative stress response of human diploid fibroblast IMR90 cells has been analysed by using high-throughput proteomics subcellular spatial razor experiments (Mulvey et al., 2013, Pinto et al., 2014).

The experimental workflow is outlined in Figure 1-10. Three data sets with their replicates were obtained: (1) nucleus-enriched protein sample (N), (2) the nucleus-depleted (cytoplasm) sample (C), and (3) a total protein sample (T). The corresponding SILAC ratios (H/L) were afforded measures for each protein of the general change in total (S_t), or of the localised change in protein abundance in the nucleus (S_n) or cytoplasm (S_c).

3.2.1 The Cellular Response to the Treatment

The TBP amount was optimised by applying increasing concentrations of TBP to IMR90 cells. Microscopic pictures show the response of IMR90 cells to different concentrations of TBP: 0, 12, 25, 50, 100 and 200μM (Figure 3-1). The highest dose of 200μM of TBP appeared to reduce the cell number compared to the control. The lowest dose of 12μM of TBP showed no effect on the number of cells. Concentrations between 50μM and 100μM did not show a severe reduction in cell numbers compared with high dosages, or the cell numbers were not changed to the levels seen in low dosages.

Analysis of cell distribution in different phases of the cell cycle revealed that at 50μM, 75μM and 100μM of TBP, oxidative stress caused arrest and accumulation of IMR90 cells in both G1 phase (57, 42 and 49%), G2/M phase (37, 53 and 44%) and very small S phase peak (6, 5 and 7%), respectively, with no sub-G1 peak for the dead cells compared to the control (Figure 3-2).

3.2.2 Western Blotting for the Oxidative Stress Associated Proteins

The TBP effect was also checked by the use of western blotting techniques. Antibodies for antioxidant proteins SOD1, GPX1, catalase, tumour suppressor protein p53 and cell division cycle 7 protein Cdc7 were tested. The WB showed that there was a change in all of these proteins compared to the control (Figure 3-3A).

Fractionating the cells into nuclear and cytoplasmic fractions, and applying WB for the antibodies Nrf2 and Keap1 with each fraction, showed that Nrf2 appeared to translocate from the cytoplasm to the nucleus and was firmly presented on the nuclear fraction under oxidative stress; in contrast, the inhibitor Keap1 appeared pale and degraded in the treated cytoplasmic fraction compared to the control (Figure 3-3B).

To obtain nuclear and cytoplasmic fractions, different nuclear fractionation buffers were used. The subcellular fractionation protocol was optimised by the use of the previously identified nuclear marker 'Lamin A/C' and the cytosolic marker 'Tubulin'; the fractionations for each sample were tested for nuclear leakage by the use of MS (for results see Appendix 1 in attached CD).

The protocol which showed the best organelle separation was chosen for the final experiment, that is, the one which gave the minimal amount of Lamin in the IMR90 cytosolic fraction and the minimal amount of Tubulin in the nuclear fraction. In the fractionation samples used for the study, the recorded cytoplasm/nucleus MS intensity ratio for Lamin A/C fluctuated between 0.2 and 0.8% for the three replicates; that is, for IMR90 cells, there was negligible nuclear leakage during the fractionation process and this did not significantly affect the measured SILAC ratios ($1.185 \leq Sn \leq 1.197$, $0.964 \leq Sc \leq 1.009$ for Lamin A/C over the three replicates).

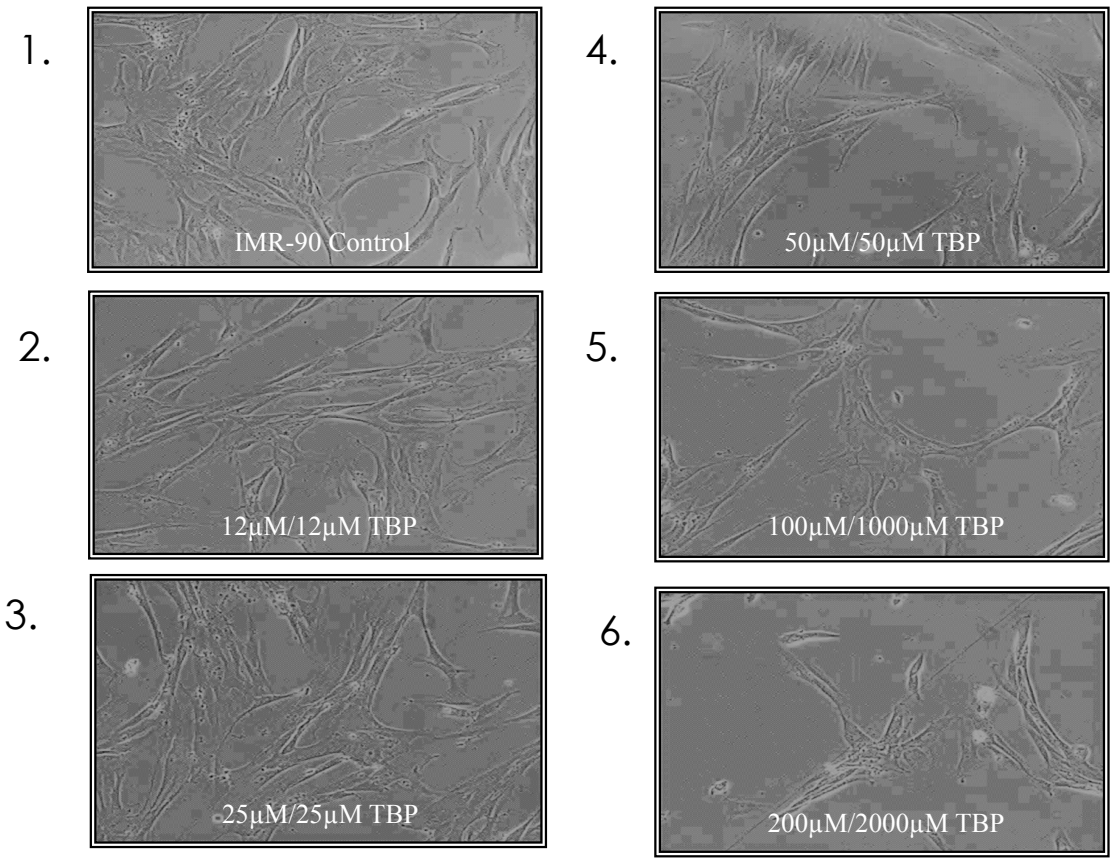

Figure 3-1. IMR90 Cells with Different Dosages of TBP. Numbers of IMR90 cells appeared to vary under the light microscope after using different concentrations of TBP: 0μM, 12μM, 25μM, 50μM, 100μM and 200μM.

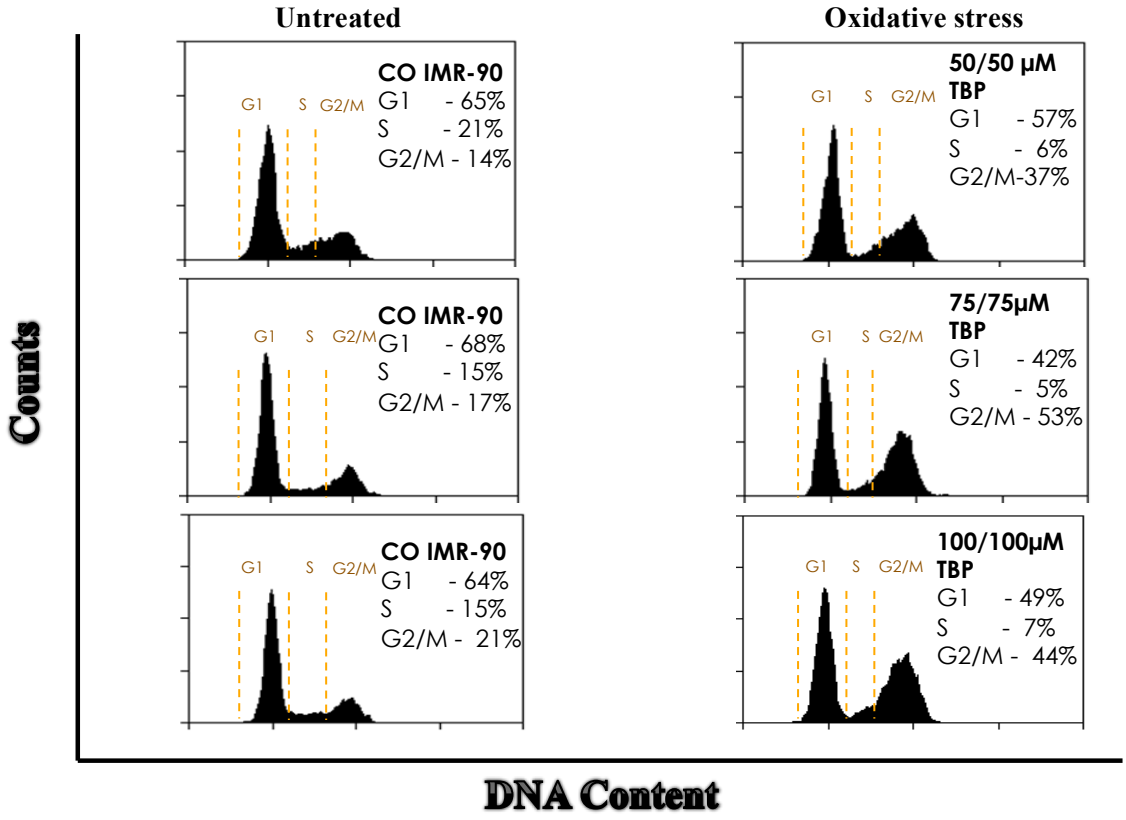

Figure 3-2. FACS Analysis for the Distribution of IMR90 Cells over the Cell Cycle Phases. The cell cycle analysis of the nominated concentrations 50µM, 75µM and 100µM showed accumulation of the cells in the G1 phase (57, 42 and 49%) and G2/M phase (37, 53 and 44%), respectively, with very small S phase peaks (6, 5 and 7%) compared to the control and no sub-G1 peaks at all.

A.

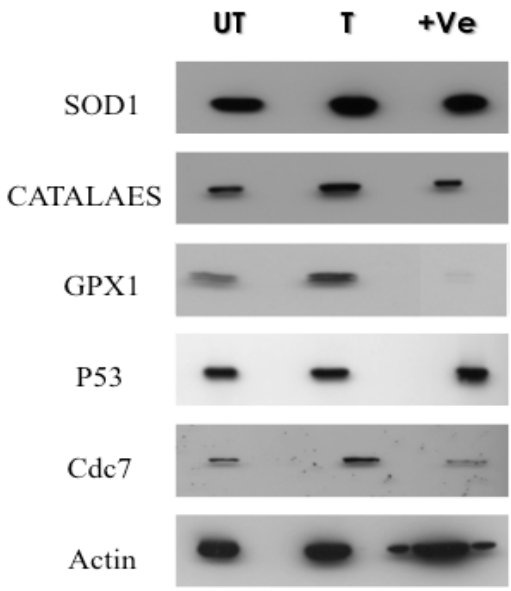

B.

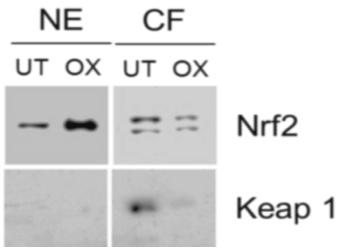

Figure 3-3. Immunoblotting for the Oxidative Stress associated Proteins. A. The antioxidant proteins SOD1, Catalase and GPX1 levels were changed after cells were treated with TBP. Also, p53 and Cdc7 accumulated in the treated cells (T) compared to the untreated ones (UT). Actin was used as a loading control while the breast cancer (MCF7) cell lines were used as positive (+Ve) control for the antibodies. **B.** Translocation of Nrf2 & degradation of Keap1 under mild oxidative stress within the IMR90 cells. The stability of the Nrf2 protein and down-regulation of the Keap1 protein between the cytoplasmic fraction (CF) and nuclear extract (NE) in treated IMR90 cells (OX) in comparison to untreated cells (UT) were easily differentiated in both populations.

3.2.3 Characterisation of the MS data

Three biological replicates were obtained for each fractionated sample (S_n, S_c and S_t) and were subjected to MS. The reproducibility of the sample preparations was verified. The data showed that there was a high correlation between each fraction replicate ($0.75 < R^2 < 0.88$), with the presence of a handful of outliers with some SILAC counts (Figure 3-4).

The MaxQuant software package (Cox and Mann, 2008, Cox et al., 2009) was used to identify proteins and determine SILAC ratios for 12 data sets: (1) each nucleus (N) sample replicate and the union of the three N samples, (2) each cytoplasm (C) sample replicate and the union of the three C samples, and (3) each C&N replicate and the union of the three C&N samples. C&N indicates that for each individual replicate, the MS data for the C and N samples were jointly processed with MaxQuant to estimate changes in total protein abundance (T). The analysis revealed that from 3589 independent consensus proteins, 1929 were detected in the C and 2751 proteins were detected in the N. The protein distribution over the nucleus and cytoplasm is shown in Figure 3-5A: 783 proteins were detected only in the cytoplasm, 1605 proteins only in the nucleus and 1146 were detected in both locations. A further 35 proteins were detected only in T. Among the C and N proteins, there were many proteins with a large number of sequenced peptides/ratio counts, which further validated the subcellular fractionation efficiency and showed that there were many proteins characteristic of one or other of the locations. With at least 2 peptides (1 unique) and 3 ratio counts in a single sample, SILAC ratios were obtained for 1658 cytoplasmic proteins (S_c), 2503 nuclear proteins (S_n), 3199 total proteins (S_t) and 981 proteins were obtained in all three fractions (S_c, S_n, S_t) (Supplementary Table 1, external CD).

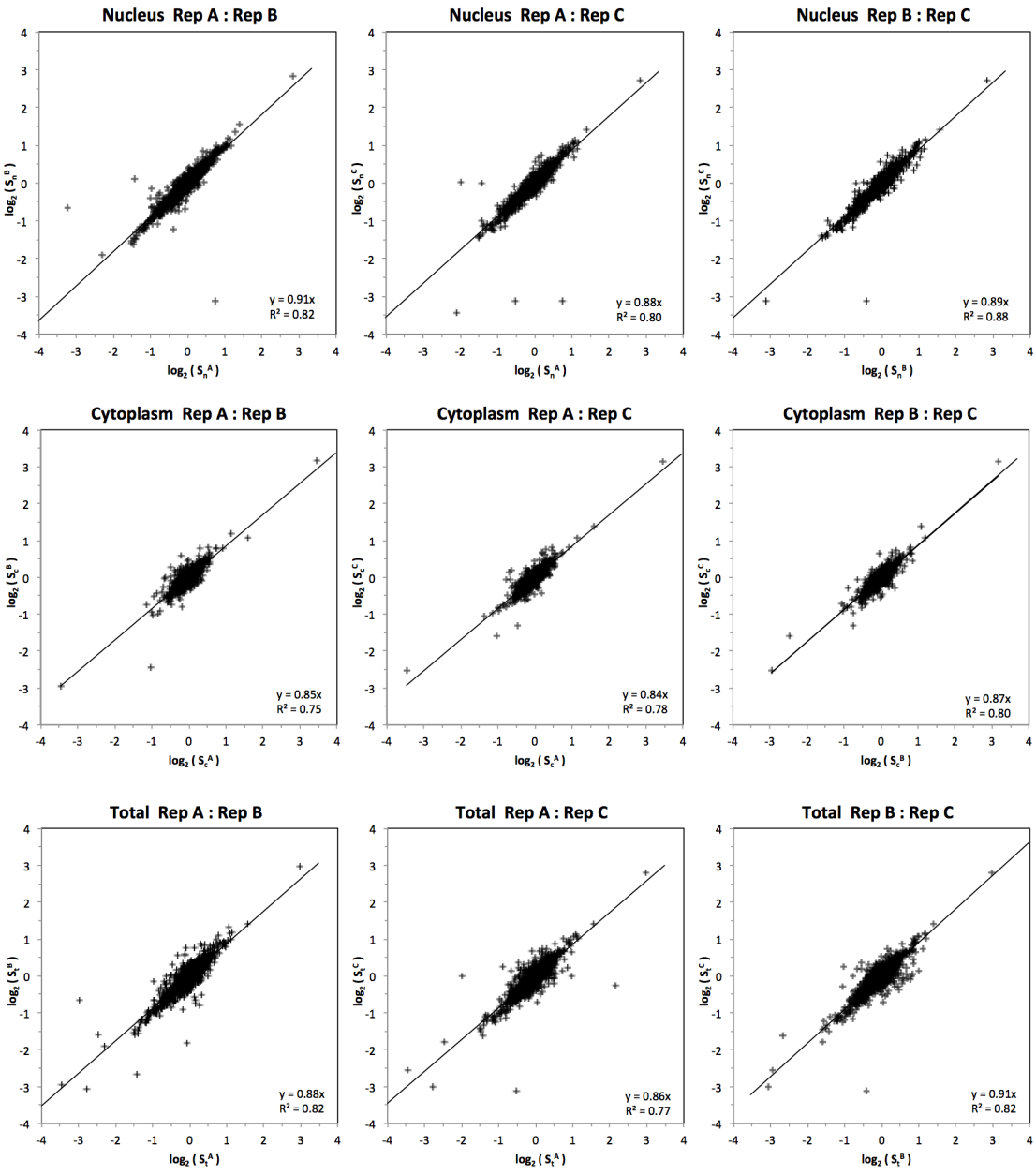

Figure 3-4. Correlation of SILAC Ratios between Three Replicates for the Nucleus, Cytoplasm and Total samples. All proteins with ≥ 3 ratio counts were included in the calculation of correlation. There is a strong correlation between replicates, even in the presence of a handful outliers of low MS recorded intensity.

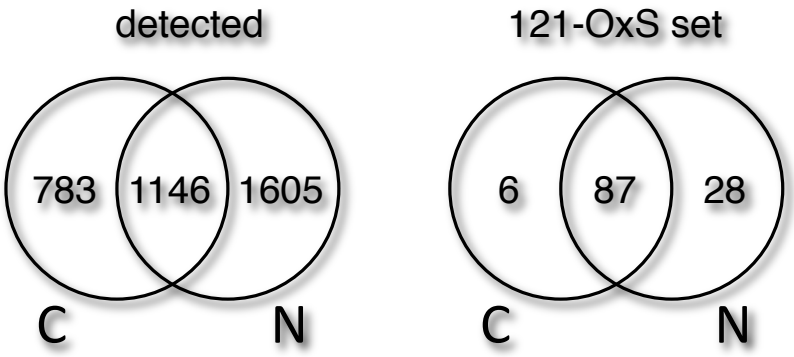

A. **B.**

Figure 3-5. Venn Diagrams for Protein Distribution over the Nucleus and Cytoplasm. A. Total number of detected proteins. From a total of 1929 C proteins and 2751 N proteins, only 783 proteins were present in the cytoplasm and 1605 proteins only in the nucleus, with 1146 proteins found in both. **B.** Significant compartmental abundance protein. From 121 significant (SigB) detected proteins: 6 were found only in C, 28 in N and 87 were present in both.

Protein ratios were normalized ($\log_2$ SILAC) in MaxQuant for each data set by the use of an algorithm within the Perseus program to calculate an outlier probability score (Significance B score, hereafter SigB) (Cox and Mann 2008, Cox, Matic et al. 2009). Also, the parameter $\log_2 (S_n/S_c)$, which aims to detect redistribution between C and N, was accompanied with SigB to find the most significant proteins. It was found that, for each of the 12 data sets, there were 121 significant proteins (121-OxS): 6 proteins only in C, 28 only in N, and 87 proteins were found in both (Figure 3-5B). These 121 significant proteins accounted for around 3.4% of all of the identified proteins and consisted of the changed proteins in S_n, S_c, S_t and/or the redistributed proteins between the nucleus and cytoplasm S_n/S_c under oxidative stress. With the rigorous selection of significant proteins: a minimum of 9 ratio counts (in a single sample type) and a median of 120 ratio counts per protein were used to classify the proteins within the 121-OxS set. It was found that there were 19 highly significant proteins in (S_c), 63 proteins in (S_n), 76 proteins in (S_t) and 43 proteins in (S_n/S_c) (Supplementary Table 2, external CD).

3.2.4 Overlook of the High Enrichment Nucleus Sample

There is growing evidence that some proteins have more than one subcellular location and may show different cellular functions in each location (see Discussion). The cellular component annotations (GO CC) for many proteins that were quantified in the nucleus sample N showed that proteins were annotated to other subcellular locations (Supplementary Table 1, external CD). For example, there were 371 proteins present within the nucleus sample and annotated to the mitochondria with 147 of them being located in the nucleus as well. Also, around 208 proteins were assigned to the endoplasmic reticulum as well, and there were other proteins ascribed to other

subcellular locations and present within the nuclear sample (Figure 3-6A and GO CC in Supplementary Table 1, external CD).

To ensure that the 121-OxS set was not contaminated with other subcellular organelle proteins, the distribution of the functional SILAC ratio of the nucleus to total SILAC ratio S_n/S_t, which is mathematically equal to the nuclear fraction stimulated to the nuclear fraction unstimulated ($S_n/S_t = f_s/f_u$), was measured (Figure 3-6, 3-7). It showed that the ratio of S_n/S_t was equal to 1 for most annotated proteins to mitochondria or to the other organelles, which means that there is no notable change in the nuclear fraction in response to oxidative stress. Only a small number of proteins such as HK1 and BAX were found to exhibit changes in the f_s/f_u ratio. In contrast, in total abundance, these proteins showed no or small changes (HK1 S_t = 1.14, and BAX S_t = 1.04). For further validation, the high abundance proteins that were present in the nucleus sample were investigated. It has been found that large numbers of these proteins, which were present in the nucleus sample with high subcellular fractionation reproducibility and very minor cross contamination from the other organelles, showed no change in measured f_s/f_u (Figure 3-6B). For example, prohibitin (PHB), which is annotated to several cellular functions such as apoptosis, cell differentiation and proliferation with known function in the organelles, nucleus, mitochondria and the plasma membrane, was a highly abundant protein in the nuclear fraction that is annotated to the mitochondria with no change in f_s/f_u and $log_2 (f_s/f_u) = 0.009$.

A.

Proteins detected in nucleus with annotation to other sites

GO annotation		quantified in nucleus	$\lvert\log_2(S_n/S_t)\rvert > 0.5$
mitochondrion	(M)	371	12
endoplasmic reticulum	(ER)	208	13
Golgi apparatus	(G)	187	13
plasma membrane	(P)	303	22
extracellular	(E)	102	3
endosome	(En)	66	9
lysosome	(L)	29	4
peroxisome	(Pe)	25	3

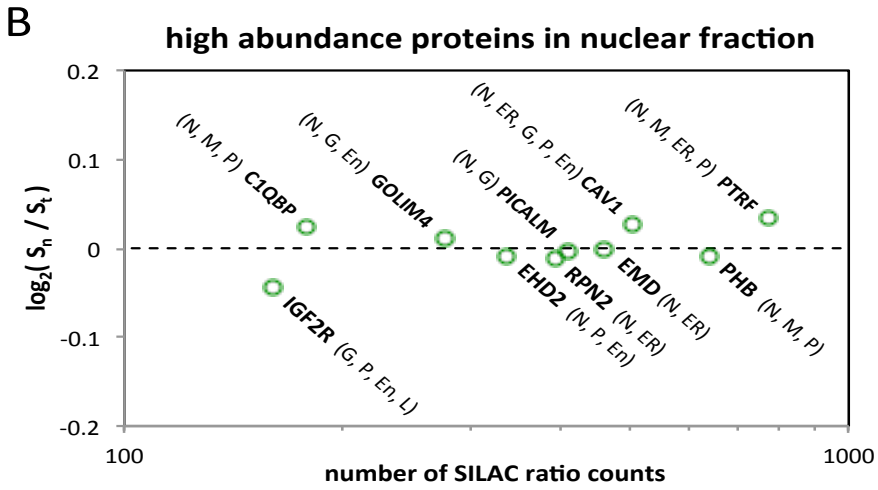

Figure 3-6. Analysis of the Enrichment of the Nuclear Fraction. A. The table illustrates the number of quantified proteins in the nuclear fraction annotated to other subcellular sites with significant changes in their nuclear fraction ($f_s/f_u = S_n/S_t$). **B.** Log_2 (S_n/S_t) for selected high abundance proteins to number of SILAC ratio counts includes that at least 50 nucleus proteins have GO CC annotation for multiple subcellular locations.

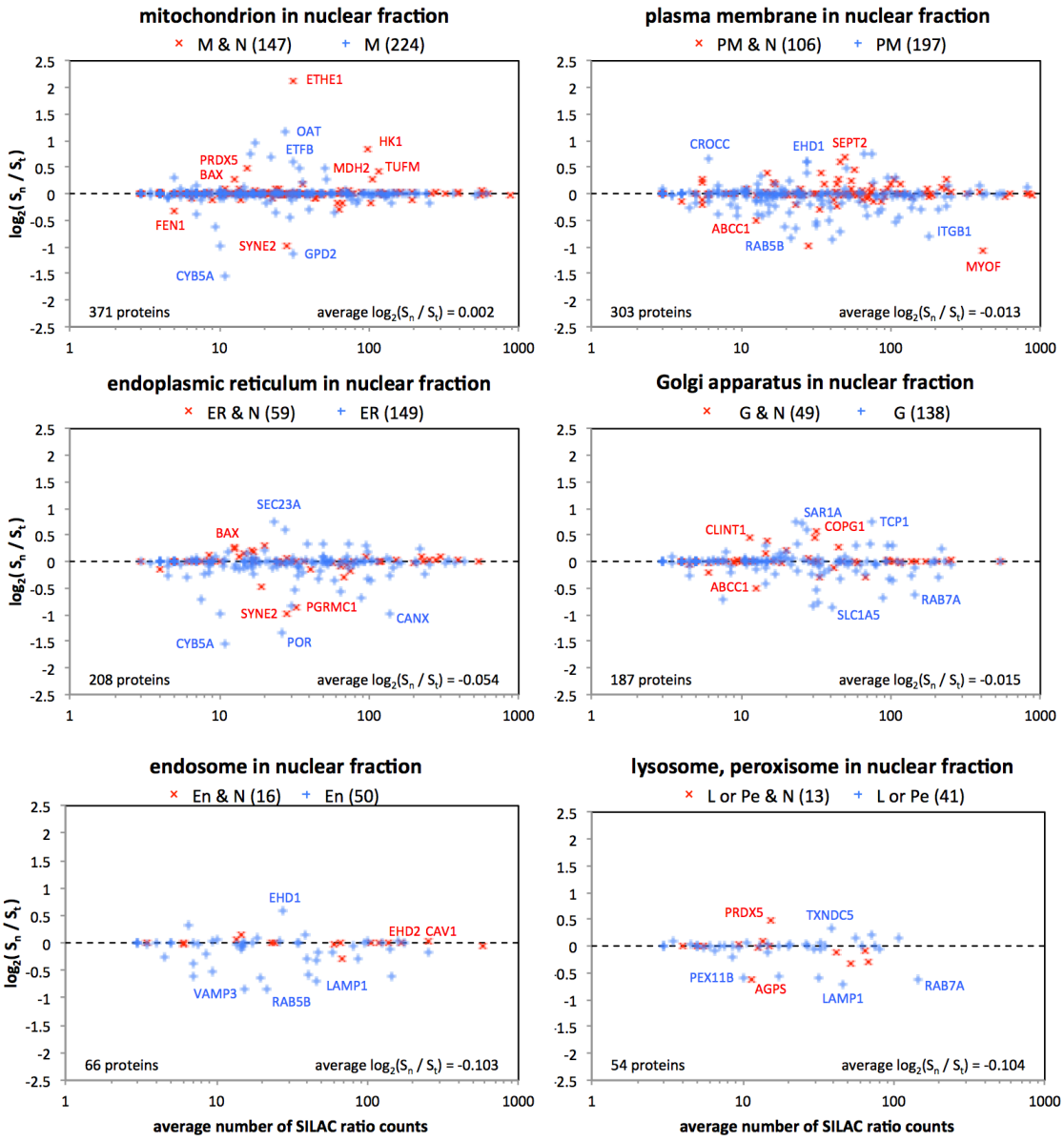

Figure 3-7. Proteins Detected in Nucleus with Annotation to other Organelles Subcellular Locations. Plots of $\log_2(S_n/S_t)$ to the average number of SILAC ratio counts over the nucleus and total data sets for proteins with GO CC annotation to the indicated subcellular organelles. For each of the subcellular organelles, the set of proteins was divided into two groups: those annotated to the location and the nucleus (red data points); and, those annotated to the location, but not to the nucleus (blue data points).

3.2.5 Correlation of Changes in Abundance and Nucleus/Cytoplasmic Distribution

Correction for the enrichment of nuclear proteins in the MS data analysis was obtained during the estimation of total protein abundance (S_t). The measurement and correction of S_t value is important to increase the number of proteins as much as possible to analyse subcellular redistribution and also to normalise the distribution plane.

It was estimated using the following equation:

$$S_t = S_t^* \left\{ \frac{\left(\frac{S_n}{S_t^*}-1\right)+\left(1-\frac{S_c}{S_t^*}\right)}{r\left(\frac{S_n}{S_t^*}-1\right)+\left(1-\frac{S_c}{S_t^*}\right)} \right\} \left\{ \frac{r\frac{S_c}{S_n}\left(\frac{S_n}{S_t^*}-1\right)+\left(1-\frac{S_c}{S_t^*}\right)}{\frac{S_c}{S_n}\left(\frac{S_n}{S_t^*}-1\right)+\left(1-\frac{S_c}{S_t^*}\right)} \right\}$$

When each given value was based on the spatial razor model (see introduction) and r was the nuclear enrichment factor these were calculated as follows: 60 µg of nuclear/cytoplasmic proteins was used for the MS analysis of each biological replicate, the fractionation gave about 250/1450 µg of nuclear/total proteins, which were effective enrichment for the nuclear proteins by r = 5.8-fold during the MS analyses. The S_t^*, which was the corrected value of S_t was found to be equal to (r $A_{n,s}$ + $A_{c,s}$)/ (r $A_{n,u}$ + $A_{c,u}$). The calculations showed that only small protein amounts were modified appreciably by correction for nuclear protein enrichment, with only 22 OxS proteins showing less than 10% variation between S_t and S_t^* (Figure 3-8).

Protein redistribution to/from the nucleus was directly measured by the following equation: $S_n/S_c = f_s(1-f_u)/f_u(1-f_s)$; when: $f_u = (S_t-S_c)$ and $f_s = S_n(S_t-S_c)/S_t(S_n-S_c)$ (see introduction). Next, 87 significant proteins from the 121-OxS set in the nucleus and cytoplasm (Supplementary Table 2, external CD) were tested to find a correlation between the changes in total abundance (S_t) and changes in the nucleus-cytoplasm distribution (S_n/S_c). It showed that there was a very small correlation because changes in

compartmental abundances were not reflected by the changes in total protein abundance (Figure 3-9A).

The orthogonal 3D spatial razor plot for S_n/S_t, S_c/S_t and S_t was used to characterise the response of these significant proteins to oxidative stress. The subcellular spatial razor basis set reflects the alterations in the total protein abundance along an S_t axis with changes in the nucleus/cytoplasm distribution in an (S_n/S_t, S_c/S_t) distribution plan, which is different from total abundance (Mulvey et al., 2013, Pinto et al., 2014).

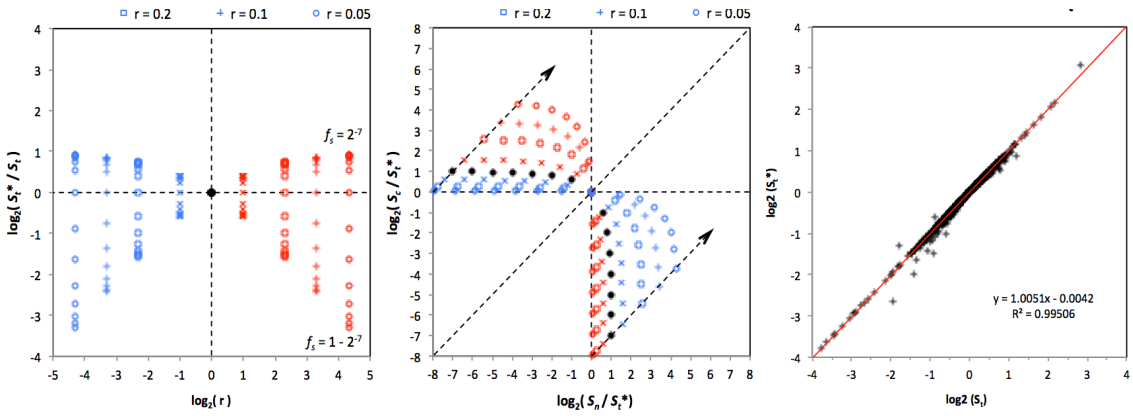

Figure 3-8. Effects of Nuclear Enrichment during MS data Collection on Values of S_t and on the Estimation of basal Nucleo-Cytoplasmic distribution. A. Variation of (S_t^*/S_t) for different values of the nuclear enrichment factor r with unstimulated nuclear fraction fu = 0.5 and variation of the stimulated nuclear fraction f_s over the range $f_s = 2^{-7}$ -> 0.5 -> $1 - 2^{-7}$ in steps of 2^{-n}. **B.** Variation in the subcellular distribution plane. **C.** Correlation between corrected (St) and uncorrected (S_t^*) changes in total abundance for the experimental MS data for the treatment of IMR90 cells with TBP.

To maintain the mass while using this distribution plan, it was obligatory for the protein points to appear in the two allowed quadrants that corresponded to N → C and C → N redistribution, respectively (Figures 3-9 B and C).

The 3D razor model was affected by three variations: changes in total abundance, compartmental protein redistribution between the nucleus and the cytoplasm in stimulated cells and the original nuclear/cytoplasm distribution in unstimulated cells. For example, the 3D razor model for 121-OxS protein data set reveals that, under classic oxidative stress, proteins such as light and heavy ferritin subunits (FTL, FTH1) showed a significant increase in total abundance with little or no C ←→ N redistribution, while the seven units of the protein-folding complex CCT showed no or slight changes in total abundance; however, there were significant changes in C → N redistribution. Proliferation cell nuclear antigen (PCNA) was redistributed from N → C with little or no changes in total protein abundance. The $\log_2 (S_c/S_t)$ for both CCT and PCNA proteins were equal to 0, which meant that the basal abundance of these proteins was clearly deviated to the cytoplasm. Also, under oxidative stress, only a small amount of CCT proteins was increased in the nucleus and a small amount of PCNA was moved to the cytoplasm. ETHE1 protein was also skewed to the cytoplasm in the basal abundance, but with a substantial decrease in total abundance and C → N redistribution (Figure 18C). Alternatively, the nucleoside diphosphate kinase A (NME1) protein had weaker skewing in basal abundance, no changes in total abundance, was redistributed from C → N, and might represent a more general "balancing" of function between different subcellular locations.

In contrast, other proteins such as ATP synthase six subunits (ATP5) appeared to show changes between total abundance and subcellular distribution. It has been found to present a 2-fold decrease in total abundance and was redistributed from N → C; basal abundance was skewed to the nucleus, which means that these proteins were more

depleted in the nucleus. Also, V-type proteins ATPase (ATP6) were skewed to the nucleus, showing a 1.8-fold increase in total abundance and C→ N redistribution.

The 87 most significant protein distributions (Supplementary Table 2, external CD) between nucleus S_n, cytoplasm S_c and nucleus-cytoplasm distribution S_n/S_c are summarised in Figure 3-10 and published in (Baqader et al., 2014). Figure 3-10 shows the significantly increased/decreased changes in protein abundance and their translocation between the nucleus and the cytoplasm. By extracting GO ontology terms from Supplementary Table 2 of the121-OxS set, Figure 3-10 illustrates the shared functional processes for each protein group. For example, cell differentiation included proteins that were also annotated in ATP synthesis, lipid metabolism, haem/iron metabolism, the negative regulation of apoptosis, cell adhesion, proline regulatory axis and protein transport.

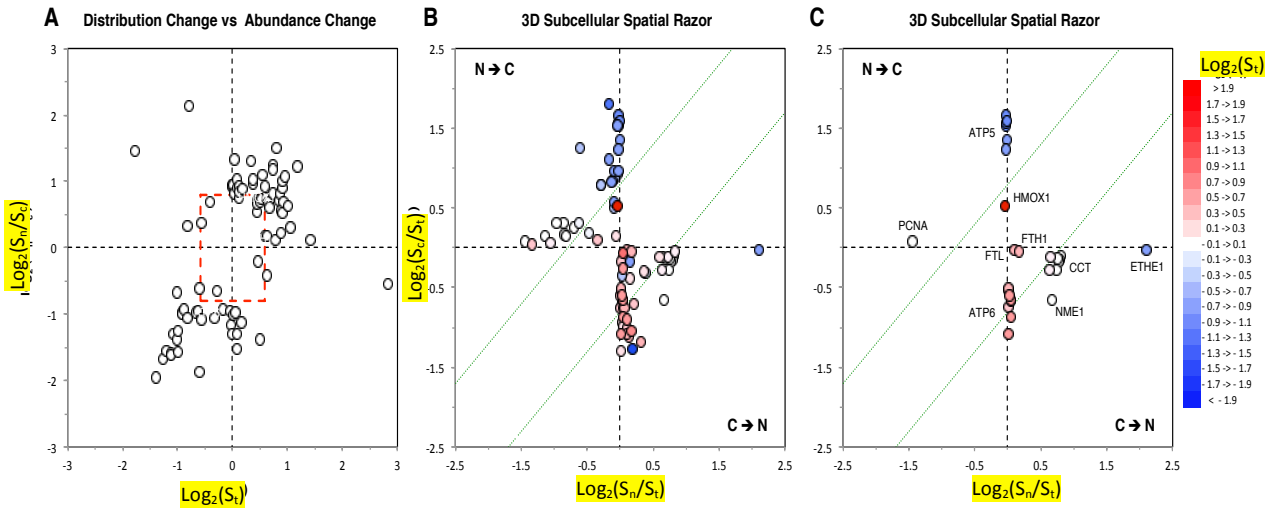

Figure 3-9. Subcellular Characterisation of the 87 Proteins of the 121-OxS set for which S_n, S_c and S_t were all measured. A. Plot of changes in nuclear-cytoplasmic distribution (S_n/S_c) versus changes in total abundance (S_t). The red bounding box corresponds to 1.5-fold changes in total abundance and $0.57 > S_n/S_c > 1.74$ ($|\log_2(S_n/S_c)| > 0.9$). A few proteins appear just inside the red boundaries because the combinations of basal distribution, changes in total abundance and changes in distribution can lead to individual compartmental abundances (S_n or S_c) being selected as significant. **B.** The 3D spatial razor plot for the 87 proteins. The dotted green lines correspond to the bound $|\log_2(S_n/S_c)| = 0.8$. Changes in total abundance (vertical dotes) are colour-coded according to the scale on the right. **C.** As for plot B, 3D spatial razor plot for selected, labelled proteins or protein complexes. Figure were designed by JGZ and published in (Baqader et al., 2014).

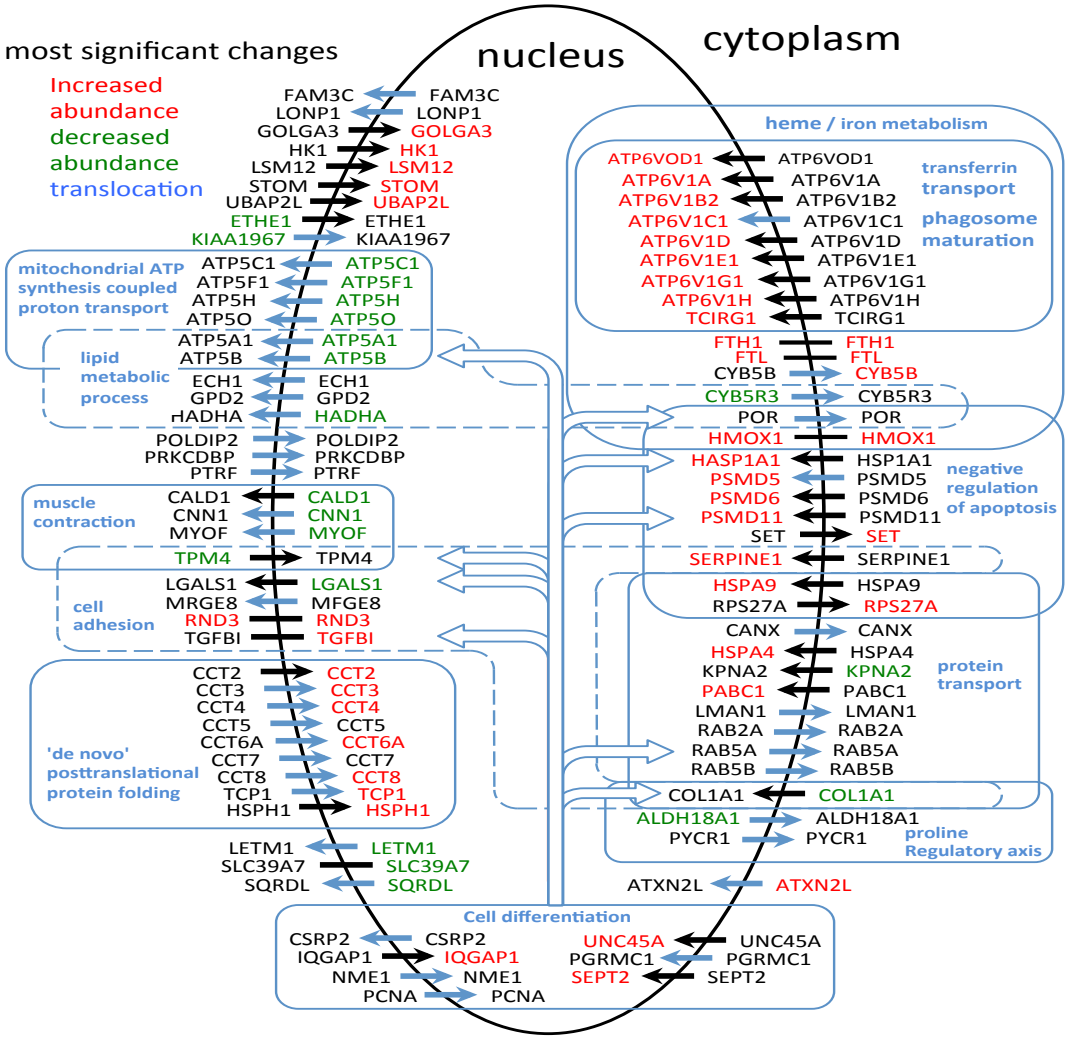

Figure 3-10. Visual Summary of the most Significant Changes in Protein Abundance and Distribution that were Quantified in the 121-OxS data set in both Nuclear and Cytoplasmic Compartments. The GO terms for biological processes were annotated to the proteins (for more details see GO BP in Supplementary Table 2, external CD). Proteins labelled with (red) mean proteins were significantly increased in abundance either in nucleus or cytoplasm, while proteins labelled with (green) mean proteins were significantly decreased in abundance due to the oxidative stress. Arrows in (blue) represent the proteins translocation between nucleus/cytoplasm, while (black →) arrows denotes no translocation in response to oxidative stress. Arrows in black without sharp edges (−) mean there is no evidence for their translocation. Figure was designed by JGZ and published in (Baqader et al., 2014).

3.2.6 Validation of Translocation for Selected Proteins

To validate several aspects of MS analysis in response to oxidative stress in order to check for the presence of some proteins in locations that are different to their original ones and to investigate the intact of subcellular organelles under various treatments, fluorescence imaging was used for validation of the results. First, to ensure that oxidative stress was mild and did not destroy the cellular morphology, images of the mitochondria and nucleus were taken. In comparison to the control, the stimulated IMR90 cells appeared intact and normal, with no alterations in mitochondria or breakage in nucleus structure (Figure 3-11A). Second, there were several groups of significant proteins that are well known to be present in specific locations that were found in the nucleus fraction. These groups included proteins such as ATP5 synthase subunits, which are known to play a role in the mitochondrial respiratory chain. ATP5A1 protein distribution within the intact nucleus under oxidative stress was investigated. It has been found that, in both stimulated and unstimulated IMR90 cells, ATP5A1 was widely distributed over the different subcellular locations such as the nucleus and mitochondria and generally was distributed over the cell (Figure 3-11B). Moreover, the GO CC for ATP5A1 was found to annotate this protein to nucleus, mitochondria, plasma membrane and the extracellular region. Another protein that was also checked was Delta-1-pyrroline-5-carboxylate synthase (ALDH18A1). ALDH18A1 is a main proline regulatory axis protein that was found in the 121-OxS data set with a 2-fold decrease in nucleus abundance under oxidative stress. Although the confocal images (Figure 3-11C) showed that the protein was redistributed from the mitochondria to the cytoplasm under oxidative stress, trace amounts of the protein were present within the nucleus in both control and treated cells. Also, ALDH18A1 seemed to be more condensed under oxidative stress. The GO annotation for this protein also showed

that ALDH18A1 was annotated to the cytoplasm, plasma membrane and mitochondrial membrane.

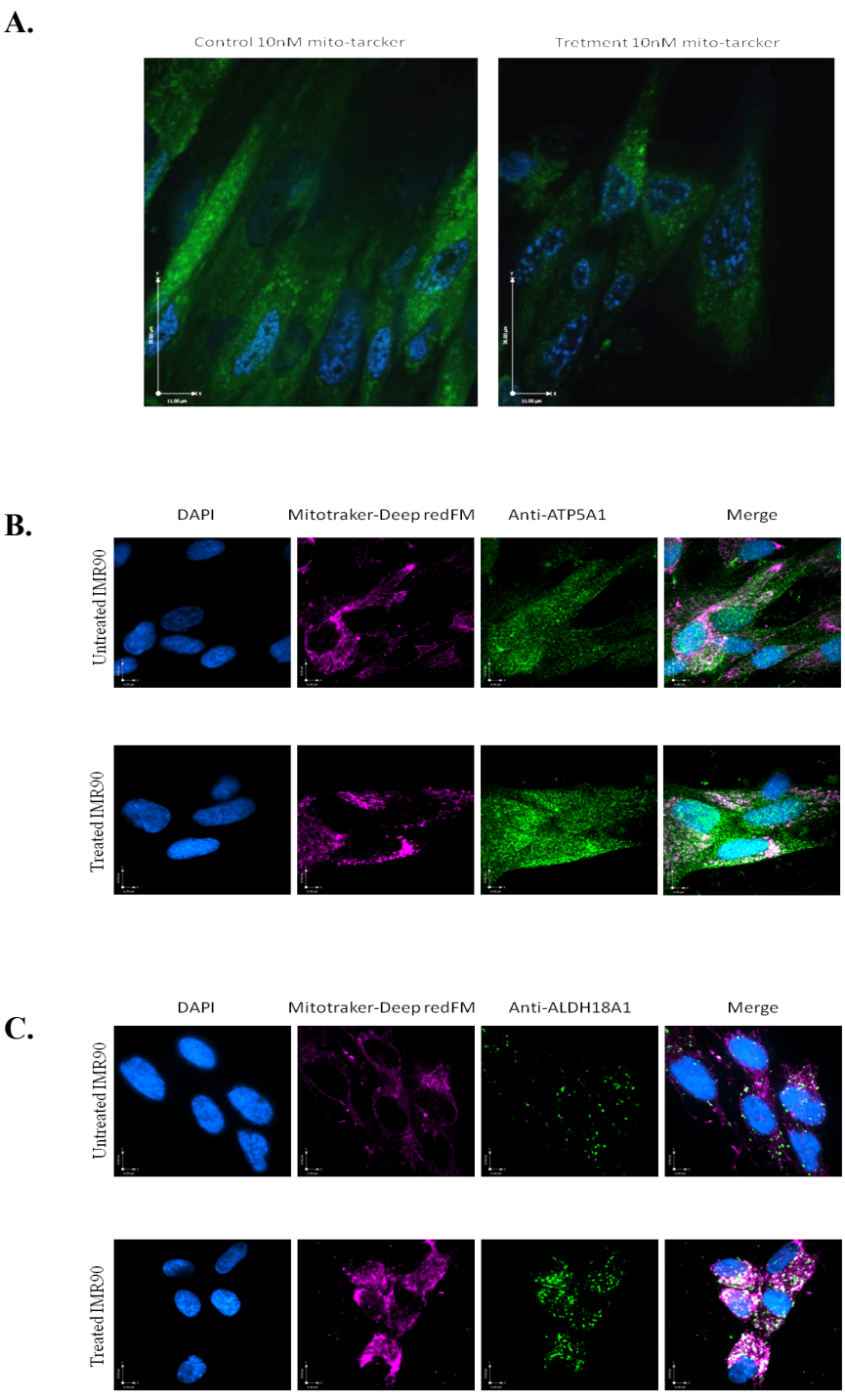

Figure 3-11. Validation of MS result with Fluorescence Imaging. A. The use of Mito-tracker (green) for the mitochondria and Hoechst 33342 (blue) for the nucleus to check the intact cellular morphology under conditions of oxidative stress. In both control and treatment conditions, cells appear intact, with no breakage in the nucleus or changes in the mitochondria. **B & C.** Confirmation of selected proteins ATP5A1 and ALDH18A1 by using fluorescence confocal microscopy. To verify the MS results in response to oxidative stress, two of the most significant mitochondrial proteins were shown to redistribute between the nucleus and cytoplasm data sets under oxidative stress; changes in the nucleus of the intact IMR90 were selected. Nuclei (DAPI blue), mitochondria (Mito-tacker red) and applied antibodies (green) to target proteins of interest for both treated and untreated cells were used. The secondary antibody for both primary antibodies was FITC. The fluorescence imaging of ALDH18A1 and ATP5A1 showed similar staining pattern that is already known in the literature. **B.** ATP5A1 appears to be widely distributed over nucleus, mitochondria and even the cytoplasm in both treatment and control populations. **C.** ALDH18A1 was similar to ATP5A1; however, after oxidative stress, the proteins seemed to become more concentrated and condensed compared to the control.

In Table 3-1, the GO term for cellular component GO CC was also used to validate the annotation of the 121-OxS set proteins. Table 3-1 shows that there were 117 proteins annotated to several locations; each protein seemed to share at least 3 locations, with the maximum being 8 locations. For example, 45 proteins were annotated to the nucleus and with 31 proteins to the cytoplasm, 18 proteins to the extracellular region and 9 proteins also to the plasma membrane. In the cytoplasm, of the 64 proteins, 34 were annotated to the cytosol with 13 in the mitochondria. However, GO CC seemed to underestimate the protein scattering over the different subcellular locations by annotating 10 of the shared proteins between nucleus and cytoplasm only to the nucleus and 33 of the proteins that were quantified in nucleus and cytoplasm only to the cytoplasm.

subcellular location	nucleus	plasma membrane	extracellular region	cytoplasm	cytosol	cytoplasmic vesicle	mitochondrion	endoplasmic reticulum	Golgi apparatus	melanosome	peroxisome	endosome	lysosome
nucleus	45	9	18	31	19	6	7	8	5	2	0	3	1
plasma membrane		32	24	20	14	11	8	3	1	5	0	7	8
extracellular region			53	37	27	16	9	7	5	7	1	7	10
cytoplasm				64	34	12	13	11	7	7	0	7	10
cytosol					43	6	9	8	2	3	0	4	8
cytoplasmic vesicle						18	1	3	4	3	0	7	4
mitochondrion							41	4	0	0	1	2	3
endoplasmic reticulum								16	3	2	0	1	2
Golgi apparatus									10	2	0	1	1
melanosome										8	0	3	2
peroxisome											1	0	0
endosome												8	4
lysosome													11
GO CC ID	GO:0005634	GO:0005886	GO:0005576	GO:0005737	GO:0005829	GO:0031410	GO:0005739	GO:0005783	GO:0005794	GO:0042470	GO:0005777	GO:0005768	GO:0005764

Table 3-1. Distribution of GO CC Annotations for the 121-OxS Proteins set Over the Subcellular Locations (Baqader, Radulovic et al. 2014).

3.2.7 Functional Network Analysis

The 121-OxS proteins set were inserted in the STRING programme for functional network analysis and visualised by Cytoscape. Interactions were investigated for three data sets: the 121-OxS; 240-OxS set that contained an additional 119 STRING suggested white nodes; and 173-OxS set that contained the 121-OxS set plus 52 nodes of the 119 white nodes which were quantified in the experiments but were not significant in the MS data. The MCODE clustering algorithm was also used with these data to identify clusters of nodes with dense interactions (see materials and methods).

GO BP enrichments were calculated by BiNGO (Maere et al., 2005) and the functions associated with protein clusters were identified by DAVID (Huang da et al., 2008).

The initial investigation of the 121-OxS by STRING was represented by a connection between the protein clusters even in the presence of some disconnected proteins (Figure 3-12). The clusters of connected proteins included ATPases, proline regulatory axis and CCT complex. However, there were some dots that appeared weakly connected or disconnected. For example, classic oxidative stress proteins FTL, FTH1 and HMOX1 appeared weakly connected by STRING. There were around 49 significant proteins such as PGRMC1, which is known to be involved in haem binding, and HK1, which is an important enzyme for glucose phosphorylation; these both appeared disconnected.

For 121- 240- 173-OxS data analysis, Table 3-2 showed most of the proteins with GO biological functions that were annotated to. The 240-OxS data described the most likely main functional processes and the 173-OxS measured exactly how these functional processes were monitored in experimental data; the 121-OxS set reflected the pure probability which might be small if only a few proteins in the network were monitored in experimental data; the 121-OxS set reflected the pure probability which might be small if only a few proteins in the network were changed.

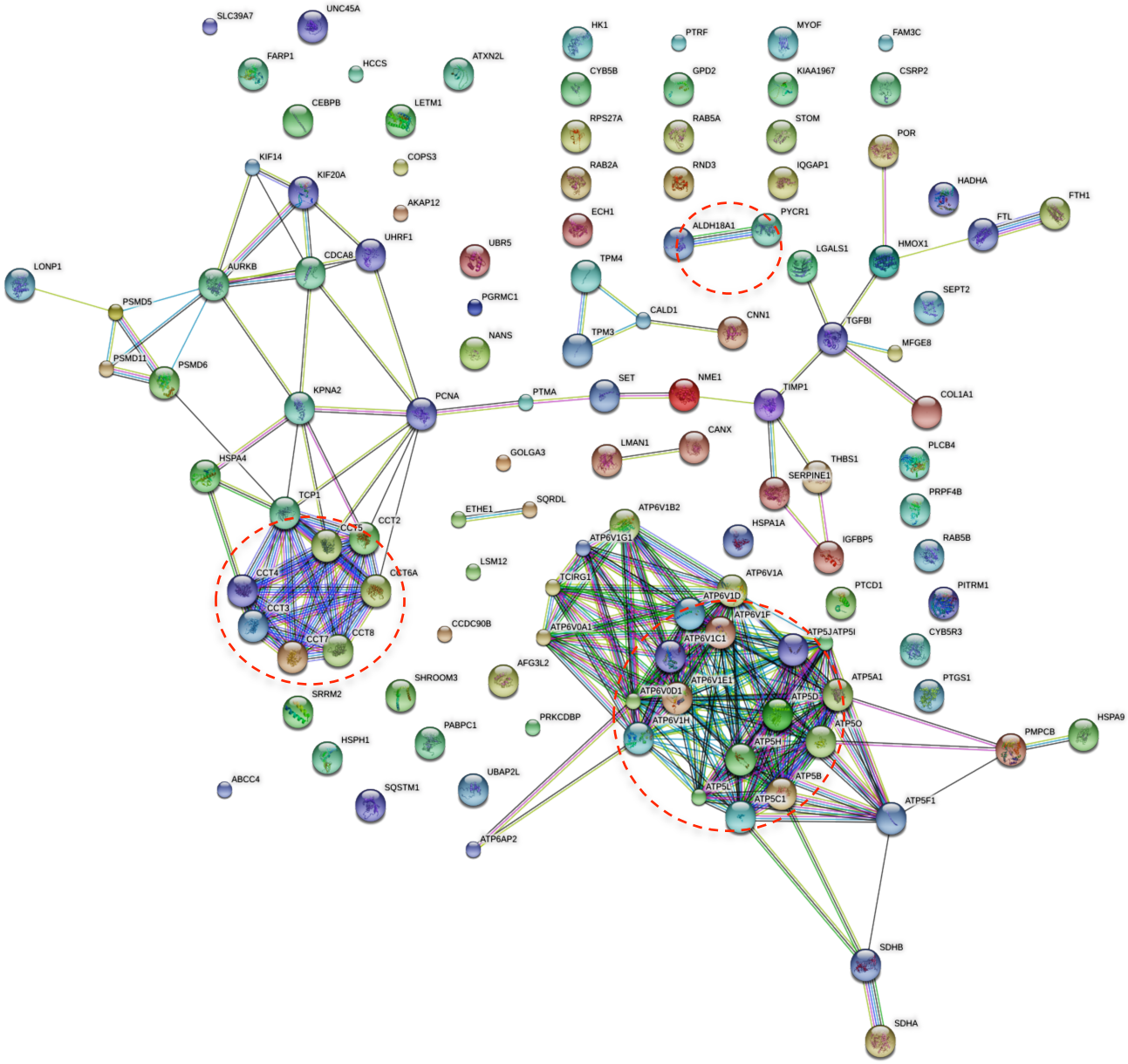

Figure 3-12. STRING Interaction Network Analysis for 121-OxS set. This shows clusters of connected proteins such ATPases, proline axis and CCT complex (red dashed circles).

Table 3-2. GO BP "Biological Process" term Associated with STRING Networks.

GO ID	GO Name	240-OxS[a]		173-OxS[b]		121-OxS[c]			Quantified[d]
		number genes	*p-value*[e]	*number genes*	*p-value*[e]	*number genes*	*p-value*[e]	*genes*	*number genes*
GO:0042776	mitochondrial ATP synthesis coupled proton transport	11	< 1.0E-17	10	1.20E-14	10	< 1.0E-17	ATP5A1, ATP5B, ATP5C1, ATP5D, ATP5F1, ATP5H, ATP5I, ATP5J, ATP5L, ATP5O	11
GO:0090382	phagosome maturation	11	3.05E-11	11	9.44E-13	11	7.11E-15	ATP6V0A1, ATP6V0D1, ATP6V1A, ATP6V1B2, ATP6V1C1, ATP6V1D, ATP6V1E1, ATP6V1F, ATP6V1G1, ATP6V1H, TCIRG1	16
GO:0033572	transferrin transport	11	2.71E-10	11	8.72E-12	11	6.83E-14	ATP6V0A1, ATP6V0D1, ATP6V1A, ATP6V1B2, ATP6V1C1, ATP6V1D, ATP6V1E1, ATP6V1F, ATP6V1G1, ATP6V1H, TCIRG1	18
GO:0008286	insulin receptor signaling pathway	13	1.53E-08	12	4.48E-09	11	5.32E-10	ATP6V0A1, ATP6V0D1, ATP6V1A, ATP6V1B2, ATP6V1C1, ATP6V1D, ATP6V1E1, ATP6V1F, ATP6V1G1, ATP6V1H, TCIRG1	32
GO:0055085	transmembrane transport	54	1.95E-10	45	1.56E-10	34	8.40E-10	ABCC4, ATP5A1, ATP5B, ATP5C1, ATP5D, ATP5F1, ATP5H, ATP5I, ATP5J, ATP5L, ATP5O, ATP6V0A1, ATP6V0D1, ATP6V1A, ATP6V1B2, ATP6V1C1, ATP6V1D, ATP6V1E1, ATP6V1F, ATP6V1G1, ATP6V1H, CCT8, FTH1, FTL, HK1, HMOX1, HSPA1A, HSPA4, LONP1, PSMD6, RPS27A, SLC39A7, TCIRG1, THBS1	313
GO:0051084	'de novo' posttranslational protein folding	10	4.69E-06	10	2.58E-07	9	6.00E-08	CCT2, CCT3, CCT4, CCT5, CCT6A, CCT7, CCT8, HSPH1, TCP1	30
GO:0022904	respiratory electron transport chain	15	1.38E-04	12	2.93E-04	12	4.21E-06	ATP5A1, ATP5B, ATP5C1, ATP5D, ATP5F1, ATP5H, ATP5I, ATP5J, ATP5L, ATP5O, SDHA, SDHB	78
GO:0043066	negative regulation of apoptotic process	41	1.65E-14	29	6.69E-10	15	1.77E-04	AURKB, CEBPB, HMOX1, HSPA1A, HSPA9, POR, PSMD11, PSMD5, PSMD6, RPS27A, SERPINE1, SET, SQSTM1, THBS1, TIMP1	156
GO:0007264	small GTPase mediated signal transduction	19	2.30E-04	15	5.10E-04	9	1.00E-02	FARP1, HMOX1, IQGAP1, KIF14, RAB2A, RAB5A, RAB5B, RND3, SQSTM1	115
GO:0055114	oxidation-reduction process	28	2.07E-01	22	1.64E-01	20	1.10E-02	ABCC4, ALDH18A1, CYB5B, CYB5R3, ECH1, ETHE1, FTH1, GPD2, HADHA, HCCS, HK1, HMOX1, IQGAP1, POR, PTGS1, PYCR1, RPS27A, SDHA, SDHB, SQRDL	334
GO:0006936	muscle contraction	6	8.04E-02	5	6.18E-02	5	1.11E-02	CALD1, CNN1, MYOF, TPM3, TPM4	51
GO:0007155	cell adhesion	18	9.75E-03	13	2.92E-02	10	1.85E-02	ATP5B, COL1A1, KIF14, LGALS1, MFGE8, RND3, SERPINE1, TGFBI, THBS1, TPM4	145
GO:0006986	response to unfolded protein	8	3.75E-02	7	2.03E-02	5	2.71E-02	ATP6V0D1, HSPA1A, HSPA4, HSPH1, THBS1	62
GO:0000209	protein polyubiquitination	21	2.75E-10	17	4.42E-09	5	3.11E-02	PSMD11, PSMD5, PSMD6, RPS27A, UBR5	64

[a]Full set of 121-OxS nodes plus 119 suggested nodes from STRING. [b]Set of 121-OxS nodes plus 52 nodes suggested by STRING that were quantified. [c]Set of 121-OxS nodes. [d]Total number of quantified proteins annotated to the indicated process. [e]Hypergeometric *p* values calculated relative to the background of MS quantified proteins.

Figure 3-13A shows the STRING network analysis for 240-OxS and suggests different protein behaviours under oxidative stress. It indicates that some proteins such as ATP5 subunits showed similar behaviours in the data (i.e. decreased S_t with N→ C distribution), while the V-type proton ATP6 proteins showed inverse behaviours (i.e. increased S_t with C→ N distribution). There were 47 quantified proteins in the MS data of proteasome protein complexes, and 16 were present in 240-OxS, with 14 quantified. However, only three of these proteins, PSMD-5, -6 and -11, were quantified in 121-OxS data, which were increased in S_t, showed C→ N distribution, and were annotated to the biological process term GO:0071158, "positive regulation of cell cycle arrest". For the nuclear COPS signalosome complex, nine proteins were presented and quantified in the 240-OxS network. However, only COPS3, ATP5A1, ATP5A69 and HSP1A1 were present and quantified in the 121-OxS set. COPS3 and HSP1A1 showed different behaviours than ATP5A1 in 121-OxS. For the CCT protein complex, all eight proteins were involved in the *de novo* post-translational protein folding (Table 3-2) and quantified in the 121-OxS data with $S_t \sim 1$ and presented C→ N distribution. RFC proteins (DNA polymerase delta subunits, replication factor C subunits) suggested that there was a connection between oxidative status and the cell cycle, although there were clear clusters of proteins associated with different specific cellular functions in 240-OxS. Proteins such as FTL, FTH1 and HMOX1 were still weakly connected with 35 un-connected proteins in 240-OxS.

Figure 3-13B shows thumbnails for the significant protein interactions in S_n, S_c, S_t and the S_n/S_c distribution within the 121-OxS set. Only 76 significant proteins that were changed in S_t were selected by the analysis. The SigB for 39 of these proteins was even smaller in S_n and S_c compared to S_t. However, there were 45 S_t significant proteins including 26 proteins that were changed in the cytoplasm with 9 proteins and in the nucleus with 17 proteins dependent on changes in S_t and S_n/S_c distribution. Also, there

were 19 proteins that appeared significant in S_n/S_c, but represented very small changes in S_t. For example, polymerase delta-interacting protein 2 (POLDIP2) was one of those proteins that was significant in S_n/S_c even though there was no GO BP for this protein suggested by the analysis. Some of the RAB proteins, including RAB2, RAB5A and RAB5B, were significantly smaller in S_t as well.

Analysis also showed that there were some proteins with more than one biological function according to their subcellular location. For example, plasminogen activator inhibitor 1 (SERPINE1) protein was annotated to 10 GO BP terms including terms related to extracellular matrix organisation, cellular component movement, and DNA-template (Table 3-2; details in Supplementary GO Terms Table, CD).

GO BP was useful for understanding protein biological functions. However, 4 proteins out of 121-OxS had no GO BP terms; also, 89 proteins of 121-OxS only had enriched terms in Table 3-2. Additionally, some terms were not reflected in the model that was used for the study of IMR90 cells. However, the same functional meaning was still given. For example, the term 'phagosome maturation' and 'insulin receptor signaling pathway' reflected lysosomal/endosomal processes. Also, the term '*de novo* post-translational protein folding" reflected the role of the CCT complex in membrane fusion and the term 'muscle contraction' was related to endocytotic processes (see discussion).

A.

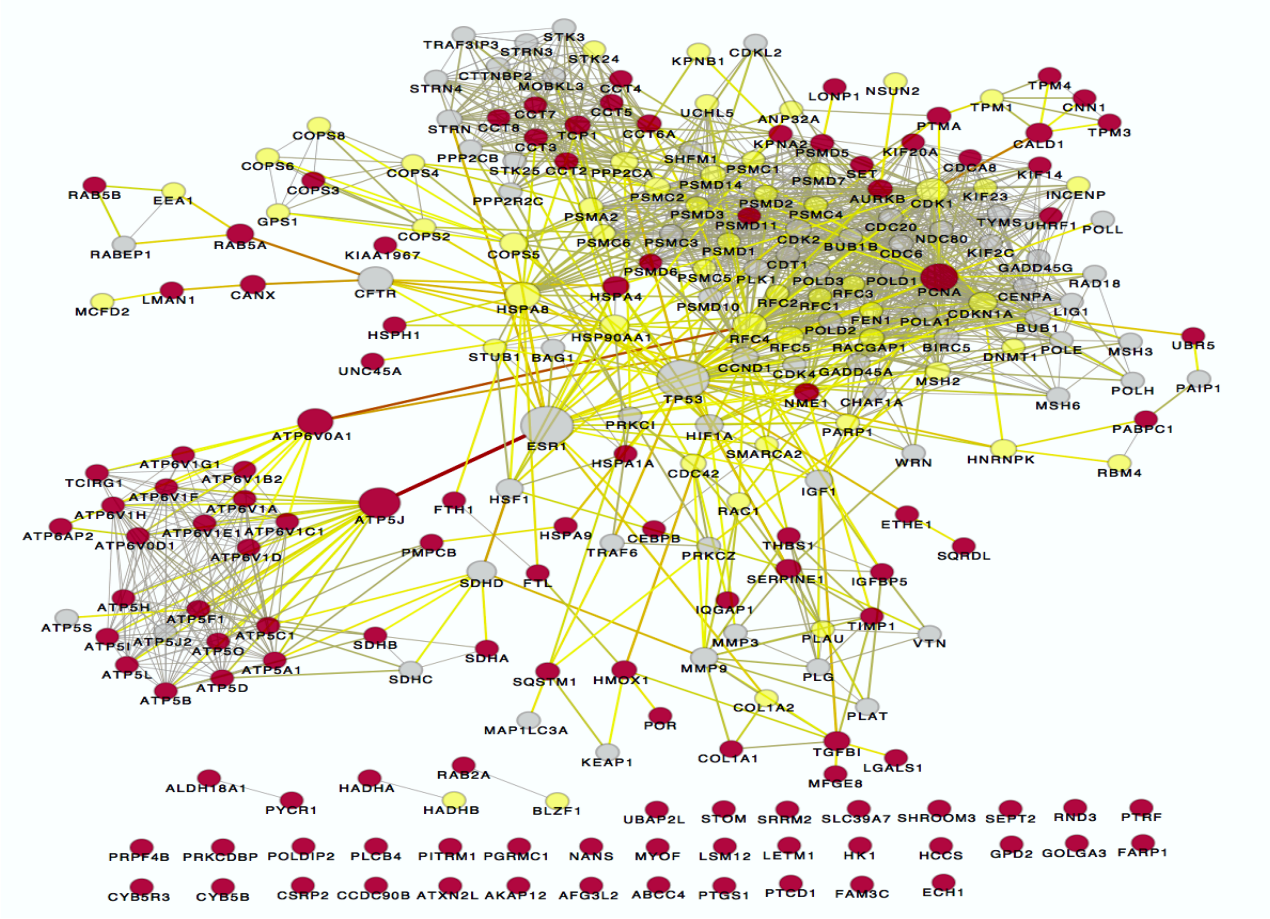

B.

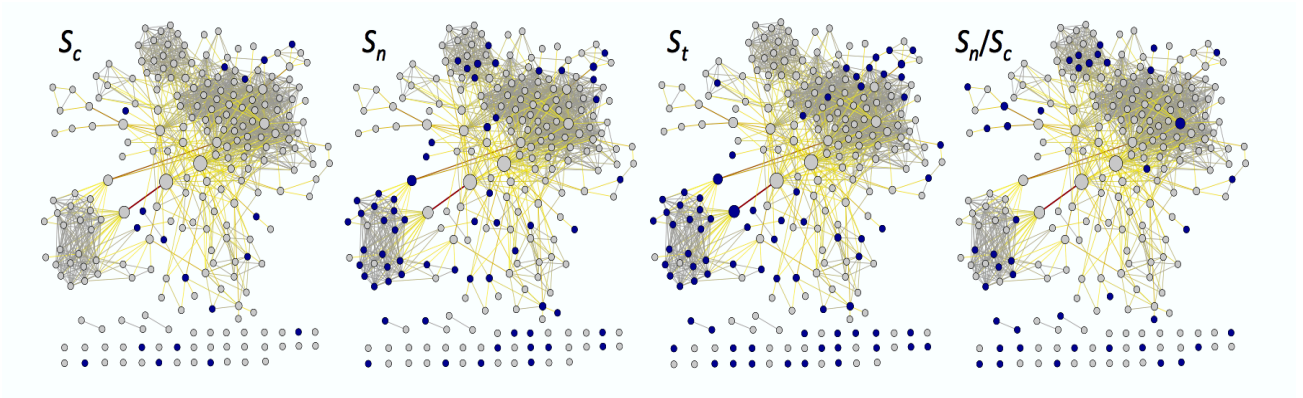

Figure 3-13. Network Analysis for 240-OxS data set Including the 121-OxS set. A. STRING interaction network for the 240-OxS set. The protein nodes for the 121-OxS set are coloured in red, the nodes for the proteins that were not significant but identified in MS are coloured in yellow, and proteins that were not found within the data sets and were only suggested by STRING are coloured in grey. Plugging the network with Cytoscape software was used to calculate the node and edge colour and size that expressed betweenness centrality values. Note: Betweenness centrality value helps to measure the node's centrality and position in a network. Edge Betweenness, which is a topological measure, is known as a normalised number of direct routes between two nodes. **B.** Thumbnails of the interaction network. The blue node represented significant protein changes in S_n, S_t, S_c *and* S_n/S_c within the 121-OxS data set. The network interactions figure was designed by Marko Radulovic (Baqader et al., 2014).

3.2.8 The Significantly Affected Metabolic Pathways under Oxidative Stress

Different important pathways that are related to oxidative stress were examined.

3.2.8.1 Affected Protein Pathways Related to Nrf2: Nuclear Respiratory Factor 2 is known to be involved in different intermediary metabolism processes such as glycolysis, the TCA cycle, generation of NADPH, glutamine metabolism, and fatty acid oxidation (Hayes and Dinkova-Kostova, 2014). In the present study, the Nrf2 protein was found to translocate to the nucleus under oxidative stress by the use of WB (Figure 3-3B). Thus, Nrf2-related pathways were investigated within the present data set by using a recent collocation of positive Nrf2-regulated genes as a reference. For example, Nrf2 was known to cause changes in pathways related to glycolysis and pentose phosphate, producing NADPH, which is important for antioxidant proteins (Hayes and Dinkova-Kostova, 2014). Numerous proteins in this pathway were observed in the study (Figure 3-14A) as follows: there was little change in total abundance detected in either of the isoforms of pyruvate kinase (S_t = 1.08, 0.99) or in the enzymes G6PD/PGLS/PGD (S_t =1.12, 0.94, 1.04) in the oxidative arm of the pentose phosphate shunt. The arm of the pentose phosphate shunt included TALDO/TKT, which showed slight increases in total abundance (S_t = 1.08, 1.39). However, MTHDF2 showed a significant decrease (S_t = 0.58), which was thought to slightly increase via MTHDF1/MTHDF1L1 (S_t = 0.96, 0.91). HK 1 was a significant protein in the 121-OxS set that was found to translocate from C → N, but was totally disconnected in the STRING network (Figure 3-12, 3-13). It was found to be the only significant protein in the glycolysis pathway (Figure 3-14A). HK1 was found to rely on redistribution of the subcellular location (S_t = 1.14, S_n = 2.02, S_c = 1.10, log2 (S_n/S_c) = 0.87). For the TCA cycle (Figure 3-14B), it has been found that 12 of the TCA cycle enzymes (SUCLA2, SUCLG2, FH, MDH2, MDH1, IDH2, IDH3A, IDH3B, IDH3G, CS, ACO2, ACO1) showed minor changes in total ($0.83 < S_t < 1.11$) or compartmental abundance.

Lipoamide E cofactor proteins showed slightly more obvious decreases in abundance (DLD, DLST, OGDH; $0.70 < S_n, S_t < 0.76$) with moderate redistribution from N → C and SUCLG1 S_t, S_c were ~0.75. These results were also accompanied with a slight reduction of succinyl-CoA production from 2-oxo-glutarate and its subsequent usage in the TCA cycle. Lipoamide E proteins of the pyruvate dehydrogenase complex (DLD, DLAT, PDHB) showed a similar modest decrease in abundance ($0.70 < S_t < 0.85$) and it was consistent with reduced production of acetyl-CoA from pyruvate. There was a modest decrease in IDH2 (S_t, $S_c \sim 0.91$) and a modest increase in cytoplasmic IDH1 (S_t, $S_c \sim 1.33$); none of these proteins were present in the 121-OxS set of the most significantly changed proteins (Figure 3-14B), and the most significant change in the TCA cycle was a decrease in SDHA and SDHB (S_n, $S_t \sim 0.37$). SDHA and SDHB were connected by STRING to ATP synthase (Figure 3-13A).

For the NADPH pathway, this is usually regulated via the generating enzymes G6PD, PGD, IDH1, 2 and NADP-dependent malic enzyme (ME1), which is known to be an alternative enzyme for pyruvate (Hayes and Dinkova-Kostova, 2014). In the present study, it was been found that there was a slight increase in abundance for ME1 ($S_t = 1.19$) with a modest change in mitochondrial NAD (P) transhydrogenase NNT ($S_t = 0.71$). Moreover, there were no notable changes detected in the levels of proteins of glutathione- or thioredoxin-based anti-oxidant systems. Glutathione peroxidases GPX1 and GPX8 ($S_t \sim 0.7$), glutaredoxin GLRX3 ($S_t = 1.02$), isoforms 1 and 3 of glutaminase GLS ($S_t = 0.93, 0.83$), and glutathione reductase GSR ($S_t = 1.32$) were slightly changed in abundance. For some antioxidants, it was found that thioredoxin TXN ($S_t = 1.23$), thioredoxin reductases TXNRD1 and TXNRD2 ($S_t = 1.16, 0.93$), and peroxiredoxins PRDX1, 2,4,5,6 ($0.93 < S_t < 1.15$) were not significantly changed in abundance. Only PRDX3 showed slightly different behaviour ($S_t = 0.77$, $S_n = 0.63$, $S_c = 0.92$). Notably, none of these anti-oxidant proteins were amongst the 121-OxS set.

For fatty acid oxidation, of the 24 proteins observed, 21 of them showed very small changes in total ($0.82 < S_t < 1.19$) or compartmental abundance. Significant changes in total and nuclear abundance were observed for subunits of the mitochondrial trifunctional enzyme HADHA/HADHB (S_t = 0.65/0.68; S_n = 0.61/0.60; S_c = 0.93/0.97). The electron transfer flavoprotein-ubiquinone oxidoreductase ETFDH appeared to show similar behaviour, but with a smaller number of SILAC ratio counts. Likewise, many proteins associated with the detoxification of drugs whose abundance is controlled by NRF2, including oxidation of drugs (aldehyde dehydrogenases, aldo-keto reductases, carbonyl reductases CBR1 and CBR3, epoxide hydrolase EPHX1, prostaglandin reductase PTGR1), conjugation of drugs (glutathione S-transferases GSTM3, GSTP1, MGST1) and drug transport (ABCC1), showed very small changes in abundance. Of the many proteins that are associated with drug detoxification, microsomal glutathione S-transferase (MGST3) showed a modest change (S_t = 1.33), and multidrug resistance-associated protein 4, ABCC4 protein (S_t, S_n = 0.50), was found in the 121-OxS set.

For glutamine metabolism, which was suggested to be regulated by Nrf2 via glutamine synthase (GLS), the pathway-related proteins were viewed in the present study. It has been found that isoforms 1 and 3 of GLS, which is part of a group of the “proline regulatory axis” proteins (Figure 3-14C) and strongly connected to redox regulation, glutamine/proline metabolism, the urea cycle, the TCA cycle, and collagen, showed only small changes in abundance (St = 0.93, 0.83). There were strong changes in abundance and subcellular distribution for the proline regulatory axis: pyrroline-5-carboxylate reductase (PYCR1), delta-1-pyrroline-5-carboxylate synthase (ALDH18A1), and collagen (COL1A1) in the 121-OxS set which might also affect the level of NADH/NADPH and cell cycle arrest.

However, it appears that antioxidant activities controlled by NRF2 were not a major contributor to the response of IMR90 cells with TBP. The activation of Nrf2 by

antioxidant response elements (ARE) was checked by studies of their related proteins. A strong increase in abundance of the CCAAT/enhancer-binding protein beta CEBPB (S_t, S_n = 2.23) and moderate increases of an accessory protein involved in NRF2 transcription MAFG (S_t = 1.48, but with only five SILAC ratio counts) was found. This suggested that there was modularity in the transcriptional activity of NRF2 and it was found in the present study for proteins involved in iron/haem metabolism and controlled by the NRF2. For example, both subunits of ferritin (FTL and FTH1; S_t = 1.72 and 1.84, respectively) and haem oxygenase (HMOX1; S_t = 7.11) presented strong increases in abundance. However, biliverdin reductase (BLVRA) and flavin reductase NADPH (BLVRB) did not show increased abundance (S_t = 1.03 and 1.00, respectively). Catalase CAT (S_t = 0.89) and superoxide dismutases SOD1 and SOD2 (S_t = 1.34 and 0.77, respectively) showed moderate changes as a specific feature of cell response to TBP. Catalase and SOD1 showed moderate increases by WB (Figure 3-3).

A.

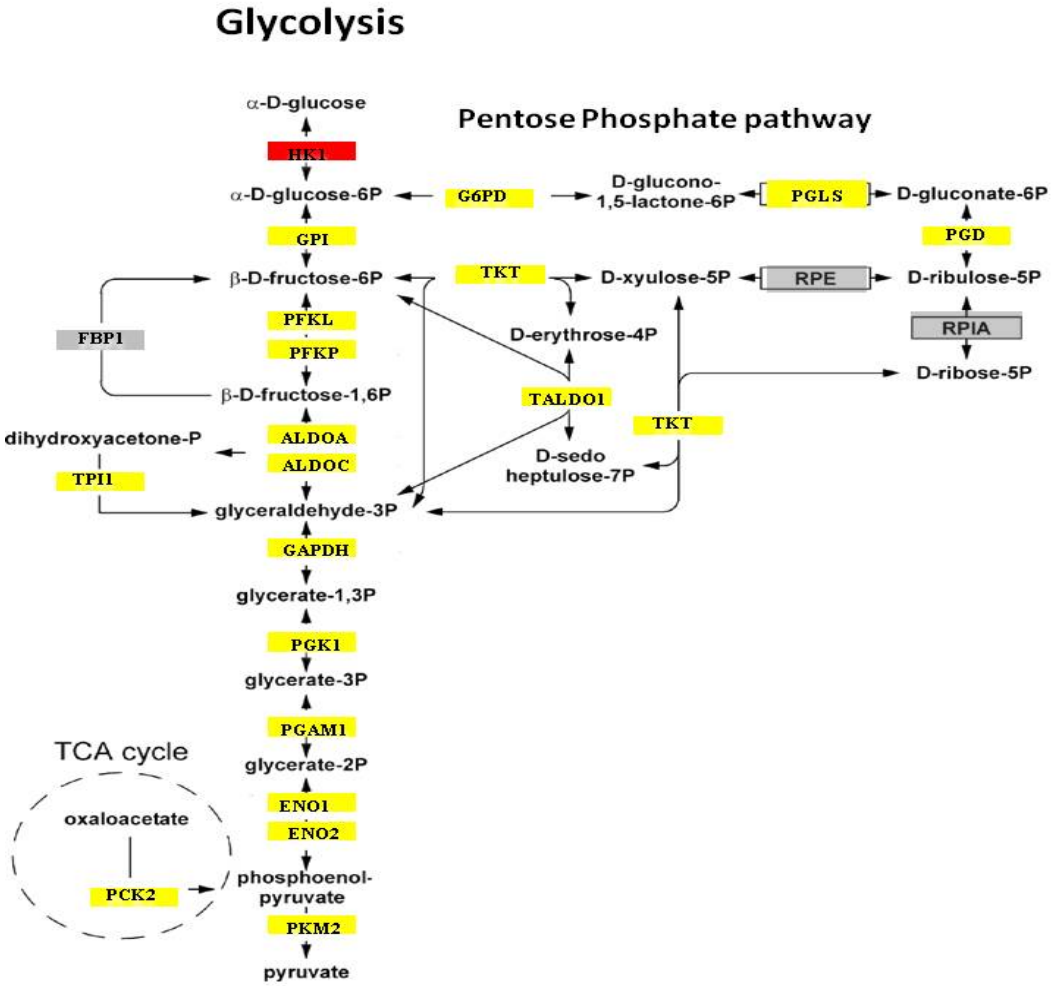
Glycolysis
Pentose Phosphate pathway
α-D-glucose
HK1
α-D-glucose-6P
G6PD
D-glucono-1,5-lactone-6P
PGLS
D-gluconate-6P
GPI
PGD
β-D-fructose-6P
TKT
D-xyulose-5P
RPE
D-ribulose-5P
PFKL
PFKP
FBP1
D-erythrose-4P
RPIA
D-ribose-5P
β-D-fructose-1,6P
TALDO1
TKT
dihydroxyacetone-P
ALDOA
ALDOC
D-sedo heptulose-7P
TPI1
glyceraldehyde-3P
GAPDH
glycerate-1,3P
PGK1
glycerate-3P
PGAM1
TCA cycle
glycerate-2P
ENO1
ENO2
oxaloacetate
phosphoenol-pyruvate
PCK2
PKM2
pyruvate

B.

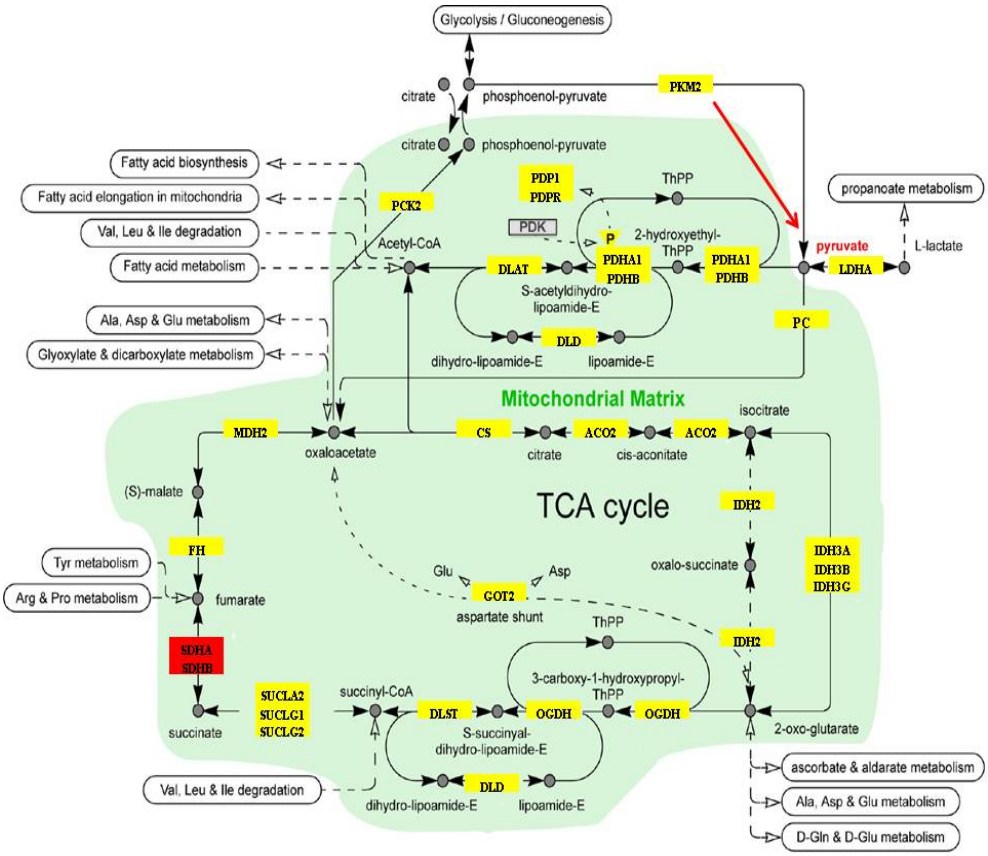

C.

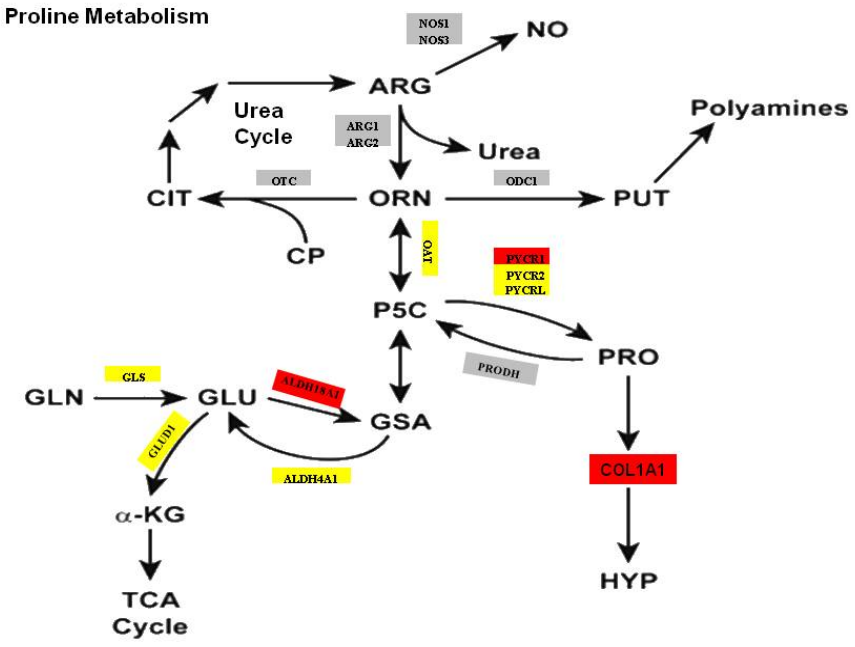

Figure 3-14. The Pathways of Proteins Regulated by Nrf2. The most significant proteins in the 121-OxS data set were marked in Red; the non-significant proteins in 121-OxS, but which were presented within the MS data, were marked in Yellow. Proteins not presented within data were marked Grey. **A.** Glycolysis pathway. **B.** TCA cycle. **C.** Proline regulatory axis pathway.

3.2.9 Affected Proteins Related to Different Cellular Functions

Proteins that relate to different subcellular locations and protein transport, and which were present in the 121-OxS data set, were checked. The use of the GO BP database showed that, in the present study, there were 448 identified proteins annotated to nuclear import/export/localisation/maintenance or regulation with 160 quantified proteins; 10 of these were suggested as possible changes in nuclear transport, of which five satisfied the more stringent conditions of presence in the 121-OxS set and were used in the network searches (Table3-3). For example, the proteins that were included in Table 3-3 were suggested by GO BP to be involved in processes related to nucleocytoplasmic trafficking; for example, collagen COL1A1 was annotated to 'protein localisation to nucleus' (GO: 0034504) and 'regulation of canonical Wnt receptor signaling pathway' (GO: 0060828), whereas karyopherin KPNA2 was annotated to 'NLS-bearing substrate import into nucleus' (GO: 0006607). Generally, most of these proteins had more than one process. However, CDKN1A was only annotated to a process related to oxidative stress: 'regulation of reactive oxygen species metabolic process' (GO: 2000377). Some of these proteins were known to be more strongly involved in other processes such as HSPA9 protein, which was known to be involved with mitochondria.

Moreover, for vesicular trafficking proteins, there were 1175 proteins annotated to "vesicle-mediated transport" (GO:0016192) and 503 proteins annotated to "cytoplasmic vesicle" (GO:0031410) in the GO database; these included a significant number of common proteins. Therefore, the set of 1427 proteins that were annotated to one or both of these terms was checked, of which 344 were quantified in the present experiments and 100 had annotations to the nucleus. Of the 251 of these proteins that were quantified in the nucleus, 70 were annotated to the nucleus (Figure 3-7, 3-8) as well as with other subcellular organelles, which showed little or no change in their nuclear

fraction and no difference between proteins that were found with/without annotation to the nucleus (Figure 3-15). It was also suggested that there was selectivity in the nucleocytoplasmic trafficking of these types of proteins. For example, for 29 of the Ras-related RAB proteins quantified in the present experiments and the 14 proteins that were annotated to vesicle-mediated transport, only 3 proteins showed evidence of nucleocytoplasmic trafficking following TBP treatment. The 121-OxS set included 28 nucleocytoplasmic trafficking proteins, of which 27 were quantified in the nucleus and 8 are presently annotated to the nucleus; 11 of these proteins showed substantial changes in the fraction of the protein in the nucleus ($|\log2(S_n/S_t)| = |\log2(f_s/f_u)| > 0.5$, Figure 3-15), including RAB2A, RAB5A, and RAB5B. Noteworthy, seven of these proteins were involved in iron metabolism (ATP6V0A1, ATP6V0D1, ATP6V1C1, ATP6V1H; FTL, FTH1, HMOX1). Also, there were a further 3 proteins involved in iron/haem metabolism that are currently annotated to the "vesicular fraction" (PGRMC1, POR, PTGS1) and 28 of these proteins were only weakly connected by STRING (Figure 3-13A).

Gene Name	Cytoplasm			Nucleus			Total		
	S_c	SigB score	Ratio Count	S_n	SigB score	Ratio Count	S_t	SigB score	Ratio Count
CDKN1A	1.90	1.02E-03	3				2.07	1.40E-04	5
COL1A1	0.51	9.26E-06	62	0.63	4.03E-02	50	0.57	1.68E-03	114
G3BP2	0.86	4.97E-01	8	1.45	1.22E-02	48	1.44	3.06E-03	53
HSPA9	1.01	7.31E-01	181	1.64	5.72E-05	476	1.58	2.27E-05	664
JUP				0.23	6.36E-08	5	0.25	3.64E-11	6
KPNA2	0.53	1.18E-05	11	0.69	1.01E-01	62	0.67	2.90E-02	73
RANBP17	0.18	7.10E-19	3						
SET	1.65	6.31E-05	57	1.22	3.61E-01	11	1.55	4.03E-04	70
TMEM173				0.54	2.78E-02	3	0.54	3.83E-03	3
UBR5				1.78	1.36E-02	15	1.78	5.47E-04	17

Table 3-3. Proteins Involved in Nuclear Import/Export/ Localization/Maintenance or its Regulation. Proteins with SigB < 0.005 and ≥3 ratio counts for at least one of S_n, S_c, or S_t. Bold gene names satisfied the more stringent conditions for selection of the 121-OxS set.

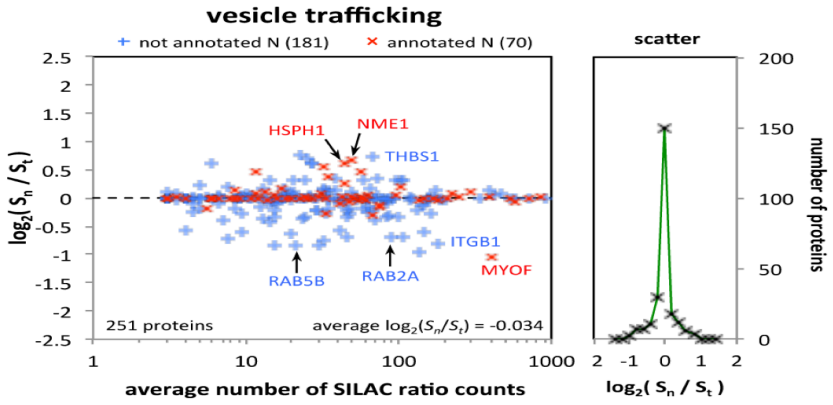

121-OxS proteins annotated to vesicle trafficking[1]

Gene Names	$\log_2(S_t)$	$\log_2(f_s/f_u)$	counts (N+T)/2	annotated nucleus
ABCC4	-0.988	-0.009	22	0
ATP6V0A1	0.746	-0.030	60	1
ATP6V0D1	0.532	0.006	119.5	0
ATP6V1C1	0.901	0.043	61.5	0
ATP6V1H	0.957	0.003	24.5	0
CANX	-0.019	-0.970	138	0
CCT6A	-0.005	0.815	57	0
FAM3C	-0.824	-0.098	32	0
FTH1	0.881	0.179	13	0
FTL	0.784	0.094	20.5	0
GOLGA3	0.737	0.044	94.5	1
HMOX1	2.831	-0.038	52	0
HSPH1	0.429	0.602	44.5	1
KIF20A	-1.939	0.000	12	1
LMAN1	0.063	-0.828	30.5	0
MFGE8	-0.324	-0.283	48	0
MYOF	0.164	-1.057	412.5	1
NME1	0.025	0.663	50	1
RAB2A	-0.051	-0.693	88.5	0
RAB5A	-0.174	-0.635	19.5	0
RAB5B	0.020	-0.844	21.5	0
RPS27A	0.450	-0.056	583	1
SERPINE1	0.621	0.005	51.5	0
SQSTM1	1.150	0.001	65.5	1
TCIRG1	0.663	0.000	124	0
TCP1	0.085	0.744	74.5	0
THBS1	0.270	0.739	67	0
TIMP1	1.145	-	10	0

Figure 3-15. Analysis of Proteins Annotated to Vesicular Trafficking. The plot in top illustrates $\log_2(S_n/S_t) = \log_2(f_s/f_u)$ as a function of the average number of ratio counts over the nucleus and total data sets for proteins annotated to "vesicle-mediated transport" or to "cytoplasmic vesicle". Proteins with (red, 70 proteins) or without (blue, 181 proteins) annotation to the nucleus are indicated. Right: number of proteins versus $\log_2(f_s/f_u)$. Table: Data for 28 proteins of the 121-OxS data set.

3.2.10 Indication of Extensive Participation of Iron/Haem Metabolism and Mitochondria

Proteins that involve iron homeostasis or haem/iron as a cofactor and were substantially enriched in the 121-OxS set were checked. In the present data, 93 proteins out of 3124 quantified proteins, with 20 proteins of the 121-OxS set, were involved in iron or haem/iron metabolism. The 20 significant proteins included 19 that were quantified in the nucleus; 13 of them represented the most significant changes in S_n, and 6 represented the most significant changes for S_t or S_n/S_c. Noteworthy, out of these 19 proteins, there were 3 that were annotated to the nucleus (ATP6V0A1, HMOX1, PGRMC1) and participated in different biological processes. However, their functions in the nucleus remain poorly understood. Ten subunits of V-type proton ATPase (ATP6) were present in the nucleus but were still not annotated to it yet, as well as both ferritin subunits (FTL, FTH1) that are important in iron homeostasis, oxidoreductases (CYB5B, CYB5R3, POR) that involve haem proteins and the succinate dehydrogenase [ubiquinone] iron−sulfur subunit (SDHB) that depends on an iron−sulfur cluster for its activity. Proteins such as haem protein prostaglandin G/H synthase 1 (PTGS1) were not quantified in the nucleus but showed a significant decrease in abundance in cytoplasm S_c. However, changes in iron metabolism-related proteins appeared to be a response to oxidative stress, especially within the nucleus. Only a few proteins, 4 out of the 20 significant proteins (such as HMOX1 and PTSG1), were annotated to oxidative stress, and few of the 19 proteins were functionally annotated to the nucleus.

For the mitochondrial proteins, 41 proteins of the 121-OxS significant set were annotated to the mitochondria, with 39 of them quantified in the nucleus, and 25 of them corresponding to the most significant changes for S_n; two proteins (CYB5B, ETHE1) corresponded to the most significant changes for S_c, and 12 corresponded to the most significant changes for S_t and/or S_n/S_c distribution. For the molecular functions,

only 7 of these proteins, including ATP5A1, ETHE1, HSPA1A, HSPA9, NME1, POLDIP2 and PTRF, are currently annotated to the nucleus. Proteins such as polymerase delta-interacting protein 2 (POLDIP2, mitochondrial nucleoid 91) and the polymerase I and transcript release factor protein (PTRF, transcription from RNA polymerase I promoter 92) seemed to play similar roles in both the nucleus and the mitochondria and both showed slight increases in total abundance with C → N redistribution. The GO biological process for proteins ATP5A1, HSPA1A (co-localisation with the COP9 signalosome 69), NME1 (positive regulation of DNA binding 93), and HSPA9 (poly (A) RNA binding and protein export from the nucleus) did not indicate nuclear functions for them. There were also 32 mitochondrial proteins with no clearly defined functions in the nucleus detected in the nuclear fraction, with 27 annotated to the mitochondrial matrix/inner membrane: 10 subunits of ATP synthase (ATP5), 2 proteins of the TCA cycle (SDHA, SDHB), 2 proteins of the proline regulatory axis (ALDH18A1, PYCR1), mitochondrial peptidases (AFG3L2, LONP1, PITRM1, PMPCB), other proteins involved in oxidation−reduction processes (CYB5B, CYB5R3, GPD2, HADHA, HCCS, POR, SQRDL), as well as LETM1 (a mitochondrial Ca_2^+ and/or K^+ transporter 96) and PTCD1. Only ATP6V1A, ATP6V1E1, CCT7, ECH1, HK1, HSPA4, POR and TCIRG1 were known to have another function beside their original function as mitochondrial proteins. Seven of the proteins that were annotated to mitochondria and detected in the nucleus also belonged to iron/haem proteins (ATP6V1A, ATP6V1E1, CYB5B, CYB5R3, POR, SDHB and TCIRG1). Furthermore, 9 of the proteins in the 121-OxS set that were annotated to mitochondria (ATP5A1, ATP5B, ATP6V1A, ATP6V1E1, CCT7, ECH1, HSPA1A, HSPA4 and HSPA9) were annotated to the extracellular vesicular exosome and one (TCIRG1) was annotated to the phagocytic vesicle membrane. For biological processes, only 4 of these mitochondrial proteins were annotated to stress responses (HSPA1A, HSPA4, LONP1

and PYCR1). Finally, 39 mitochondrial proteins (of the 371 quantified in the nucleus) were thought to represent the cellular response to oxidative stress (see discussion).

Chapter 4: Discussion of Findings

The proteomics subcellular spatial razor is a powerful approach for the study of dynamic changes and protein redistribution between different cellular locations such as the nucleus and the cytoplasm. The previously published results related to protein distributions during cell cycle arrest in IMR90 cells (Mulvey et al., 2013, Mulvey et al., 2010), cellular response to oestradiol in breast cancer MCF7 cell lines (Pinto et al., 2014) and fluorescence-based results on genome-wide spatial response to hypoxia in yeast (Henke et al., 2011) all suggested that the subcellular distribution of proteins is highly dynamic and context-dependent. In the present experiment, the experimental model was based on treatment of the normal human fibroblast IMR90 cell lines with *tert*-butyl-hydrogen peroxide TBP in cell culture to generate a mild oxidative stress response within the cells. This was with the aim of arresting cell cycle by activating specific cell cycle checkpoints to test the hypothesis that the novel DNA origin activation checkpoint response in somatic cells is a normal response driven by a novel pathway.

The subcellular proteomics analysis revealed that there was dynamic redistribution of numerous proteins over the defined compartments (i.e. nucleus and cytoplasm) as a response to oxidative stress; these findings revealed several aspects of cellular response to oxidative stress that are still poorly understood. It is now clear that cellular response to oxidative stress and ROS signaling affect different cellular processes. In this experiment, these processes were primarily viewed from a nuclear-defined perspective. The data discussed four key topics: the first topic covered the general properties of the proteomics subcellular spatial razor, especially the compartmentalised changes in protein abundance between the nucleus and cytoplasm. The second topic included a simple overview of the most significant proteins in the data that are known to

participate in different cellular processes such as control of the cell cycle, autophagy/mitophagy, and other signaling systems. The third topic provided intensive analysis for the two most prominent features that seemed to be related and to be more novel in current understanding of cellular response to oxidative stress. This has included the participation of proteins that play crucial roles in iron metabolism or with haem/iron as cofactors, and how that was connected to nuclear hormone metabolism/receptors that are involved in cancer. The final topic generally suggested constructing models of cellular function that include functional systems that are spatially distributed over different subcellular locations and dynamic changes in the spatial dispersion of proteins. To achieve these topics the experiments were firstly optimised to ensure the cellular response to TBP. Optimising and testing the cells response to TBP was achieved by the use of FACS analysis and western blotting, which helped to select the best dosage that caused mild oxidative stress without harming cells. It has been found that a high level of oxidative stress can be lethal for cells (Fatemi et al., 2014). Conversely, in the present study, from initial light microscopic pictures, cell numbers appeared normal with the optimised doses (50-100μM) of TBP, which means that modest dosage might still affect the cells without harming them (Figure 3-1). These results were also monitored by the use of FACS analysis for the nominated doses to test cell cycle arrest between G1/S after the treatment and also to confirm the cellular viability by checking the accumulation of dead cells at sub-G1. Accumulation of cells at the G1/S and G2/M boundaries with no sub-G1 under oxidative stress indicated that the cell cycle checkpoints were activated due to the treatment effect (Figure 3-2); these results were also compatible with the previously published results that found cell cycle was suspended after the activation of a specific checkpoint, the origin activation checkpoint (Tudzarova et al., 2010).

Elevation of ROS is known to increase antioxidant levels; for example, SODs normally elevate to convert the free radical oxygen into hydrogen peroxide. In contrast, antioxidants such as PRX, GPX and catalase participate in protein oxidation and redox biology by converting the excess of H_2O_2 into water. This antioxidants system is mainly controlled by Nrf2 (Schieber and Chandel, 2014). Western blotting for most of these antioxidant proteins showed modest elevation with TBP (Figure 3-3.A). In a previous study of cell cycle arrest at the original activation checkpoint for DNA replication induced by knockdown of the Cdc7 kinase by siRNA (Mulvey et al., 2013, Mulvey et al., 2010), Cdc7, tumour suppresser p53 and other oxidative stress proteins were shown to be involved in the cellular response. In the present study treatment, TBP was found to cause changes to both Cdc7 and TP53 in IMR90 cells (Figure 3-3A), highlighting that the cell cycle and oxidative stress have functional overlaps (Burhans and Heintz, 2009a). In parallel, translocation of the Nrf2 protein from the cytoplasm to the nucleus after the indication of oxidative stress provided evidence that the ROS level and antioxidant systems were activated due the TBP effect (Figure 3-3B). Thus, these results were suitable for proceeding with proteomic investigations.

4.1 Properties of the Subcellular Spatial Razor

A general overview of the results has shown that large numbers of either significant or non-significant proteins that were found in the nucleus were annotated by GO to different subcellular locations. The protein set of each organelle (Figure 3-6, 3-7) proved that a small number of the proteins, which were annotated to non-nuclear locations, represented changes in compartmental abundance as a response to oxidative stress. The changes in protein abundance between different subcellular organelles were obtained via a combination of changes in the subcellular distributions and total

abundance, with redistribution being at least equally important as changes in the total. The consistency of the results proved that there was no artefact from nuclear enrichment; this was also found with previously published experiments, making the results more reliable. For example, 36% of human proteins within the GO database are annotated to different subcellular locations. Also, the previously published spatial razor results for Cdc7 knock-down in IMR90 cells related to cell cycle arrest showed the same context, whereby nuclear enrichment was achieved by the same protocol with only 14 significant proteins shared between the two data sets (Mulvey et al., 2013). By comparing the significance of these two data sets of $Cdc7^{KD}$ (here after, origin activation checkpoint, 124-OAC) and 121-OxS (Supplementary Table 4, 5, external CD), a high variation in abundance and distribution has been found as a response to different cellular stimulations. The TCA cycle, glycolysis and proline regulatory axis were checked in both data sets. For glycolysis, HK1 showed strong reduction under oxidative stress, but was not significant under the $Cdc7^{KD}$ data set. For the proline regulatory axis, the significant proteins in the 121-OxS set were PYCR1 and ALDH18A1; in contrast, GLS, GLUD1 and OAT were changed in the Cdc7-depletion data set. Proteins such as collagen (COL1A1) were significant in both but were decreased in OxS and increase in $Cdc7^{KD}$. In relation to TCA cycle, 6 proteins include ACO2, DLD, FH, IDH2, MDH2, and SUCLG1 were significant in the nucleus for the $Cdc7^{KD}$ data set (Mulvey et al., 2013), whereas only SDHA and SDHB had changes detected in the 121-OxS data set. Hypoxia is also known to be a form of oxidative stress and genome-wide scans of subcellular protein distribution in yeast cells in response to hypoxia (Henke et al., 2011) resulted in the redistribution of SDHA. The spatial razor showed the changes in these three pathways in both data sets. The selectivity/reliability of the subcellular spatial razor was proven by direct comparison of the proteome of mitochondria and nuclei in MCF7 breast cancer cells. In these experiments, nuclei were

enriched with similar protocols as well. The results from MCF7 cells revealed that there were around 1000 proteins separated into the two subcellular locations and that this separation was highly reproducible (Qattan et al., 2012). Stimulation of MCF7 cells with oestrogen results in the major nucleocytoplasmic redistribution of proteins, which encompassed more than 100 proteins detected in the mitochondria (Pinto et al., 2014). This allowed us to conclude that the subcellular redistribution is more prominent than changes in total abundance, which led to the hypothesis that strong perturbation of subcellular spatial control may be a main feature of cancer cells (Pinto et al., 2014). In IMR90 cells, there was no massive nucleocytoplasmic redistribution detected in IMR90 cells under oxidative stress or cell Cdc7 depletion related to cycle arrest. However, it has been found that oestrogen receptor alpha (ESR1) was prominent in the 240-OxS STRING network (Figure 3-13) and there were no changes detected for proteins with direct connections to a progesterone receptor in the 121-OxS set. Although there is still the need for technical improvements in the proteomics experimental procedures, the nuclear spatial razor provides important information on the role of nucleocytoplasmic subcellular redistribution in cellular function. The spatial razor approach can also be applicable to other subcellular organelles such as mitochondria.

4.2 Overview of Cell Cycle Control, Autophagy/Mitophagy, Signaling Systems, and Mitochondrial Response

4.2.1 Cell Cycle Control

It is already known that there is a strong relationship between oxidative stress and the cell cycle (Burhans and Heintz, 2009b, Chiu and Dawes, 2012). However, it was initially surprising that only a few common proteins were strongly altered between

oxidative stress and cell cycle arrest within the IMR90 cells (Supplementary table 6, external CD). Noteworthy, by including proteins that showed similarities and differences in the joint analysis of the two data sets, oxidative stress and cell cycle arrest, there were a variety of nuclear processes and DNA replication that were changed in similar ways. However, these changes were achieved by detecting subtle alterations in the protein identity, total abundance, and protein redistribution of numerous proteins that were involved in the process; for example, polymerase delta-interacting protein 2 (POLDIP2), the homozygous deletion of which is lethal in mice (Sutliff et al., 2013), was detected within both data sets. POLDIP2 is already known to have functional roles that involve binding to DNA polymerases and ubiquitinating PCNA in the nucleus. These functions were suggested to offer cells the ability to bypass lesions such as 8-oxo-7, 8-dihydroguanine during DNA replication (Liu et al., 2003, Maga et al., 2013, Tissier et al., 2010). It has also been found to participate in the formation of mitotic spindles and chromatin segregation (Klaile et al., 2008). POLDIP2 has also been shown to be involved in the spliceosome and is essential for alternative splicing of MDM2 in response to UV irradiation, possibly as a consequence of ROS signaling (Wong et al., 2013). This also can be related to p53 (Dutertre et al., 2011), as p53 induces the transcription of HMOX1 (Nam and Sabapathy, 2011) and haem interactions (Shen et al., 2014). It has been reported that the plasma membrane interaction with CEACAM1, which is the homophilic cell−cell adhesion receptor carcinoembryonic antigen-related cell adhesion molecule 1, is related to the nuclear import of POLDIP2 under specific conditions such as quiescence, proliferation and cell division cycle (Klaile et al., 2007). Related to the reduced production of H_2O_2 and increased collagen secretion in focal adhesions and stress fibres, with the aim of regulating ROS signaling, extracellular matrix composition, and vascular structure and function in mice, NOX4 enzymes, which are

ROS-generating proteins, have been found to interact with POLDIP2 (Lyle et al., 2009, Sutliff et al., 2013).

In our data sets, a massive increase in nuclear abundance for POLDIP2 (S_n = 1.79) coupled with increases in total abundance with C → N redistribution (S_t = 1.67, $\log_2$ (S_n/S_c) = 1.18) and moderate decrease in cytoplasmic abundance (S_c = 0.79) were observed. Joint analysis with Cdc7-depletion-induced cell cycle arrest, in relation to DNA replication, showed that the proteins POLD and PCNA, and the replication factor C complex, were all included in the 240-OxS set (Figure 3-13, and supplementary table 3). Although the relative amounts of POLDIP2 over the different subcellular locations are not clear (Klaile et al., 2007), POLDIP2 has been found to have a mitochondrial targeting sequence in order to be predominantly expressed in the mitochondria of certain cell types (Cheng et al., 2005, Xie et al., 2005). It is also known to be associated with TFAM and LONP1 proteins in the mitochondrial nucleoid (Cheng et al., 2005). It not surprising therefore that POLDIP2 may be a link between DNA metabolism in the nucleus and mitochondria in related ROS signaling systems. Noteworthy, the POLDIP2 gene, which is known to be part of the complex sense-antisense architecture, has been linked with ERBB2, which is a member of the epidermal growth factor family, and associated with breast cancer (Grinchuk et al., 2010).

4.2.2 NRF2 and FOXO Signaling Systems

NRF2-related signaling is important in the response to oxidative stress and control of the antioxidants system (Ray et al., 2012, Hayes and Dinkova-Kostova, 2014, Pickering et al., 2013, Schieber and Chandel, 2014), and was clearly predominant in our experiments. Although NRF2 is known to affect glycolysis, the TCA cycle,

NADPH generation, and antioxidant systems, NRF2 response on these pathways seemed not predominant in our experiments (Figure 3-14). However, NRF2 expression clearly led to activation of antioxidant response elements (i.e. up-regulation of CEBPB, MAGF) and haem/iron proteins under NRF2 transcriptional control (HMOX1, FTL, FTH) including the strongest alterations in total protein abundance. Connection between p53, cell cycle processes and Nrf2 signaling, are believed to be coordinating via the FOXO transcription factor (Tudzarova et al., 2010, Sainsbury et al., 2010, Gorrini et al., 2013). FOXO is also known to participate in mitochondrial ROS signaling and the apoptotic pathway (Hagenbuchner and Ausserlechner, 2013). In our data set, it was found that 269 proteins were quantified and functionally annotated to apoptosis, with 16 of them being significant in the 121-OxS data set (supplementary table 2, external CD). These proteins were equally divided between anti-apoptosis proteins (SERPINE1, HSPA1A, HMOX1, HSPA9, POR), apoptosis proteins (LGALS1, PSMD6, PSMD5, NME1, PSMD11), or both (RPS27A, SQSMT1). Also, a similar mixed pattern was detected for the positive or negative regulation of apoptosis, with no clear patterns of changes in total or compartmental abundances that differentiated between apoptosis/anti-apoptosis. GO showed that 28 proteins were annotated to caspase activity (GO:0004197) or regulation of cysteine-type endopeptidase activity involved in apoptotic processes (GO:0043281), with only thrombospondin-1 (THBS1) being included in the 121-OxS set. These proteins have several other activities. Although, the data are consistent with a modular response to TBP, these did not include FoxO3-mediated connections to apoptosis. This led us to postulate that the data were consistent with no visible increase in dead cells and only very small changes in Annexin A5 (S_t = 1.09). This was suggested modularity in the NRF2-related response to TBP and other interactions involving NRF2; in particular,

the transcription of haematopoietic proteins and interaction with SQSTM1 may be crucial.

4.2.3 Autophagy and Sequestosome-1 (p62/SQSMT1)

In our data, GO annotated 10 quantified proteins to autophagy; these proteins included PARK7, FIS1, NPC1, and GABARAPL2 (Supplementary table 2, external CD). P62/SQSMT1 was the only protein found within the 121-OxS set, which has been shown to play a crucial role in autophagy as a response to oxidative damage (Szeto et al., 2006) and has a protective effect in huntingtin-induced cell death by lowering p26 levels (Bjorkoy et al., 2005). In other studies, SQSMT1 in association with Parkin has been found to be involved in the clustering of mitochondria in the perinuclear region (Okatsu et al., 2010) but not in mitophagy (Narendra et al., 2010). In promyelocytic leukaemia bodies, p26/SQSMT1 was found to translocate from the cytoplasm to the nucleus via NLS import/export sequences under phosphorylation control for the targeting of proteins for degradation (Pankiv et al., 2010). Under oxidative stress, SQSMT1 has been found to bind to Keap1 and help to initiate Nrf2 activation through the creation of a feedback loop (Komatsu et al., 2010, Jain et al., 2010). It is also known that, under stress, SQSMT1 plays a role in the formation of protein aggregates in the perinuclear region which are to be degraded by selective autophagy. However, this finding of protein aggregates was not sufficient to explain the observation of dynamic nucleocytoplasmic distributions in our data. For example, in our data, 371 unstimulated mitochondrial proteins were detected in the nucleus with only 41 quantified in the 121-OxS data set. Thirty-nine of mitochondrial proteins within the 121-OxS data were found to increase and decrease in nuclear abundance with protein redistribution between the nucleus and cytoplasm, with little or no change in total

abundance (Figure 3-9, 3-10; supplementary Table 2, external CD). It was suggested that SQSMT1 might have additional roles in the nucleocytoplasmic trafficking of (ubiquitinated) proteins as well as its role in the aggregation of damaged proteins such as PCNA, which binds both POLDIP2 and Flap endonuclease 1 (FEN1) (Sakurai et al., 2005). Many autophagic proteins have different roles (Subramani and Malhotra, 2013) and SQSMT1 might have other roles as well. In our data, GO showed that SQSMT1 was annotated to the negative regulation of apoptotic processes and small GTPase-mediated signal transduction (Table 3-2) which indicates that SQSMT1 might be more directly connected with changes related to cancer and interactions with mTOR in lysosomes (Moscat and Diaz-Meco, 2012). It has been argued that clustering of mitochondria in the perinuclear region is not unique to autophagy and that this clustering might be important for oxidant-rich nuclear domain production, which is crucial for hypoxia-induced transcription (Al-Mehdi et al., 2012). Also, some conditions that support mitophagy may encourage the movement of mitochondria toward lysosomes (Twig and Shirihai, 2011). PGRMC1, which has recently been found to promote autophagy (Mir et al., 2013, Mir et al., 2012), was also found in our 121-OxS set. However, in general in our experiments, it was shown that there was limited direct connection to autophagy/mitophagy, with clearer indications for other processes.

4.2.4 Mitochondria and the Retrograde Response

Although our experiments were concentrated more on the nucleus, they indirectly included mitochondrial processes. Noteworthy, there were 39 proteins out of 121 significant proteins that were located in the nucleus but also annotated to the mitochondria, consistent with extensive retrograde signaling from mitochondria to the

nucleus in response to TBP-induced oxidative stress. Mitochondrial retrograde signaling to nucleus is a crucial process that is vital within many cellular processes and is context-dependent (Kotiadis et al., 2014). The interpretation of the functions of these 39 proteins and their roles within our data with oxidative stress was not easy to achieve due to the limited knowledge regarding their functions within the nucleus. KIAA1967 (also known as deleted-in-breast-cancer-1, DBC1) has recently been shown growing interest in the context of cancer mechanisms. Although it is still unknown whether KIAA1967 is normally deleted or involved in cancer (Chini et al., 2013), clear evidence has shown that this protein is located in the nucleus and involved in important processes such as the regulation of histone deacetylase chromatin remodelling enzymes, transcription factor expression (Joshi et al., 2013) and alternative mRNA splicing (Close et al., 2012). It also directly interacts with important nuclear receptors such as the α and β oestrogen receptors (Trauernicht et al., 2007, Koyama et al., 2010). KIAA1967 or DBC1 was also observed within the mitochondria (Sundararajan et al., 2005). In our data, changes in KIAA1967 were observed, with moderate changes in S_n and $S_t \approx 1.25$, $S_c = 0.5$, C → N redistribution with $\log_2 (S_n/S_c) = 1.3$ in response to oxidative stress. Under oxidative stress, it is interesting to assume that KIAA1967 might also have crucial mitochondrial functions connected to the metabolic changes via the presence of important receptors such as oestrogen and other nuclear hormone receptors in the mitochondria (Chen et al., 2009a).

On the other hand, it was shown in our data that some proteins have a clear function in the mitochondria with no established function in the nucleus. For example, Lon protease (LONP1), which is an ATP-dependent protease, was annotated to the mitochondrial nucleoid and has well-known functions in the proteolytic clearance of damaged proteins (Ngo et al., 2013). LONP1 is also a context-dependent protein; for

example, under acute stress, within the mitochondrial matrix, it has been found to play a role as a protector protein in the degradation of oxidised proteins, while under chronic conditions, Lon level decreases and there is a loss of function (Ngo et al., 2013). Lon can act as a chaperone (Suzuki et al., 1997) and attaches to the promoter sequence in mDNA (Liu et al., 2004) and to transcription factor mitochondrial proteins (Matsushima et al., 2010). It has been found to bind to the POLDIP2 protein in the mitochondrial nucleoid (Cheng et al., 2005). In our data, Lon was found to show considerable nuclear changes with $S_c = 1.17$, $S_n = 0.55$, $S_t = 0.67$, N → C redistribution with $\log_2 (S_n/S_c) = -1.08$. These findings suggest that LONP1 might have nuclear functions that are modulated and controlled by oxidative stress.

Many other mitochondrial proteins were detected in the nucleus with interesting changes in response to oxidative stress. This might be due to the extensive retrograde signaling from the mitochondria to the nucleus, which might include the variable, dynamic distribution of proteins between the nucleus and mitochondria. The *C. elegans* ATFS-1 (activating transcription factor associated with stress-1) protein is considered a prototype for this type of mitochondrial retrograde control, as it detects mitochondrial stress and connects with the nucleus during the mitochondrial unfolded protein response. Under normal conditions, ATFS-1 is imported to the mitochondria and targeted for degradation. However, under stress conditions, changes in the nuclear/mitochondrial distribution are achieved by reduced mitochondrial import (Nargund et al., 2012). In this context, several proteins in the 121-OxS set were found to be linked with mitochondrial import processes such as HSPA9, PITRM1 and PMPCB. This suggested that Nrf2 and Keap1 might have a similar retrograde system as it has been previously found that the Nrf2/Keap1 complex is tied to the outer mitochondrial membrane via interactions with PGAM5, close to sources of ROS from the respiratory chain (Lo and Hannink, 2008).

4.3 Haem/Iron Metabolism

From the previous examples above, it is clear that many proteins in our data were identified with recognised connections to oxidative stress, mitochondrial pathways and the different signaling systems. The information on protein dynamic spatial distribution is largely new and for many of these proteins, an explanation of possible nuclear functions is now more attractive. Our results suggested that other subcellular organelles as well as mitochondria are involved in protein signaling to the nucleus in response to oxidative stress and this might include more novel systems that were not previously explained. Iron metabolism, for example, was one of the most attractive systems in our data. It is already well known to be associated with oxidative stress and connected to many diseases such as Alzheimer's, Parkinson's and other neurodegenerative diseases (Chtourou et al., 2014), as well as type-2 diabetes (Fernandez-Real and Manco, 2013). Iron metabolism and iron haemostasis are also intimately connected to cancer, such as in colorectal and breast cancer (Marques et al., 2014, Lamy et al., 2014); also, iron chelators have been used as therapeutic agents in cancer chemotherapy (Buss et al., 2004). Iron transport, molecular mechanisms and the subcellular trafficking of proteins involved in iron homeostasis have been well established for the important iron systems such as the transferrin cycle (Anderson and Vulpe, 2009, Lawen and Lane, 2013). In our data, results related to iron systems were indicated as follows: 93 proteins out of 3569 proteins were annotated to haem/iron with 20 of them being included in the 121-OxS data set (Supplementary Table 2, external CD). Noteworthy, these proteins were annotated to different subcellular locations as follows: 10 proteins were annotated to the plasma membrane, 9 to the lysosome, 7 to mitochondria, 5 to the endoplasmic reticulum, 4 to endosomes and 1 to Golgi apparatus, with only 4 proteins annotated to the nucleus. Cytochrome-b5 type B (CYB5B) and NADH-cytochrome-b5 reductase 3

(CYBR3), which are part of the mitochondrial outer membrane, both showed moderate increases in abundance as a response to TBP treatment in the cytoplasmic compartment (S_c = 1.58 and 1.18, respectively) with the strong redistribution from N → C, showing an appreciable decrease in total abundance ($S_t \approx 0.65$), with clearly significantly reduced abundance in the nucleus (S_n = 0.43 and 0.61 respectively). Ferritin heavy/light chains (FTL and FTH1) as well as haemoxygenase (HMOX1) showed a massive increase in total abundance from two- to seven-fold that seem to be mainly equilibrated over the two subcellular compartments as a response to the TBP challenge. V-type ATP synthase showed an increase in total abundance ($S_t \approx 1.8$) with moderate C → N redistribution for many V-type ATP subunits (Figure 3-9). V-type ATP synthase is known to be involved in iron homeostasis regulation by providing acidic conditions for iron metabolism within lysosomes and endosomes (Diab and Kane, 2013). PGRMC1, which is a haem-binding protein with connections to both sterol receptors and autophagy, has been found to promote tumorigenesis (Ahmed et al., 2010b). This protein was not disconnected by STRING (Figure 3-12, 3-13). The cause of this was suggested to have emerged due to a lack of information in the STRING database at the time of analysis, even with extensive reports in the literature about the functional roles of these proteins. However, this defect did not appear to be because of a drawback in the STRING programme, as GeneMania also showed the same results. This means that the currently available databases might be dominated by large-scale co-expression and physical interaction data sets.

Many iron- and haem-related proteins also play additional roles that are associated with vesicle-mediated subcellular trafficking or are present in the extracellular vesicular exosome. The current experiments provided strong evidence for an important role of trafficking of iron/haem proteins in the response to oxidative stress. However, the interpretation of results was complex, due to the shortage of details about the

subcellular trafficking of iron/haem and proteins containing these cofactors in both yeast (Cyert and Philpott, 2013) and metazoans (Hamza and Dailey, 2012). This is supported by the evidence that mitochondria are highly dynamic organelles with constitutive processes, including the transfer of proteins by vesicular trafficking to organelles such as peroxisomes and lysosomes (Braschi et al., 2010, Mohanty and McBride, 2013).

It has been reported that, under acute oxidative stress, mitochondria are located close to the nucleus and fragment in order to initiate the damage control process mitoptosis, which is a novel mitochondrial death mechanism, leading to the release of mitochondrial proteins into the vesicular exosome (Arnoult et al., 2005, Lyamzaev et al., 2008). Some of these proteins have been shown to be altered in nuclear abundance in our data. Recent evidence has been found to suggest that mitochondrial cristae vesicularise in ageing cells and ATP synthase dissociates into monomers in the inner membrane vesicles, which results in reduced cellular function (Daum et al., 2013). One of the mitochondrial proteins, LETM1, which was significantly decreased in nuclear abundance within the 121-OxS data set (Supplementary Table 2, external CD), is known to be involved in crista formation. Reduced expression of the ATP synthase subunits has been believed to be essential for the oligomerisation of ATP synthase dimers, which may result in fission and the altered organisation of mitochondria (Habersetzer et al., 2013). Noteworthy, ATP synthase dimmers, which are different to those in mitochondrial cristae, are from the mitochondrial permeability transition pore (Bernardi, 2013, Giorgio et al., 2013). Also, TBP has been found to encourage mitochondrial depolarisation (Greco and Fiskum, 2010, Greco et al., 2011). This might help to explain the changes in many ATP synthase subunits that were observed in our data with regard to nuclear abundance, and may offer a clear mechanism for this.

ROS bursts in mitochondria may play different roles under normal or disease conditions

(Xu et al., 2013, Wang et al., 2008b, Wang et al., 2012). Recently, it has been suggested that mitochondrial proteins can be transferred by vesicle-mediated transport to lysosomes under oxidative stress, which is a different process than mitophagy (Soubannier et al., 2012).

Chapter 5: Comparison of Changes for Oxidative Stress and Cell Cycle Arrest Data

The analyses of the changes in nucleus-cytoplasm subcellular abundance and distribution for IMR90 cells subjected either to: (a) siRNA repression of the Cdc7 kinase, which leads to cell cycle arrest at the G1/S transition via the origin activation checkpoint (OAC) for DNA replication (Mulvey et al., 2013); or, (b) mild oxidative stress initiated with treatment of the cells with tert-butyl hydrogen peroxide (TBP), have been described by (Mulvey et al., 2013, Mulvey et al., 2010) and in previous chapters.

In each individual study for SILAC ratios for several thousand proteins were obtained, a set of about 120 proteins with the most significant changes was identified, and analysis with a subcellular spatial razor approach (Mulvey et al., 2013, Pinto et al., 2014) revealed that changes both in total protein abundance and in nucleo-cytoplasmic distribution resulted in distinctive patterns of protein abundance changes in the nuclear/cytoplasmic compartments that are the basis of the cellular response to each type of stimulation (Mulvey et al., 2013). In this chapter I present a joint analysis of the data from the two experiments to further explore connections between oxidative status and the cell cycle.

The original experiments and MS data collected for Cdc7-depletion-induced cell cycle arrest at the origin activation checkpoint for DNA replication (OAC-set (Mulvey et al., 2013)) and on mild tert-butyl-peroxide-induced oxidative stress (OxS-set (Chapter 3)) have been described in detail. These studies included extensive evidence that the cells remained viable without perceptible cell death and that the protocols used for subcellular fractionation gave highly enriched nuclear fractions with very little or no cross contamination with other subcellular components such as mitochondria, endoplasmic reticulum, plasma membrane, etc. Flow cytometery analysis indicated cell

cycle arrest for both stimulations. In order to compare the changes for oxidative stress and cell cycle arrest the original MS data from the two experiments were reprocessed under identical conditions against a common UniProt proteome set using MaxQuant (Cox and Mann, 2008). For each of the two experiments SILAC ratios were calculated for 12 data subsets: each nucleus (N) replicate and the union of the three replicates, each cytoplasm (C) replicate and the union of the three replicates, and each (C&N) replicate and the union of the three replicates. C&N denotes that the MS data for the nucleus and cytoplasm samples was jointly processed to estimate changes in total abundance. Correlation of the identified peptides across all biological samples detected 4733 distinct proteins. With a limit of at least two sequenced peptides and at least one sample with a minimum of three SILAC ratio counts, 4048 proteins were quantified (Supplementary Table 4, external CD).

A. SELECTION LIMITS						
SILAC ratio counts >=		SigB limit <=				
abundance		STRINGENT	STRICT	MODERATE	RELAXED	MINIMUM
union	6	0.0025	0.0075	0.015	0.02	0.05
replicates						
Sn	3	0.0075	0.015	0.03	0.05	0.07
Sc	3	0.0075	0.015	0.03	0.05	0.07
St (C&N)	3	0.0075	0.015	0.03	0.05	0.07
distribution				| log2(Sn/Sc) | >=		
union	6	0.9	0.8	0.6	0.5	0.4
replicate	3	0.8	0.6	0.5	0.4	0.3
B. NUMBER OF SIGNIFICANT PROTEINS						
data set		STRINGENT	STRICT	MODERATE	RELAXED	MINIMUM
OXS only		112	145	196	229	308
OAC only		98	125	156	195	263
TOTAL		224	289	382	467	633
BOTH		14	19	30	43	62

[1] Proteins accepted as significant for changes in abundance and/or distribution satisfy the limits for the union and for at least two replicates .

Table 5-1. Summary of Significance B Selection Significant Proteins in Both OAC and OxS data sets[1] (Supplementary Table 5, external CD).

Because the absolute magnitude of the changes in protein abundance are dependent on the degree of Cdc7 kinase suppression (OAC) or on the concentration of tert-butyl peroxide to which the cells are exposed (OxS), it is not very helpful to directly compare the absolute changes in protein abundance between the two experiments. Instead, we used a procedure that identifies sets of proteins with the most significant changes in abundance relative to all quantified proteins in each individual experiment. MaxQuant uses a procedure that takes into account the recorded MS intensity for each protein to calculate an outlier probability (Significance B score, hereafter SigB) that identifies the most significantly changed proteins in each data set (Cox and Mann, 2008). Table 5-1 shows the number of significant proteins for different cutoffs of $SigB^{union}$, $SigB^{replicate}$ and the distribution parameter $\log_2(S_n/S_c)$, which detects changes in subcellular distribution even in the absence of changes in total abundance. In constructing the sets of proteins in Table 5-1 we restricted the proteins accepted as significant to those with appreciable recorded MS intensity and substantial numbers of SILAC ratio counts by using a $SigB^{union}$ limit for the union of the three replicates, a $SigB^{replicate}$ limit to ensure reproducibility over the replicates, as well as a minimum number of SILAC ratio counts. At all cutoff limits, roughly equal numbers of proteins were identified as significant in the OxS and OAC data sets, i.e. the response to the two different cellular stimulations is sampled approximately equally. As an initial test for possible similarities/differences between response to oxidative stress and cell cycle arrest, we compared the OxS and OAC sets of proteins using the stringent selection criteria (Supplementary Table 5, external CD). For the 224 proteins selected as most significant there were 112 proteins significant only for OxS, 98 proteins significant only for OAC and 14 proteins that were significant for both cellular stimulations.

For 110 proteins, S_c and S_n were quantified in both experiments. Their behavior in the two experiments is shown in a 3D spatial razor plot (Figure 5-1A). In this type of plot,

changes in subcellular nucleo-cytoplasmic distribution are displayed in a (S_n/S_t, S_c/S_t) distribution plane that is independent of changes in total abundance while changes in total abundance are displayed on an orthogonal S_t axis that is color-coded according to the scale at the right (Figure 5-1). Conservation of mass restricts the data points to two quadrants of the distribution plane corresponding to N → C or N ← C redistribution (Mulvey et al., 2013, Pinto et al., 2014). Out of these 110 proteins, 45 showed greater than 1.5-fold changes in total abundance (S_t) and 62 showed $|\log_2(S_n/S_c)| > 0.9$ in one or both of the OxS and OAC data sets. That is, changes both in total abundance and in nuclear-cytoplasmic distribution are prominent in the cellular responses. We have previously shown that changes in total abundance (S_t) and in subcellular distribution (S_n/S_c) are not correlated for either OxS or OAC (Mulvey et al., 2013), i.e., the changes in compartmental abundance (S_n and/or S_c) do not simply mirror changes in total abundance.

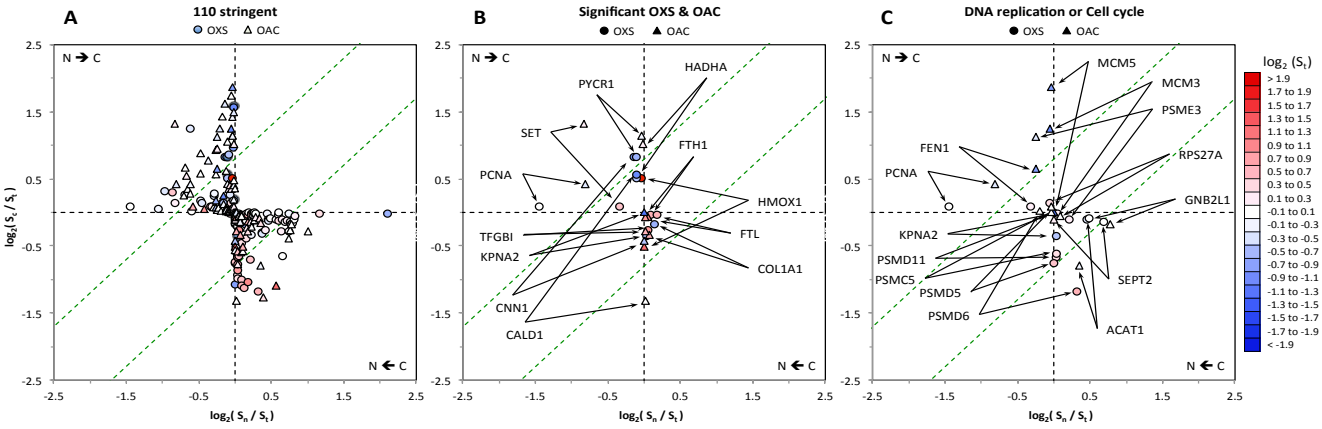

Figure 5-1. 3D Spatial Razor Plots Comparing Response to OxS and OAC. Quadrants corresponding to N → C and N ← C redistribution are shown in the distribution plane and changes in total abundance are colour coded according to the scale at the right. (A) 110 proteins that were significant in both the OxS and OAC data sets with stringent selection criteria. (B) 12 proteins that were most significant in both the OxS and OAC data sets. (C) 14 proteins with GO annotation to DNA replication and/or cell cycle.

Of the 14 proteins common to the OxS and OAC stringent sets, both S_c and S_n were quantified in both experiments for 12 proteins (Figure 5-1B). Although over the different proteins the changes in abundance and distribution tend to vary continuously and hence the classes are not completely separable, comparison of OxS and OAC distinguishes four approximate types of response behavior. (a) Proteins for which changes show the same trend for OxS and OAC. For example FTL, FTH1 and TGFBI show large increase in total abundance with little redistribution in both experiments, KPNA2 shows decreased total abundance with limited redistribution in both experiments, while PYCR1 shows decreased total abundance and N → C redistribution in both experiments. (b) Proteins for which total abundance changes show the same trend, but distribution changes tend to be different (SET, CNN1, HMOX1). (c) Proteins for which total abundance changes are different, but redistribution shows the same trend (PCNA, HADHA, COL1A1), (d) Proteins for which both total abundance and distribution show opposing trends (HSPA9). Such differences suggest that there may be some protein networks with similar behavior for OxS and OAC, other networks that are characteristic of one or the other of OxS or OAC, and some networks that behave differently between the two cellular responses. Further evidence for differential behavior was obtained from the 12 proteins that were quantified in both the nucleus and cytoplasm and were annotated by GO to DNA replication and/or cell cycle, which were the dominant biological processes determined for OAC (Mulvey et al., 2013). As shown in Figure 5-1C, changes for subunits of the MCM helicase complex (MCM3, MCM5), which is essential for pre-Replication Complex loading at DNA replication origins and is a direct substrate of Cdc7 kinase, are limited to OAC. Conversely, changes in several proteasome subunits (PSMC5, PSMD5, PSMD6, PSMD11), Ubiquitin-40S (RPS27A) and Septin 2 (SEPT2) are limited to OxS. The proteins PCNA, FEN1, PSME3, KPNA2, ACAT1 and GNB2L1 show indications of participating in response to both OxS and

OAC. In general the results in Figure 5-1 indicate that changes in both total abundance and in subcellular distribution are important to determining the compartmental abundance of proteins and hence in determining cellular response. Furthermore, at all levels of stringency in the selection criteria for significant proteins (Table 5-1), a small proportion of the significant proteins (6-9%) is common to both OxS and OAC.

Although these initial analyses are helpful in understanding and visualizing trends, individual determination of the sets of most significant OxS and OAC proteins restricts the number of proteins that can be compared, limits ability to identify network responses that are similar, different or exclusive to one or the other of OxS and OAC, and limits identification of possible connections between the networks. We therefore carried out a direct, joint analysis of the full OxS and OAC data sets.

5.1 Joint Spatial Razor Plots for OxS and OAC

At the level of at least three SILAC ratio counts in the union, there were a total of 6099 pairwise values of one or more of S_c, S_n, S_t and S_n/S_c for the same protein in both the OAC and OxS data sets. These corresponded to 2388 different proteins. To jointly analyze the data sets for similarities and differences in cellular response, to include proteins which were quantified in only one of the subcellular compartments and to handle all four types of comparisons (S_c, S_n, S_t, S_n/S_c) equivalently, we plotted S^{OXS} / S^{OAC} versus $S^{OXS} \bullet S^{OAC}$ for each of the four types of SILAC ratios. In this "joint spatial razor" plot the 6099 data points cluster around the origin, that is, only a minority of proteins show major changes in their SILAC ratios in either experiment (Figure 5-2A,B). The radial distance from the origin for the data points gave highly similar distributions for each of the four types of comparison, as shown for S_n and the union over (S_c, S_n, S_t, S_n/S_c) in Figure 5-2C.

The “joint spatial razor” plot classifies the SILAC ratios into regions such that the cellular response can be analyzed for dominance of one stimulation, for similarity in both responses or for opposite response to the two stimulations (see the colored radial regions in Figure 5-2D). This is very helpful for visualizing the nature of any correlation in the changes for OxS and OAC. For example, the heavy subunit of ferritin (FTH1) shows a strong increase in total abundance for both OxS and OAC, but little or no subcellular redistribution, so that abundance in both the nuclear and cytoplasmic compartments is strongly increased for both OxS and OAC. Conversely, proliferating cell nuclear antigen (PCNA) shows strong N → C redistribution, but limited change in total abundance for both OxS and OAC, so that nuclear abundance is substantially decreased for both OxS and OAC. OAC is strongly dominant for DNA replication licensing factor MCM5. The combination of reduced total abundance and strong N → C redistribution leads to a major reduction in nuclear abundance coupled to an appreciable increase in cytoplasmic abundance. Pyrroline-5-carboxylate reductase 1 (PYCR1) shows strong N → C redistribution for both OxS and OAC, but reduction in total abundance predominantly for OxS.

This results in strong reduction in nuclear abundance mainly for OxS and strong increase in cytoplasmic abundance mainly for OAC. In short, the combination of changes in total abundance and in subcellular distribution can lead to complex patterns of changes in the compartmental abundances that vary between OxS and OAC.

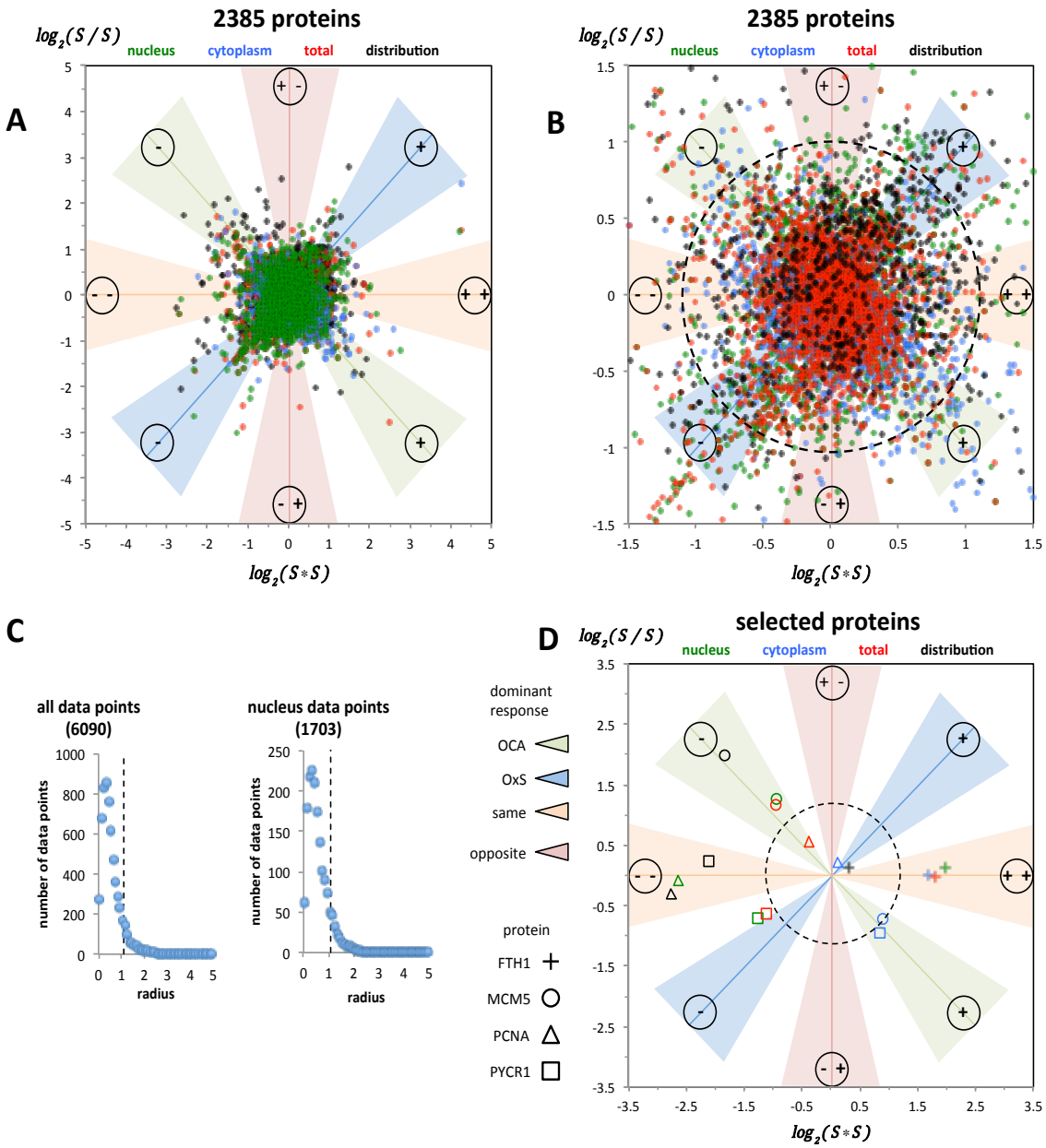

Figure 5-2. Joint Spatial Razor Plot of the OxS and OAC data sets. (A) Plots of $\log_2(S^{OXS}/S^{OAC})$ vs $\log_2(S^{OXS} \bullet S^{OAC})$ for S_n/S_c, S_t, S_c, S_n, (back to front). The four types of comparisons are color coded according to the legend at the top. (B) Expansion of the central region of (A) with reverse back to front order. (C) Radial distribution of the data points in (A) for the union over all 6090 data points and for the 1703 nuclear data points. (D) Examples of response for four selected proteins (see text). The dashed black circles in (B) and (D) correspond to radius = 1.1 as indicated in (C). The colored radial slices (see D) represent angular regions where the dominant response is at least twice that of the neighboring regions. The circled + and – symbols denote increases/decreases in abundance (S_n, S_c, S_t) or C → N / N → C redistribution (S_n/S_c) respectively. Figure was designed by JGZ for publication in preparation by Radulovic et all, 2015.

By selecting proteins that correspond to specific functional processes, e.g. glycolysis (Figure 5-3A), or to specific subcellular locations, e.g. mitochondria (Figure 5-3B), the functional interplay between changes in abundance and in subcellular location can begin to be visualized. For example, 8 proteins of the glycolysis/gluconeogenesis enzymatic cascade were monitored in both the cytoplasm and nucleus in both experiments. Only hexokinase 1 (HK1) showed appreciable change: N ← C redistribution without change in total abundance led to strongly increased nuclear abundance only for OxS (Figure 5-3A). This is a known effect that is related to the metabolic fate of glucose and to metabolism in cancer cells (Mathupala et al., 1997, Neary and Pastorino, 2010, Wilson, 2003, John et al., 2011).

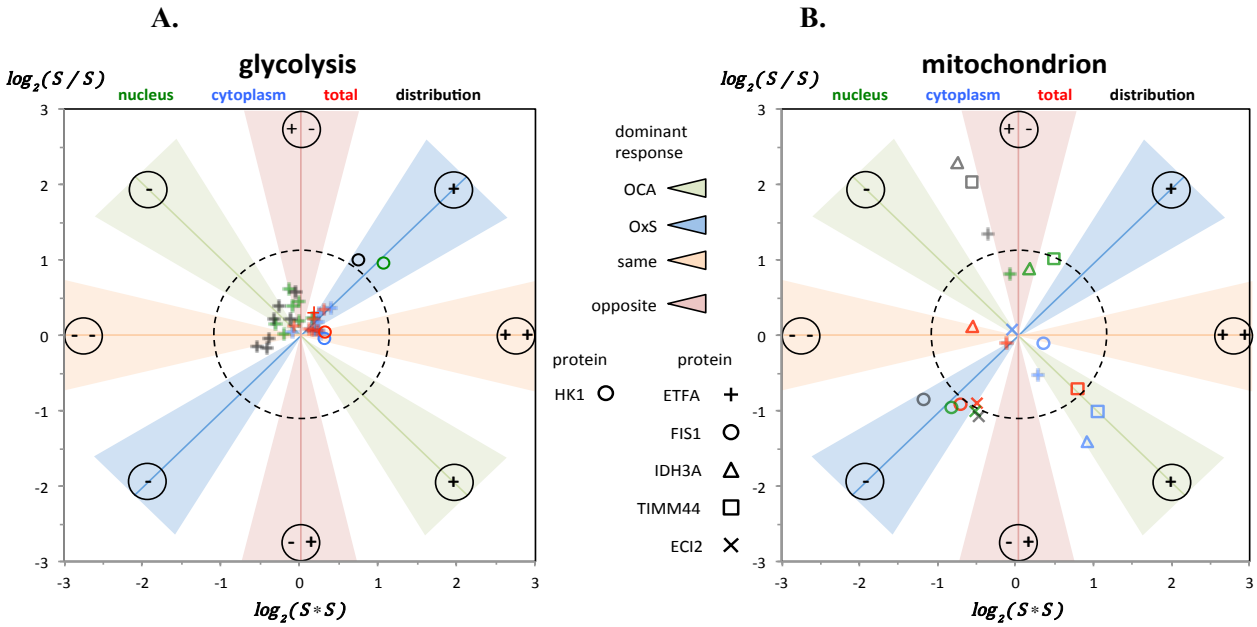

Figure 5-3. Joint Spatial Razor Plots for Selected Proteins. A. Eight proteins of the glycolytic enzymatic cascade (HK1, GAPDH, TPI1, ALDOA, ENO1, PKM2, PGAM1, LDHA). **B.** Five proteins with GO annotation to mitochondria.

None of the other seven enzymes (GAPDH, TPI1, ALDOA, ENO1, PKM2, PGAM1, LDHA) showed major changes in either experiment.

Similarly, Figure 5-3B shows the joint analysis for 5 proteins with GO annotations of mitochondrion. Mitochondrial fission 1 protein (FIS1) and Enoyl-CoA delta isomerase 2 (ECI2) show similar, predominant response for OxS involving decreased total abundance and N → C redistribution, hence strong decreases in nuclear abundance with little change in cytoplasmic abundance. Subunit alpha of the electron transfer flavoprotein (ETFA) shows little change in total abundance and opposite N ←→ C redistribution for OxS and OAC, hence moderate, opposed changes in nuclear abundance. Subunit alpha of isocitrate dehydrogenase [NAD] (IDH3A) shows small decreases in total abundance for OxS and OAC and largely opposite N ←→ C redistribution, which results in a modest increase in nuclear abundance for OxS and an appreciable increase in cytoplasmic abundance for OAC.

Finally, mitochondrial import inner membrane translocase subunit TIM44 shows increased total abundance only for OAC and strong, opposite N ←→ C redistribution, which results in a substantial increase in abundance in the cytoplasmic compartment for OAC (S_c = 2.04, S_n = 0.83) and in the nuclear compartment for OxS (S_c = 1.04, S_n = 1.68). These and other changes are considered further in the context of a joint network analysis (in preparation by Radulovic et all, 2015). Overall these results suggested that nucleo-cytoplasmic trafficking of proteins is an integral component of the cellular response to both stimulations and provided an additional evidence for the possible involvement of nuclear import/export processes and/or of vesicle-mediated transport processes.

Chapter 6: Conclusions and Impact of these Findings

Major conclusion of the thesis can be summarised as follows:

Different conditions can affect protein behaviours and distributions over the subcellular compartments, as in mild oxidative stress, which also activates cell cycle checkpoints within the IMR90 fibroblasts, leading to cell cycle arrest.

The results of the thesis clearly show the involvement of numerous proteins with various functions, including cell cycle control, mitochondrial function, iron metabolism, signaling systems and other functional processes, with significant changes in nucleo-cytoplasmic compartmental abundance in response to oxidative stress.

These changes also included proteins that are known to be present in different non-nuclear subcellular locations.

Protein redistribution between the nucleus and cytoplasm is equally as important as changes in total protein abundance in order to achieve the appropriate changes in compartmental abundance; this is because changes in total protein abundance alone still give a general overview without a comprehensive picture for the appropriate changes the cellular response to TBP.

The cellular behaviours and characteristics have been observed before under different conditions, including cell cycle arrest (Mulvey et al., 2013) at the original activation checkpoint for DNA replication and in response to hypoxia (Henke et al., 2011).

Nucleocyoplasmic trafficking of proteins has also been observed in breast cancer in response to oestrogen stimulation (Pinto et al., 2014), which supports the concept of the need to learn more about the mechanism of protein distribution and their behaviours in different subcellular locations, such as the nucleus.

A total of 115 proteins in 121-OxS were found in the nucleus, with 45 also annotated by GO to the nucleus. However, the nuclear function of 80 proteins was unclear. There were sixty-three proteins found in our data with highly significant changes in S_n; however, 40 proteins were found not to be annotated to the nucleus. These proteins are linked to many functional processes and suggest many interesting entry points in the context of oxidative stress.

The involvement of iron/haem proteins in response to oxidative stress is not surprising, as haem has been shown to be crucial for eukaryotic evolution (Chiabrando et al., 2014).

Moreover, the specific selection of RAB proteins and kinesins that are known to be intimately involved in vesicular trafficking (Huotari and Helenius, 2011) (RAB2A, RAB5A, RAB5B, KIF14, KIF20A) gave a strong indication of the contribution of vesicular trafficking in the nucleus in response to TBP treatment.

Apart from cancer cells, around 2-5% of the total of cellular proteins showed significant changes under specific conditions.

These results clearly show very selective changes in the local abundance over the different subcellular locations, which can help to improve the model for cellular function. This can be achieved by the inclusion of spatial location as an explicit factor coupled with powerful databases to further understand the cellular interactions.

Chapter 7: Future Studies

Spatial razor proteomics coupled with downstream bioinformatics analysis are a potent way to study protein abundance and behaviour under specific conditions. As mentioned before, our present experiments coupled with suggestive evidence from the literature can enable an interpretation of this data, which would seem to be that vesicular trafficking occurs more widely in higher eukaryotic cells than is presently known. The supporting evidence for that is that GO annotated around 1427 proteins in our data to "vesicle-mediated transport" or to "cytoplasmic vesicle". This also suggests that the nucleus, mitochondria, other subcellular organelles and haem/iron proteins participate in vesicular trafficking. Therefore, the involvement of iron/haem proteins in trafficking led us to suggest three possibilities for further investigation of the possible role of proteins involved in iron/haem metabolism in subcellular trafficking in response to oxidative stress. First, subcellular trafficking of the membrane-associated progesterone receptor (MAPR) family PGRMC1, PGRMC2, neudesin and neuferricin of cytochrome-*b*-related, haem-containing proteins (Kimura et al., 2012) could be investigated. The prototype of this family is PGRMC1, which showed strong N → C redistribution with $\log_2 (S_n/S_c) = -1.17$ in our data with no change in total abundance ($St = 0.99$), resulting in a strong decrease in nuclear abundance ($S_n = 0.54$) and a moderate increase in cytoplasmic abundance ($S_c = 1.22$). PGRMC1 has been widely reported as part of a plasma membrane receptor for progesterone that acts independently of the classical progesterone nuclear hormone receptor in most cells, including in neuronal cells (Bali et al., 2013, Petersen et al., 2013).

PGRMC1 has recently been suggested as an attractive target for future investigations for several reasons: it was found to be part of a protein complex that has the binding site for the enigmatic sigma-2-recptor, which is known to regulate lipid metabolism,

hormone signaling, and it is certified as a biomarker for tumour cell proliferation, with both the receptor and PGRMC1 being important for cancer (Xu et al., 2011). According to previously published reports, PGRMC1 is located within several cellular compartments such as the ER and mitochondria (Xu et al., 2011), the cellular vesicular fraction (Ahmed et al., 2010a), in the perinuclear region and in the nucleus (Bali et al., 2013). PGRMC1 has been found to play a role in autophagy (Mir et al., 2013), regulating genes that inhibit apoptosis via progesterone (Peluso et al., 2010, Peluso et al., 2012) and can also act as an adaptor protein for membrane receptors (Thomas et al., 2014). PGRMC1 has been found to interact with plasminogen activator inhibitor 1 RNA-binding protein (PAIRBP1) for nuclear transcriptional functions (Peluso et al., 2013) and co-localises with aurora kinase b (AURKB) in chromatin during oocyte maturation processes (Luciano et al., 2010). AURKB and plasminogen activator inhibitor 1 (SERPINE1) were found in our significant 121-OxS data set. This suggests intimate connections between oxidative stress and various PGRMC1 functions, and PGRMC1 may have redox ability that could be crucial for its multitude of functions. As a haem-containing protein with multiple known subcellular locations, interactions, and functions, PGRMC1 seems to be an excellent candidate for the further elucidation of possible connections between haem protein trafficking and oxidative stress. Cytochrome b5 type B (CYB5B) and its partner NADH-cytochrome b5 reductase 3 (CYB5R3) were also found in our data, which are mitochondrial outer membrane proteins; these showed noticeable N → C redistribution, and may also be useful candidates for further investigation.

The second target for further investigation and future work is the subcellular trafficking of NADPH oxidase 4 (NOX 4). NOX4 is an integral membrane protein that consists of six transmembrane helices that contain two haem groups (Bedard and Krause, 2007). Under specific conditions that apparently include H_2O_2, NOX4 and POLDIP2

dynamically co-localise to the nucleus for the production of collagen (Lyle et al., 2009). In our data, NOX4 was not quantified; however, there was an increase in the nuclear POLDIP2 and a reduction in cellular collagen (COL1A1) that may be mediated via the proline regulatory axis (Figure 3-14C). NOX4 has been detected in different subcellular locations, including the endoplasmic reticulum (Van Buul et al., 2005), mitochondria (Ago et al., 2010, Block et al., 2009) and particular plasma membrane subcellular domains such as focal adhesions (Hilenski et al., 2004) and invadopodia (Diaz et al., 2009, Diaz and Courtneidge, 2012). NOX4 can produce ROS in the nucleus (Matsushima et al., 2010, Spencer et al., 2011), mitochondria (Kartha et al., 2008, Ago et al., 2010) and ER (Sciarretta et al., 2013) and it has been found to be associated with different cellular functions and diseases such as cancer, diabetic kidney disease, cardiovascular disease, Alzheimer's disease, fibrosis, and atherosclerosis (For review, see (Barnes and Gorin, 2011, Drummond et al., 2011, Block and Gorin, 2012, Bedard and Krause, 2007)). As mentioned before, the structure and catalytic function of NOX4 allow it to transfer electrons from NADPH across the cellular membrane to molecular oxygen locations (Bedard and Krause, 2007). However, the mechanism responsible for NOX4 transport to different subcellular locations is still unclear due to limited information. Thus, vesicular trafficking might help to understand how for an integral membrane protein such NOX4 with unknown function to import/export via nuclear pore reaches the nucleus.

The third interesting suggestion involves the possibility of vesicle trafficking in iron homeostasis via studying the subcellular trafficking of the V-type ATPases (ATP6). V-type ATPases regulate the cellular pH of the cytoplasm and acidic organelles (Beyenbach and Wieczorek, 2006, Diab and Kane, 2013) to protect cells against the loss of pH homeostasis due to oxidative stress and iron misregulation (Milgrom et al., 2007). This might be an attractive target for studying the functional roles of V-type ATPases.

Iron interacts with hydrogen peroxide causing cellular damage; for that reason, V-type ATPases mitigate and prevent this effect by stabilising the acidic environment within the endosomes and lysosomes (Valko et al., 2005).

P26/SQSMT1 interacts with V-type ATPase in the lysosomes and activates the rapamycin mTOR pathway, which is involved in important cellular functions such as cell growth and autophagy (Duran et al., 2011), senescence and amino acid metabolism (Zoncu et al., 2011). The insulin receptor-signaling pathway is also affected by V-type ATPases; for example, it has been found that the acidic environment in the endosomes leads insulin to dissociate from its receptor via V-type ATPases (O'Callaghan et al., 2010). This pathway was also observed in our data (Table 3-2). However, there were 21 proteins known to be involved in the insulin receptor pathway that were not significant in our data in either total or compartmental abundance. This might reflect the fact that there was a consequence of changes, which might occur as a response to the processes acidification/depolarisation of endosomes/lysosomes. As a result, the depolarisation of endosomes and lysosomes due to cyclic bursts of pH (Valko et al., 2005, Diab and Kane, 2013) might explain normal physiological mechanisms for discarding V-type ATPases. Most V-type ATPase subunits are currently annotated by GO to most of the cellular compartments, such as the mitochondria, plasma membrane, endosomes, lysosomes, Golgi apparatus, vacuoles, nucleus, and cytoplasmic vesicles. Noteworthy, V-type ATPases have also been found to be involved in vesicle trafficking (Beyenbach and Wieczorek, 2006, Brown et al., 2009, Gu and Gruenberg, 2000). One of these subunits is ATP6V0C, which has been found to regulate the metabolism of autophagy proteins that are accumulated in age-related neurodegenerative diseases (Mangieri et al., 2014). Moreover, the renin receptor ATP6AP2 was found in our data with S_t = 1.59, S_n = 1.71. ATP6AP2 is also known to interact with V-type ATPases in the Wnt/β-catenin signaling pathway, but there are still unclear connections to the renin−angiotensin

hormonal system, similar to various other signaling systems (Kops et al., 2002b). Interestingly, subunits of V-type ATPases might be involved in a variety of processes/locations different to those that have been well studied, such as the transfer of these subunits to the nucleus under conditions of oxidative stress.

References

ADACHI, M., FISCHER, E. H., IHLE, J., IMAI, K., JIRIK, F., NEEL, B., PAWSON, T., SHEN, S., THOMAS, M., ULLRICH, A. & ZHAO, Z. 1996. Mammalian SH2-containing protein tyrosine phosphatases. *Cell,* 85**,** 15.

ADAM, J., HATIPOGLU, E., O'FLAHERTY, L., TERNETTE, N., SAHGAL, N., LOCKSTONE, H., BABAN, D., NYE, E., STAMP, G. W., WOLHUTER, K., STEVENS, M., FISCHER, R., CARMELIET, P., MAXWELL, P. H., PUGH, C. W., FRIZZELL, N., SOGA, T., KESSLER, B. M., EL-BAHRAWY, M., RATCLIFFE, P. J. & POLLARD, P. J. 2011. Renal cyst formation in Fh1-deficient mice is independent of the Hif/Phd pathway: roles for fumarate in KEAP1 succination and Nrf2 signaling. *Cancer Cell,* 20**,** 524-37.

AEBERSOLD, R. & MANN, M. 2003. Mass spectrometry-based proteomics. *Nature,* 422**,** 198-207.

AGO, T., KURODA, J., PAIN, J., FU, C., LI, H. & SADOSHIMA, J. 2010. Upregulation of Nox4 by hypertrophic stimuli promotes apoptosis and mitochondrial dysfunction in cardiac myocytes. *Circ Res,* 106**,** 1253-64.

AHMED, I. S., ROHE, H. J., TWIST, K. E. & CRAVEN, R. J. 2010a. Pgrmc1 (progesterone receptor membrane component 1) associates with epidermal growth factor receptor and regulates erlotinib sensitivity. *J Biol Chem,* 285**,** 24775-82.

AHMED, I. S., ROHE, H. J., TWIST, K. E., MATTINGLY, M. N. & CRAVEN, R. J. 2010b. Progesterone receptor membrane component 1 (Pgrmc1): a heme-1 domain protein that promotes tumorigenesis and is inhibited by a small molecule. *J Pharmacol Exp Ther,* 333**,** 564-73.

AL-MEHDI, A. B., PASTUKH, V. M., SWIGER, B. M., REED, D. J., PATEL, M. R., BARDWELL, G. C., PASTUKH, V. V., ALEXEYEV, M. F. & GILLESPIE, M.

N. 2012. Perinuclear mitochondrial clustering creates an oxidant-rich nuclear domain required for hypoxia-induced transcription. *Sci Signal,* 5**,** ra47.

ALFADDA, A. A. & SALLAM, R. M. 2012. Reactive oxygen species in health and disease. *J Biomed Biotechnol,* 2012**,** 936486.

ANDERSON, G. J. & VULPE, C. D. 2009. Mammalian iron transport. *Cell Mol Life Sci,* 66**,** 3241-61.

ANDERSON, L. & SEILHAMER, J. 1997. A comparison of selected mRNA and protein abundances in human liver. *Electrophoresis,* 18**,** 533-7.

ANDERSON, N. L. & ANDERSON, N. G. 1998. Proteome and proteomics: New technologies, new concepts, and new words. *Electrophoresis,* 19**,** 1853-1861.

ARNOULT, D., RISMANCHI, N., GRODET, A., ROBERTS, R. G., SEEBURG, D. P., ESTAQUIER, J., SHENG, M. & BLACKSTONE, C. 2005. Bax/Bak-dependent release of DDP/TIMM8a promotes Drp1-mediated mitochondrial fission and mitoptosis during programmed cell death. *Curr Biol,* 15**,** 2112-8.

AU, C. E., BELL, A. W., GILCHRIST, A., HIDING, J., NILSSON, T. & BERGERON, J. J. 2007. Organellar proteomics to create the cell map. *Curr Opin Cell Biol,* 19**,** 376-85.

BABIOR, B. M., LAMBETH, J. D. & NAUSEEF, W. 2002. The neutrophil NADPH oxidase. *Arch Biochem Biophys,* 397**,** 342-4.

BADER, G. D. & HOGUE, C. W. 2003. An automated method for finding molecular complexes in large protein interaction networks. *BMC Bioinformatics,* 4**,** 2.

BAE, Y. S., KANG, S. W., SEO, M. S., BAINES, I. C., TEKLE, E., CHOCK, P. B. & RHEE, S. G. 1997. Epidermal growth factor (EGF)-induced generation of hydrogen peroxide. Role in EGF receptor-mediated tyrosine phosphorylation. *J Biol Chem,* 272**,** 217-21.

BALI, N., MORGAN, T. E. & FINCH, C. E. 2013. Pgrmc1: new roles in the microglial mediation of progesterone-antagonism of estradiol-dependent neurite sprouting and in microglial activation. *Front Neurosci,* 7**,** 157.

BAQADER, N. O., RADULOVIC, M., CRAWFORD, M., STOEBER, K. & GODOVAC-ZIMMERMANN, J. 2014. Nuclear-Cytoplasmic Trafficking of Proteins is a Major Response of Human Fibroblasts to Oxidative Stress. *J Proteome Res*.

BARNES, J. L. & GORIN, Y. 2011. Myofibroblast differentiation during fibrosis: role of NAD(P)H oxidases. *Kidney Int,* 79**,** 944-56.

BARTEK, J., LUKAS, C. & LUKAS, J. 2004. Checking on DNA damage in S phase. *Nat Rev Mol Cell Biol,* 5**,** 792-804.

BEDARD, K. & KRAUSE, K. H. 2007. The NOX family of ROS-generating NADPH oxidases: physiology and pathophysiology. *Physiol Rev,* 87**,** 245-313.

BELL, S. P. & DUTTA, A. 2002. DNA replication in eukaryotic cells. *Annual review of biochemistry,* 71**,** 333-74.

BERNARDI, P. 2013. The mitochondrial permeability transition pore: a mystery solved? *Front Physiol,* 4**,** 95.

BEYENBACH, K. W. & WIECZOREK, H. 2006. The V-type H+ ATPase: molecular structure and function, physiological roles and regulation. *J Exp Biol,* 209**,** 577-89.

BEYNON, R. J. & BOND, J. S. 1989. *Proteolytic enzymes : a practical approach,* Oxford, IRL.

BIAMONTI, G., PAIXAO, S., MONTECUCCO, A., PEVERALI, F. A., RIVA, S. & FALASCHI, A. 2003. Is DNA sequence sufficient to specify DNA replication origins in metazoan cells? *Chromosome research : an international journal on the molecular, supramolecular and evolutionary aspects of chromosome biology,* 11**,** 403-12.

BINNS, D., DIMMER, E., HUNTLEY, R., BARRELL, D., O'DONOVAN, C. & APWEILER, R. 2009. QuickGO: a web-based tool for Gene Ontology searching. *Bioinformatics,* 25**,** 3045-6.

BJORKOY, G., LAMARK, T., BRECH, A., OUTZEN, H., PERANDER, M., OVERVATN, A., STENMARK, H. & JOHANSEN, T. 2005. p62/SQSTM1 forms protein aggregates degraded by autophagy and has a protective effect on huntingtin-induced cell death. *Journal of Cell Biology,* 171**,** 603-614.

BLOCK, K. & GORIN, Y. 2012. Aiding and abetting roles of NOX oxidases in cellular transformation. *Nat Rev Cancer,* 12**,** 627-37.

BLOCK, K., GORIN, Y. & ABBOUD, H. E. 2009. Subcellular localization of Nox4 and regulation in diabetes. *Proc Natl Acad Sci U S A,* 106**,** 14385-90.

BLOOM, D., DHAKSHINAMOORTHY, S. & JAISWAL, A. K. 2002. Site-directed mutagenesis of cysteine to serine in the DNA binding region of Nrf2 decreases its capacity to upregulate antioxidant response element-mediated expression and antioxidant induction of NAD(P)H:quinone oxidoreductase1 gene. *Oncogene,* 21**,** 2191-200.

BLOW, J. J. & GILLESPIE, P. J. 2008. Replication licensing and cancer--a fatal entanglement? *Nature reviews. Cancer,* 8**,** 799-806.

BOLAND, M. L., CHOURASIA, A. H. & MACLEOD, K. F. 2013. Mitochondrial dysfunction in cancer. *Front Oncol,* 3**,** 292.

BONUCCELLI, G., WHITAKER-MENEZES, D., CASTELLO-CROS, R., PAVLIDES, S., PESTELL, R. G., FATATIS, A., WITKIEWICZ, A. K., VANDER HEIDEN, M. G., MIGNECO, G., CHIAVARINA, B., FRANK, P. G., CAPOZZA, F., FLOMENBERG, N., MARTINEZ-OUTSCHOORN, U. E., SOTGIA, F. & LISANTI, M. P. 2010. The reverse Warburg effect: glycolysis inhibitors prevent the tumor promoting effects of caveolin-1 deficient cancer associated fibroblasts. *Cell Cycle,* 9**,** 1960-71.

BRASCHI, E., GOYON, V., ZUNINO, R., MOHANTY, A., XU, L. Q. & MCBRIDE, H. M. 2010. Vps35 Mediates Vesicle Transport between the Mitochondria and Peroxisomes. *Current Biology,* 20**,** 1310-1315.

BROOKHEART, R. T., MICHEL, C. I., LISTENBERGER, L. L., ORY, D. S. & SCHAFFER, J. E. 2009. The non-coding RNA gadd7 is a regulator of lipid-induced oxidative and endoplasmic reticulum stress. *J Biol Chem,* 284**,** 7446-54.

BROWN, D., PAUNESCU, T. G., BRETON, S. & MARSHANSKY, V. 2009. Regulation of the V-ATPase in kidney epithelial cells: dual role in acid-base homeostasis and vesicle trafficking. *J Exp Biol,* 212**,** 1762-72.

BROWNLEE, M. 2001. Biochemistry and molecular cell biology of diabetic complications. *Nature,* 414**,** 813-20.

BRUNET, S., THIBAULT, P., GAGNON, E., KEARNEY, P., BERGERON, J. J. M. & DESJARDINS, M. 2003. Organelle proteomics: looking at less to see more. *Trends in Cell Biology,* 13**,** 629-638.

BURHANS, W. C. & HEINTZ, N. H. 2009a. The cell cycle is a redox cycle: Linking phase-specific targets to cell fate. *Free Radical Biology and Medicine,* 47**,** 1282-1293.

BURHANS, W. C. & HEINTZ, N. H. 2009b. The cell cycle is a redox cycle: linking phase-specific targets to cell fate. *Free radical biology & medicine,* 47**,** 1282-93.

BUSS, J. L., GREENE, B. T., TURNER, J., TORTI, F. M. & TORTI, S. V. 2004. Iron chelators in cancer chemotherapy. *Curr Top Med Chem,* 4**,** 1623-35.

CAIRNS, R. A., HARRIS, I. S. & MAK, T. W. 2011. Regulation of cancer cell metabolism. *Nat Rev Cancer,* 11**,** 85-95.

CAMPOS, P. B., PAULSEN, B. S. & REHEN, S. K. 2014. Accelerating neuronal aging in in vitro model brain disorders: a focus on reactive oxygen species. *Front Aging Neurosci,* 6**,** 292.

CAO, J., SCHULTE, J., KNIGHT, A., LESLIE, N. R., ZAGOZDZON, A., BRONSON, R., MANEVICH, Y., BEESON, C. & NEUMANN, C. A. 2009. Prdx1 inhibits tumorigenesis via regulating PTEN/AKT activity. *EMBO J,* 28**,** 1505-17.

CHANDEL, N. S. 2010. Mitochondrial complex III: an essential component of universal oxygen sensing machinery? *Respir Physiol Neurobiol,* 174**,** 175-81.

CHEN, J. H., STOEBER, K., KINGSBURY, S., OZANNE, S. E., WILLIAMS, G. H. & HALES, C. N. 2004. Loss of proliferative capacity and induction of senescence in oxidatively stressed human fibroblasts. *The Journal of biological chemistry,* 279**,** 49439-46.

CHEN, J. Q., CAMMARATA, P. R., BAINES, C. P. & YAGER, J. D. 2009a. Regulation of mitochondrial respiratory chain biogenesis by estrogens/estrogen receptors and physiological, pathological and pharmacological implications. *Biochim Biophys Acta,* 1793**,** 1540-70.

CHEN, K., KIRBER, M. T., XIAO, H., YANG, Y. & KEANEY, J. F., JR. 2008. Regulation of ROS signal transduction by NADPH oxidase 4 localization. *J Cell Biol,* 181**,** 1129-39.

CHEN, Y., AZAD, M. B. & GIBSON, S. B. 2009b. Superoxide is the major reactive oxygen species regulating autophagy. *Cell Death Differ,* 16**,** 1040-52.

CHENG, X., KANKI, T., FUKUOH, A., OHGAKI, K., TAKEYA, R., AOKI, Y., HAMASAKI, N. & KANG, D. 2005. PDIP38 associates with proteins constituting the mitochondrial DNA nucleoid. *J Biochem,* 138**,** 673-8.

CHIABRANDO, D., VINCHI, F., FIORITO, V., MERCURIO, S. & TOLOSANO, E. 2014. Heme in pathophysiology: a matter of scavenging, metabolism and trafficking across cell membranes. *Front Pharmacol,* 5**,** 61.

CHINI, E. N., CHINI, C. C. S., NIN, V. & ESCANDE, C. 2013. Deleted in breast cancer-1 (DBC-1) in the interface between metabolism, aging and cancer. *Bioscience Reports,* 33**,** 637-643.

CHIU, J. & DAWES, I. W. 2012. Redox control of cell proliferation. *Trends Cell Biol,* 22**,** 592-601.

CHTOUROU, Y., FETOUI, H. & GDOURA, R. 2014. Protective Effects of Naringenin on Iron-Overload-Induced Cerebral Cortex Neurotoxicity Correlated with Oxidative Stress. *Biol Trace Elem Res*.

CHUN, K. S., KUNDU, J., KUNDU, J. K. & SURH, Y. J. 2014. Targeting Nrf2-Keap1 signaling for chemoprevention of skin carcinogenesis with bioactive phytochemicals. *Toxicol Lett,* 229**,** 73-84.

CLOSE, P., EAST, P., DIRAC-SVEJSTRUP, A. B., HARTMANN, H., HERON, M., MASLEN, S., CHARIOT, A., SODING, J., SKEHEL, M. & SVEJSTRUP, J. Q. 2012. DBIRD complex integrates alternative mRNA splicing with RNA polymerase II transcript elongation. *Nature,* 484**,** 386-9.

COOPER, G. M. & HAUSMAN, R. E. 2004. *The cell : a molecular approach,* Washington, D.C., ASM Press.

CORTHALS, G. L., WASINGER, V. C., HOCHSTRASSER, D. F. & SANCHEZ, J. C. 2000. The dynamic range of protein expression: A challenge for proteomic research. *Electrophoresis,* 21**,** 1104-1115.

COX, J. & MANN, M. 2008. MaxQuant enables high peptide identification rates, individualized p.p.b.-range mass accuracies and proteome-wide protein quantification. *Nature biotechnology,* 26**,** 1367-72.

COX, J. & MANN, M. 2011. Quantitative, high-resolution proteomics for data-driven systems biology. *Annu Rev Biochem,* 80**,** 273-99.

COX, J., MATIC, I., HILGER, M., NAGARAJ, N., SELBACH, M., OLSEN, J. V. & MANN, M. 2009. A practical guide to the MaxQuant computational platform for SILAC-based quantitative proteomics. *Nature protocols,* 4**,** 698-705.

COX, J., NEUHAUSER, N., MICHALSKI, A., SCHELTEMA, R. A., OLSEN, J. V. & MANN, M. 2011. Andromeda: a peptide search engine integrated into the MaxQuant environment. *J Proteome Res,* 10**,** 1794-805.

CRAIG, R. & BEAVIS, R. C. 2003. A method for reducing the time required to match protein sequences with tandem mass spectra. *Rapid Commun Mass Spectrom,* 17**,** 2310-6.

CRAIG, R. & BEAVIS, R. C. 2004. TANDEM: matching proteins with tandem mass spectra. *Bioinformatics,* 20**,** 1466-7.

CROSS, C. E., HALLIWELL, B., BORISH, E. T., PRYOR, W. A., AMES, B. N., SAUL, R. L., MCCORD, J. M. & HARMAN, D. 1987. Oxygen radicals and human disease. *Ann Intern Med,* 107**,** 526-45.

CYERT, M. S. & PHILPOTT, C. C. 2013. Regulation of cation balance in Saccharomyces cerevisiae. *Genetics,* 193**,** 677-713.

DANSEN, T. B. & BURGERING, B. M. 2008. Unravelling the tumor-suppressive functions of FOXO proteins. *Trends Cell Biol,* 18**,** 421-9.

DAUM, B., WALTER, A., HORST, A., OSIEWACZ, H. D. & KUHLBRANDT, W. 2013. Age-dependent dissociation of ATP synthase dimers and loss of inner-membrane cristae in mitochondria. *Proc Natl Acad Sci U S A,* 110**,** 15301-6.

DE BRITO, O. M. & SCORRANO, L. 2008. Mitofusin 2 tethers endoplasmic reticulum to mitochondria. *Nature,* 456**,** 605-10.

DENICOLA, G. M., KARRETH, F. A., HUMPTON, T. J., GOPINATHAN, A., WEI, C., FRESE, K., MANGAL, D., YU, K. H., YEO, C. J., CALHOUN, E. S., SCRIMIERI, F., WINTER, J. M., HRUBAN, R. H., IACOBUZIO-DONAHUE,

C., KERN, S. E., BLAIR, I. A. & TUVESON, D. A. 2011. Oncogene-induced Nrf2 transcription promotes ROS detoxification and tumorigenesis. *Nature,* 475**,** 106-9.

DETMER, S. A. & CHAN, D. C. 2007. Functions and dysfunctions of mitochondrial dynamics. *Nat Rev Mol Cell Biol,* 8**,** 870-9.

DIAB, H. I. & KANE, P. M. 2013. Loss of Vacuolar H+-ATPase (V-ATPase) Activity in Yeast Generates an Iron Deprivation Signal That Is Moderated by Induction of the Peroxiredoxin TSA2. *Journal of Biological Chemistry,* 288**,** 11366-11377.

DIAZ, B. & COURTNEIDGE, S. A. 2012. Redox signaling at invasive microdomains in cancer cells. *Free Radical Biology and Medicine,* 52**,** 247-256.

DIAZ, B., SHANI, G., PASS, I., ANDERSON, D., QUINTAVALLE, M. & COURTNEIDGE, S. A. 2009. Tks5-Dependent, Nox-Mediated Generation of Reactive Oxygen Species Is Necessary for Invadopodia Formation. *Science Signaling,* 2.

DINKOVA-KOSTOVA, A. T., HOLTZCLAW, W. D., COLE, R. N., ITOH, K., WAKABAYASHI, N., KATOH, Y., YAMAMOTO, M. & TALALAY, P. 2002. Direct evidence that sulfhydryl groups of Keap1 are the sensors regulating induction of phase 2 enzymes that protect against carcinogens and oxidants. *Proc Natl Acad Sci U S A,* 99**,** 11908-13.

DIZDAROGLU, M. & JARUGA, P. 2012. Mechanisms of free radical-induced damage to DNA. *Free Radic Res,* 46**,** 382-419.

DONALD, S. P., SUN, X. Y., HU, C. A., YU, J., MEI, J. M., VALLE, D. & PHANG, J. M. 2001. Proline oxidase, encoded by p53-induced gene-6, catalyzes the generation of proline-dependent reactive oxygen species. *Cancer Res,* 61**,** 1810-5.

DOUGLAS, D. J., FRANK, A. J. & MAO, D. 2005. Linear ion traps in mass spectrometry. *Mass Spectrom Rev,* 24**,** 1-29.

DRISSI, R., DUBOIS, M. L. & BOISVERT, F. M. 2013. Proteomics methods for subcellular proteome analysis. *FEBS J,* 280**,** 5626-34.

DROGE, W. 2002. Free radicals in the physiological control of cell function. *Physiol Rev,* 82**,** 47-95.

DRUMMOND, G. R., SELEMIDIS, S., GRIENDLING, K. K. & SOBEY, C. G. 2011. Combating oxidative stress in vascular disease: NADPH oxidases as therapeutic targets. *Nature Reviews Drug Discovery,* 10**,** 453-471.

DUMONT, M. & BEAL, M. F. 2011. Neuroprotective strategies involving ROS in Alzheimer disease. *Free Radic Biol Med,* 51**,** 1014-26.

DURAN, A., AMANCHY, R., LINARES, J. F., JOSHI, J., ABU-BAKER, S., POROLLO, A., HANSEN, M., MOSCAT, J. & DIAZ-MECO, M. T. 2011. p62 Is a Key Regulator of Nutrient Sensing in the mTORC1 Pathway. *Molecular Cell,* 44**,** 134-146.

DUTERTRE, M., SANCHEZ, G., BARBIER, J., CORCOS, L. & AUBOEUF, D. 2011. The emerging role of pre-messenger RNA splicing in stress responses: sending alternative messages and silent messengers. *RNA Biol,* 8**,** 740-7.

ENG, J. K., MCCORMACK, A. L. & YATES, J. R. 1994. An approach to correlate tandem mass spectral data of peptides with amino acid sequences in a protein database. *J Am Soc Mass Spectrom,* 5**,** 976-89.

FATEMI, N., SANATI, M. H., SHAMSARA, M., MOAYER, F., ZAVAREHEI, M. J., POUYA, A., SAYYAHPOUR, F., AYAT, H. & GOURABI, H. 2014. TBHP-induced oxidative stress alters microRNAs expression in mouse testis. *J Assist Reprod Genet*.

FENN, J. B., MANN, M., MENG, C. K., WONG, S. F. & WHITEHOUSE, C. M. 1989. Electrospray ionization for mass spectrometry of large biomolecules. *Science,* 246**,** 64-71.

FERBER, E. C., PECK, B., DELPUECH, O., BELL, G. P., EAST, P. & SCHULZE, A. 2012. FOXO3a regulates reactive oxygen metabolism by inhibiting mitochondrial gene expression. *Cell Death Differ,* 19**,** 968-79.

FERNANDEZ-REAL, J. M. & MANCO, M. 2013. Effects of iron overload on chronic metabolic diseases. *Lancet Diabetes Endocrinol*.

FINKEL, T. 2012. From sulfenylation to sulfhydration: what a thiolate needs to tolerate. *Sci Signal,* 5**,** pe10.

FINKEL, T., SERRANO, M. & BLASCO, M. A. 2007. The common biology of cancer and ageing. *Nature,* 448**,** 767-74.

FRANCESCHINI, A., SZKLARCZYK, D., FRANKILD, S., KUHN, M., SIMONOVIC, M., ROTH, A., LIN, J., MINGUEZ, P., BORK, P., VON MERING, C. & JENSEN, L. J. 2013. STRING v9.1: protein-protein interaction networks, with increased coverage and integration. *Nucleic Acids Res,* 41**,** D808-15.

FREZZA, C., ZHENG, L., FOLGER, O., RAJAGOPALAN, K. N., MACKENZIE, E. D., JERBY, L., MICARONI, M., CHANETON, B., ADAM, J., HEDLEY, A., KALNA, G., TOMLINSON, I. P., POLLARD, P. J., WATSON, D. G., DEBERARDINIS, R. J., SHLOMI, T., RUPPIN, E. & GOTTLIEB, E. 2011. Haem oxygenase is synthetically lethal with the tumour suppressor fumarate hydratase. *Nature,* 477**,** 225-8.

FRIDOVICH, I. 1984. Overview: biological sources of O2. *Methods Enzymol,* 105**,** 59-61.

FRIDOVICH, I. 1997. Superoxide anion radical (O2-.), superoxide dismutases, and related matters. *J Biol Chem,* 272**,** 18515-7.

FRIEDMAN, J. R., LACKNER, L. L., WEST, M., DIBENEDETTO, J. R., NUNNARI, J. & VOELTZ, G. K. 2011. ER tubules mark sites of mitochondrial division. *Science,* 334**,** 358-62.

FU, Z. & TINDALL, D. J. 2008. FOXOs, cancer and regulation of apoptosis. *Oncogene,* 27**,** 2312-9.

FUKUI, M. & ZHU, B. T. 2010. Mitochondrial superoxide dismutase SOD2, but not cytosolic SOD1, plays a critical role in protection against glutamate-induced oxidative stress and cell death in HT22 neuronal cells. *Free Radic Biol Med,* 48**,** 821-30.

FURUKAWA-HIBI, Y., KOBAYASHI, Y., CHEN, C. & MOTOYAMA, N. 2005. FOXO transcription factors in cell-cycle regulation and the response to oxidative stress. *Antioxid Redox Signal,* 7**,** 752-60.

GAO, P., ZHANG, H., DINAVAHI, R., LI, F., XIANG, Y., RAMAN, V., BHUJWALLA, Z. M., FELSHER, D. W., CHENG, L., PEVSNER, J., LEE, L. A., SEMENZA, G. L. & DANG, C. V. 2007. HIF-dependent antitumorigenic effect of antioxidants in vivo. *Cancer Cell,* 12**,** 230-8.

GARRETT, M. A. 2001. Cell cycle control and cancer. *Current Science,* 81**,** 515-522.

GARTEL, A. L. & RADHAKRISHNAN, S. K. 2005. Lost in transcription: p21 repression, mechanisms, and consequences. *Cancer Res,* 65**,** 3980-5.

GAUTHIER, D. J. & LAZURE, C. 2008. Complementary methods to assist subcellular fractionation in organellar proteomics. *Expert Review of Proteomics,* 5**,** 603-617.

GIORGIO, V., VON STOCKUM, S., ANTONIEL, M., FABBRO, A., FOGOLARI, F., FORTE, M., GLICK, G. D., PETRONILLI, V., ZORATTI, M., SZABO, I., LIPPE, G. & BERNARDI, P. 2013. Dimers of mitochondrial ATP synthase form the permeability transition pore. *Proc Natl Acad Sci U S A,* 110**,** 5887-92.

GO, Y. M. & JONES, D. P. 2008. Redox compartmentalization in eukaryotic cells. *Biochim Biophys Acta,* 1780**,** 1273-90.

GODOVAC-ZIMMERMANN, J. & BROWN, L. R. 2001. Perspectives for mass spectrometry and functional proteomics. *Mass spectrometry reviews,* 20**,** 1-57.

GODOVAC-ZIMMERMANN, J. & BROWN, L. R. 2003. Proteomics approaches to elucidation of signal transduction pathways. *Current opinion in molecular therapeutics,* 5**,** 241-9.

GORRINI, C., HARRIS, I. S. & MAK, T. W. 2013. Modulation of oxidative stress as an anticancer strategy. *Nat Rev Drug Discov,* 12**,** 931-47.

GOUGH, D. R. & COTTER, T. G. 2011. Hydrogen peroxide: a Jekyll and Hyde signalling molecule. *Cell Death Dis,* 2**,** e213.

GRECO, T. & FISKUM, G. 2010. Brain mitochondria from rats treated with sulforaphane are resistant to redox-regulated permeability transition. *J Bioenerg Biomembr,* 42**,** 491-7.

GRECO, T., SHAFER, J. & FISKUM, G. 2011. Sulforaphane inhibits mitochondrial permeability transition and oxidative stress. *Free Radic Biol Med,* 51**,** 2164-71.

GRINCHUK, O. V., MOTAKIS, E. & KUZNETSOV, V. A. 2010. Complex sense-antisense architecture of TNFAIP1/POLDIP2 on 17q11.2 represents a novel transcriptional structural-functional gene module involved in breast cancer progression. *BMC Genomics,* 11 Suppl 1**,** S9.

GU, F. & GRUENBERG, J. 2000. ARF1 regulates pH-dependent COP functions in the early endocytic pathway. *J Biol Chem,* 275**,** 8154-60.

GUERRERA, I. C. & KLEINER, O. 2005. Application of mass spectrometry in proteomics. *Bioscience reports,* 25**,** 71-93.

GUO, S., CHENG, X., LIM, J. H., LIU, Y. & KAO, H. Y. 2014. Control of antioxidative response by the tumor suppressor protein PML through regulating Nrf2 activity. *Mol Biol Cell*.

GYGI, S. P., RIST, B., GERBER, S. A., TURECEK, F., GELB, M. H. & AEBERSOLD, R. 1999a. Quantitative analysis of complex protein mixtures using isotope-coded affinity tags. *Nat Biotechnol,* 17**,** 994-9.

GYGI, S. P., ROCHON, Y., FRANZA, B. R. & AEBERSOLD, R. 1999b. Correlation between protein and mRNA abundance in yeast. *Molecular and cellular biology,* 19**,** 1720-30.

HABERSETZER, J., LARRIEU, I., PRIAULT, M., SALIN, B., ROSSIGNOL, R., BRETHES, D. & PAUMARD, P. 2013. Human F1F0 ATP synthase, mitochondrial ultrastructure and OXPHOS impairment: a (super-)complex matter? *PLoS One,* 8**,** e75429.

HAGENBUCHNER, J. & AUSSERLECHNER, M. J. 2013. Mitochondria and FOXO3: breath or die. *Front Physiol,* 4**,** 147.

HALES, K. G. 2004. The machinery of mitochondrial fusion, division, and distribution, and emerging connections to apoptosis. *Mitochondrion,* 4**,** 285-308.

HALLIWELL, B. 2007. Biochemistry of oxidative stress. *Biochemical Society transactions,* 35**,** 1147-50.

HALLIWELL, B. & GUTTERIDGE, J. M. C. 2007. *Free radicals in biology and medicine,* Oxford, Oxford University Press.

HAMANAKA, R. B. & CHANDEL, N. S. 2010. Mitochondrial reactive oxygen species regulate cellular signaling and dictate biological outcomes. *Trends Biochem Sci,* 35**,** 505-13.

HAMZA, I. & DAILEY, H. A. 2012. One ring to rule them all: trafficking of heme and heme synthesis intermediates in the metazoans. *Biochim Biophys Acta,* 1823**,** 1617-32.

HANAHAN, D. & WEINBERG, R. A. 2011. Hallmarks of cancer: the next generation. *Cell,* 144**,** 646-74.

HANSEN, J. M., GO, Y. M. & JONES, D. P. 2006. Nuclear and mitochondrial compartmentation of oxidative stress and redox signaling. *Annu Rev Pharmacol Toxicol,* 46**,** 215-34.

HARBOUR, J. W. & DEAN, D. C. 2000. The Rb/E2F pathway: expanding roles and emerging paradigms. *Genes Dev,* 14**,** 2393-409.

HARDMAN, M. & MAKAROV, A. A. 2003. Interfacing the orbitrap mass analyzer to an electrospray ion source. *Anal Chem,* 75**,** 1699-705.

HARTWELL, L. H. & WEINERT, T. A. 1989. Checkpoints: controls that ensure the order of cell cycle events. *Science,* 246**,** 629-34.

HAVENS, C. G., HO, A., YOSHIOKA, N. & DOWDY, S. F. 2006. Regulation of late G1/S phase transition and APC Cdh1 by reactive oxygen species. *Mol Cell Biol,* 26**,** 4701-11.

HAYES, J. D. & DINKOVA-KOSTOVA, A. T. 2014. The Nrf2 regulatory network provides an interface between redox and intermediary metabolism. *Trends Biochem Sci,* 39**,** 199-218.

HENKE, R. M., DASTIDAR, R. G., SHAH, A., CADINU, D., YAO, X., HOODA, J. & ZHANG, L. 2011. Hypoxia elicits broad and systematic changes in protein subcellular localization. *Am J Physiol Cell Physiol,* 301**,** C913-28.

HILENSKI, L. L., CLEMPUS, R. E., QUINN, M. T., LAMBETH, J. D. & GRIENDLING, K. K. 2004. Distinct subcellular localizations of Nox1 and

Nox4 in vascular smooth muscle cells. *Arterioscler Thromb Vasc Biol,* 24**,** 677-83.

HITOSUGI, T., ZHOU, L., ELF, S., FAN, J., KANG, H. B., SEO, J. H., SHAN, C., DAI, Q., ZHANG, L., XIE, J., GU, T. L., JIN, P., ALECKOVIC, M., LEROY, G., KANG, Y., SUDDERTH, J. A., DEBERARDINIS, R. J., LUAN, C. H., CHEN, G. Z., MULLER, S., SHIN, D. M., OWONIKOKO, T. K., LONIAL, S., ARELLANO, M. L., KHOURY, H. J., KHURI, F. R., LEE, B. H., YE, K., BOGGON, T. J., KANG, S., HE, C. & CHEN, J. 2012. Phosphoglycerate mutase 1 coordinates glycolysis and biosynthesis to promote tumor growth. *Cancer Cell,* 22**,** 585-600.

HO, C. S., LAM, C. W., CHAN, M. H., CHEUNG, R. C., LAW, L. K., LIT, L. C., NG, K. F., SUEN, M. W. & TAI, H. L. 2003. Electrospray ionisation mass spectrometry: principles and clinical applications. *Clin Biochem Rev,* 24**,** 3-12.

HOUSTIS, N., ROSEN, E. D. & LANDER, E. S. 2006. Reactive oxygen species have a causal role in multiple forms of insulin resistance. *Nature,* 440**,** 944-8.

HUANG DA, W., SHERMAN, B. T., STEPHENS, R., BASELER, M. W., LANE, H. C. & LEMPICKI, R. A. 2008. DAVID gene ID conversion tool. *Bioinformation,* 2**,** 428-30.

HUOTARI, J. & HELENIUS, A. 2011. Endosome maturation. *EMBO J,* 30**,** 3481-500.

HUSSAIN, S. P., AMSTAD, P., HE, P. J., ROBLES, A., LUPOLD, S., KANEKO, I., ICHIMIYA, M., SENGUPTA, S., MECHANIC, L., OKAMURA, S., HOFSETH, L. J., MOAKE, M., NAGASHIMA, M., FORRESTER, K. S. & HARRIS, C. C. 2004. p53-induced up-regulation of MnSOD and GPx but not catalase increases oxidative stress and apoptosis. *Cancer Research,* 64**,** 2350-2356.

ITOH, K., CHIBA, T., TAKAHASHI, S., ISHII, T., IGARASHI, K., KATOH, Y., OYAKE, T., HAYASHI, N., SATOH, K., HATAYAMA, I., YAMAMOTO, M. & NABESHIMA, Y. 1997. An Nrf2/small Maf heterodimer mediates the

induction of phase II detoxifying enzyme genes through antioxidant response elements. *Biochem Biophys Res Commun,* 236**,** 313-22.

JAIN, A., LAMARK, T., SJOTTEM, E., LARSEN, K. B., AWUH, J. A., OVERVATN, A., MCMAHON, M., HAYES, J. D. & JOHANSEN, T. 2010. p62/SQSTM1 Is a Target Gene for Transcription Factor NRF2 and Creates a Positive Feedback Loop by Inducing Antioxidant Response Element-driven Gene Transcription. *Journal of Biological Chemistry,* 285**,** 22576-22591.

JARAMILLO, M. C. & ZHANG, D. D. 2013. The emerging role of the Nrf2-Keap1 signaling pathway in cancer. *Genes Dev,* 27**,** 2179-91.

JE, E. M., AN, C. H., YOO, N. J. & LEE, S. H. 2012. Mutational and expressional analyses of NRF2 and KEAP1 in sarcomas. *Tumori,* 98**,** 510-5.

JENKINS, R. R. 2000. Exercise and oxidative stress methodology: a critique. *Am J Clin Nutr,* 72**,** 670S-4S.

JOHN, S., WEISS, J. N. & RIBALET, B. 2011. Subcellular localization of hexokinases I and II directs the metabolic fate of glucose. *PLoS One,* 6**,** e17674.

JONES, R. G., PLAS, D. R., KUBEK, S., BUZZAI, M., MU, J., XU, Y., BIRNBAUM, M. J. & THOMPSON, C. B. 2005. AMP-activated protein kinase induces a p53-dependent metabolic checkpoint. *Mol Cell,* 18**,** 283-93.

JOSHI, P., QUACH, O. L., GIGUERE, S. S. & CRISTEA, I. M. 2013. A Functional Proteomics Perspective of DBC1 as a Regulator of Transcription. *J Proteomics Bioinform,* Suppl 2.

JUNG, S., SMITH, J. J., VON HALLER, P. D., DILWORTH, D. J., SITKO, K. A., MILLER, L. R., SALEEM, R. A., GOODLETT, D. R. & AITCHISON, J. D. 2013. Global analysis of condition-specific subcellular protein distribution and abundance. *Mol Cell Proteomics,* 12**,** 1421-35.

KAELIN, W. G., JR. & RATCLIFFE, P. J. 2008. Oxygen sensing by metazoans: the central role of the HIF hydroxylase pathway. *Mol Cell,* 30**,** 393-402.

KANETO, H., KATAKAMI, N., MATSUHISA, M. & MATSUOKA, T. A. 2010. Role of reactive oxygen species in the progression of type 2 diabetes and atherosclerosis. *Mediators Inflamm,* 2010**,** 453892.

KAO, R. T., HALL, J. & STERN, R. 1986. Collagen and elastin synthesis in human stroma and breast carcinoma cell lines: modulation by the extracellular matrix. *Connect Tissue Res,* 14**,** 245-55.

KARTHA, G. K., MOSHAL, K. S., SEN, U., JOSHUA, I. G., TYAGI, N., STEED, M. M. & TYAGI, S. C. 2008. Renal mitochondrial damage and protein modification in type-2 diabetes. *Acta Diabetol,* 45**,** 75-81.

KASPAR, J. W., NITURE, S. K. & JAISWAL, A. K. 2009. Nrf2:INrf2 (Keap1) signaling in oxidative stress. *Free Radic Biol Med,* 47**,** 1304-9.

KIM, K. Y., AHN, J. H. & CHEON, H. G. 2007. Apoptotic action of peroxisome proliferator-activated receptor-gamma activation in human non small-cell lung cancer is mediated via proline oxidase-induced reactive oxygen species formation. *Mol Pharmacol,* 72**,** 674-85.

KIMURA, I., NAKAYAMA, Y., KONISHI, M., TERASAWA, K., OHTA, M., ITOH, N. & FUJIMOTO, M. 2012. Functions of MAPR (Membrane-Associated Progesterone Receptor) Family Members As Heme/Steroid-Binding Proteins. *Current Protein & Peptide Science,* 13**,** 687-696.

KIRCHNER, M. & SELBACH, M. 2012. In vivo quantitative proteome profiling: planning and evaluation of SILAC experiments. *Methods Mol Biol,* 893**,** 175-99.

KITO, K. & ITO, T. 2008. Mass spectrometry-based approaches toward absolute quantitative proteomics. *Curr Genomics,* 9**,** 263-74.

KLAILE, E., KUKALEV, A., OBRINK, B. & MULLER, M. M. 2008. PDIP38 is a novel mitotic spindle-associated protein that affects spindle organization and chromosome segregation. *Cell Cycle,* 7**,** 3180-3186.

KLAILE, E., MULLER, M. M., KANNICHT, C., OTTO, W., SINGER, B. B., REUTTER, W., OBRINK, B. & LUCKA, L. 2007. The cell adhesion receptor carcinoembryonic antigen-related cell adhesion molecule 1 regulates nucleocytoplasmic trafficking of DNA polymerase delta-interacting protein 38. *J Biol Chem,* 282**,** 26629-40.

KOBAYASHI, M. & YAMAMOTO, M. 2005. Molecular mechanisms activating the Nrf2-Keap1 pathway of antioxidant gene regulation. *Antioxid Redox Signal,* 7**,** 385-94.

KOMATSU, M., KUROKAWA, H., WAGURI, S., TAGUCHI, K., KOBAYASHI, A., ICHIMURA, Y., SOU, Y. S., UENO, I., SAKAMOTO, A., TONG, K. I., KIM, M., NISHITO, Y., IEMURA, S., NATSUME, T., UENO, T., KOMINAMI, E., MOTOHASHI, H., TANAKA, K. & YAMAMOTO, M. 2010. The selective autophagy substrate p62 activates the stress responsive transcription factor Nrf2 through inactivation of Keap1. *Nature Cell Biology,* 12**,** 213-U17.

KOPS, G. J., DANSEN, T. B., POLDERMAN, P. E., SAARLOOS, I., WIRTZ, K. W., COFFER, P. J., HUANG, T. T., BOS, J. L., MEDEMA, R. H. & BURGERING, B. M. 2002a. Forkhead transcription factor FOXO3a protects quiescent cells from oxidative stress. *Nature,* 419**,** 316-21.

KOPS, G. J., MEDEMA, R. H., GLASSFORD, J., ESSERS, M. A., DIJKERS, P. F., COFFER, P. J., LAM, E. W. & BURGERING, B. M. 2002b. Control of cell cycle exit and entry by protein kinase B-regulated forkhead transcription factors. *Mol Cell Biol,* 22**,** 2025-36.

KOTIADIS, V. N., DUCHEN, M. R. & OSELLAME, L. D. 2014. Mitochondrial quality control and communications with the nucleus are important in maintaining mitochondrial function and cell health. *Biochim Biophys Acta,* 1840**,** 1254-65.

KOYAMA, S., WADA-HIRAIKE, O., NAKAGAWA, S., TANIKAWA, M., HIRAIKE, H., MIYAMOTO, Y., SONE, K., ODA, K., FUKUHARA, H., NAKAGAWA, K., KATO, S., YANO, T. & TAKETANI, Y. 2010. Repression of estrogen receptor beta function by putative tumor suppressor DBC1. *Biochem Biophys Res Commun,* 392**,** 357-62.

KROCK, B. L., SKULI, N. & SIMON, M. C. 2011. Hypoxia-induced angiogenesis: good and evil. *Genes Cancer,* 2**,** 1117-33.

KULKARNI, A. A., KINGSBURY, S. R., TUDZAROVA, S., HONG, H. K., LODDO, M., RASHID, M., RODRIGUEZ-ACEBES, S., PREVOST, A. T., LEDERMANN, J. A., STOEBER, K. & WILLIAMS, G. H. 2009. Cdc7 kinase is a predictor of survival and a novel therapeutic target in epithelial ovarian carcinoma. *Clinical cancer research : an official journal of the American Association for Cancer Research,* 15**,** 2417-25.

LACKNER, L. L., PING, H., GRAEF, M., MURLEY, A. & NUNNARI, J. 2013. Endoplasmic reticulum-associated mitochondria-cortex tether functions in the distribution and inheritance of mitochondria. *Proc Natl Acad Sci U S A,* 110**,** E458-67.

LAMY, P. J., DURIGOVA, A. & JACOT, W. 2014. Iron homeostasis and anemia markers in early breast cancer: Iron and breast cancer. *Clin Chim Acta*.

LATELLA, L., SACCO, A., PAJALUNGA, D., TIAINEN, M., MACERA, D., D'ANGELO, M., FELICI, A., SACCHI, A. & CRESCENZI, M. 2001. Reconstitution of cyclin D1-associated kinase activity drives terminally differentiated cells into the cell cycle. *Mol Cell Biol,* 21**,** 5631-43.

LAWEN, A. & LANE, D. J. 2013. Mammalian iron homeostasis in health and disease: uptake, storage, transport, and molecular mechanisms of action. *Antioxid Redox Signal,* 18**,** 2473-507.

LEE, J., GIORDANO, S. & ZHANG, J. H. 2012. Autophagy, mitochondria and oxidative stress: cross-talk and redox signalling. *Biochemical Journal,* 441**,** 523-540.

LEE, S. L., SON, A. R., AHN, J. & SONG, J. Y. 2014. Niclosamide enhances ROS-mediated cell death through c-Jun activation. *Biomed Pharmacother*.

LEE, S. R., KWON, K. S., KIM, S. R. & RHEE, S. G. 1998. Reversible inactivation of protein-tyrosine phosphatase 1B in A431 cells stimulated with epidermal growth factor. *J Biol Chem,* 273**,** 15366-72.

LEMMON, M. A. & SCHLESSINGER, J. 2010. Cell signaling by receptor tyrosine kinases. *Cell,* 141**,** 1117-34.

LIN, M. T. & BEAL, M. F. 2006. Mitochondrial dysfunction and oxidative stress in neurodegenerative diseases. *Nature,* 443**,** 787-95.

LIU, L., RODRIGUEZ-BELMONTE, E. M., MAZLOUM, N., XIE, B. & LEE, M. Y. 2003. Identification of a novel protein, PDIP38, that interacts with the p50 subunit of DNA polymerase delta and proliferating cell nuclear antigen. *J Biol Chem,* 278**,** 10041-7.

LIU, T., LU, B., LEE, I., ONDROVICOVA, G., KUTEJOVA, E. & SUZUKI, C. K. 2004. DNA and RNA binding by the mitochondrial Lon protease is regulated by nucleotide and protein substrate. *Journal of Biological Chemistry,* 279**,** 13902-13910.

LIU, W., ZABIRNYK, O., WANG, H., SHIAO, Y. H., NICKERSON, M. L., KHALIL, S., ANDERSON, L. M., PERANTONI, A. O. & PHANG, J. M. 2010. miR-23b targets proline oxidase, a novel tumor suppressor protein in renal cancer. *Oncogene,* 29**,** 4914-24.

LIU, Y., BORCHERT, G. L., DONALD, S. P., DIWAN, B. A., ANVER, M. & PHANG, J. M. 2009. Proline oxidase functions as a mitochondrial tumor suppressor in human cancers. *Cancer Res,* 69**,** 6414-22.

LIU, Y., BORCHERT, G. L., DONALD, S. P., SURAZYNSKI, A., HU, C. A., WEYDERT, C. J., OBERLEY, L. W. & PHANG, J. M. 2005. MnSOD inhibits proline oxidase-induced apoptosis in colorectal cancer cells. *Carcinogenesis,* 26**,** 1335-42.

LO, S. C. & HANNINK, M. 2008. PGAM5 tethers a ternary complex containing Keap1 and Nrf2 to mitochondria. *Exp Cell Res,* 314**,** 1789-803.

LOPEZ-LAZARO, M. 2008. The warburg effect: why and how do cancer cells activate glycolysis in the presence of oxygen? *Anticancer Agents Med Chem,* 8**,** 305-12.

LOVRIC, J. 2011. *Introducing proteomics : from concepts to sample separation, mass spectrometry and data analysis,* Oxford, Wiley-Blackwell.

LUCIANO, A. M., LODDE, V., FRANCIOSI, F., CECILIANI, F. & PELUSO, J. J. 2010. Progesterone receptor membrane component 1 expression and putative function in bovine oocyte maturation, fertilization, and early embryonic development. *Reproduction,* 140**,** 663-72.

LYAMZAEV, K. G., NEPRYAKHINA, O. K., SAPRUNOVA, V. B., BAKEEVA, L. E., PLETJUSHKINA, O. Y., CHERNYAK, B. V. & SKULACHEV, V. P. 2008. Novel mechanism of elimination of malfunctioning mitochondria (mitoptosis): formation of mitoptotic bodies and extrusion of mitochondrial material from the cell. *Biochim Biophys Acta,* 1777**,** 817-25.

LYLE, A. N., DESHPANDE, N. N., TANIYAMA, Y., SEIDEL-ROGOL, B., POUNKOVA, L., DU, P., PAPAHARALAMBUS, C., LASSEGUE, B. & GRIENDLING, K. K. 2009. Poldip2, a novel regulator of Nox4 and cytoskeletal integrity in vascular smooth muscle cells. *Circ Res,* 105**,** 249-59.

MA, Q., CAVALLIN, L. E., YAN, B., ZHU, S., DURAN, E. M., WANG, H., HALE, L. P., DONG, C., CESARMAN, E., MESRI, E. A. & GOLDSCHMIDT-CLERMONT, P. J. 2009. Antitumorigenesis of antioxidants in a transgenic Rac1 model of Kaposi's sarcoma. *Proc Natl Acad Sci U S A,* 106**,** 8683-8.

MAERE, S., HEYMANS, K. & KUIPER, M. 2005. BiNGO: a Cytoscape plugin to assess overrepresentation of gene ontology categories in biological networks. *Bioinformatics,* 21**,** 3448-9.

MAGA, G., CRESPAN, E., MARKKANEN, E., IMHOF, R., FURRER, A., VILLANI, G., HUBSCHER, U. & VAN LOON, B. 2013. DNA polymerase delta-interacting protein 2 is a processivity factor for DNA polymerase lambda during 8-oxo-7,8-dihydroguanine bypass. *Proceedings of the National Academy of Sciences of the United States of America,* 110**,** 18850-18855.

MAILLOUX, R. J., JIN, X. & WILLMORE, W. G. 2013. Redox regulation of mitochondrial function with emphasis on cysteine oxidation reactions. *Redox Biol,* 2**,** 123-139.

MAKAROV, A. 2000. Electrostatic axially harmonic orbital trapping: a high-performance technique of mass analysis. *Anal Chem,* 72**,** 1156-62.

MANGIERI, L. R., MADER, B. J., THOMAS, C. E., TAYLOR, C. A., LUKER, A. M., TSE, T. E., HUISINGH, C. & SHACKA, J. J. 2014. ATP6V0C knockdown in neuroblastoma cells alters autophagy-lysosome pathway function and metabolism of proteins that accumulate in neurodegenerative disease. *PLoS One,* 9**,** e93257.

MANN, M., HENDRICKSON, R. C. & PANDEY, A. 2001. Analysis of proteins and proteomes by mass spectrometry. *Annu Rev Biochem,* 70**,** 437-73.

MANN, M. & WILM, M. 1995. Electrospray mass spectrometry for protein characterization. *Trends Biochem Sci,* 20**,** 219-24.

MARQUES, O., DA SILVA, B. M., PORTO, G. & LOPES, C. 2014. Iron homeostasis in breast cancer. *Cancer Lett,* 347**,** 1-14.

MATHUPALA, S. P., REMPEL, A. & PEDERSEN, P. L. 1997. Aberrant glycolytic metabolism of cancer cells: a remarkable coordination of genetic,

transcriptional, post-translational, and mutational events that lead to a critical role for type II hexokinase. *J Bioenerg Biomembr,* 29**,** 339-43.

MATSUSHIMA, Y., GOTO, Y. & KAGUNI, L. S. 2010. Mitochondrial Lon protease regulates mitochondrial DNA copy number and transcription by selective degradation of mitochondrial transcription factor A (TFAM). *Proc Natl Acad Sci U S A,* 107**,** 18410-5.

MAXWELL, S. A. & RIVERA, A. 2003. Proline oxidase induces apoptosis in tumor cells, and its expression is frequently absent or reduced in renal carcinomas. *J Biol Chem,* 278**,** 9784-9.

MCMAHON, M., ITOH, K., YAMAMOTO, M. & HAYES, J. D. 2003. Keap1-dependent proteasomal degradation of transcription factor Nrf2 contributes to the negative regulation of antioxidant response element-driven gene expression. *J Biol Chem,* 278**,** 21592-600.

MCMAHON, M., LAMONT, D. J., BEATTIE, K. A. & HAYES, J. D. 2010. Keap1 perceives stress via three sensors for the endogenous signaling molecules nitric oxide, zinc, and alkenals. *Proc Natl Acad Sci U S A,* 107**,** 18838-43.

MECHALI, M. 2001. DNA replication origins: from sequence specificity to epigenetics. *Nature reviews. Genetics,* 2**,** 640-5.

MILGROM, E., DIAB, H., MIDDLETON, F. & KANE, P. M. 2007. Loss of vacuolar proton-translocating ATPase activity in yeast results in chronic oxidative stress. *J Biol Chem,* 282**,** 7125-36.

MIR, S. U., AHMED, I. S., ARNOLD, S. & CRAVEN, R. J. 2012. Elevated progesterone receptor membrane component 1/sigma-2 receptor levels in lung tumors and plasma from lung cancer patients. *Int J Cancer,* 131**,** E1-9.

MIR, S. U., SCHWARZE, S. R., JIN, L., ZHANG, J., FRIEND, W., MIRIYALA, S., ST CLAIR, D. & CRAVEN, R. J. 2013. Progesterone receptor membrane

component 1/Sigma-2 receptor associates with MAP1LC3B and promotes autophagy. *Autophagy,* 9**,** 1566-78.

MITRA, K., WUNDER, C., ROYSAM, B., LIN, G. & LIPPINCOTT-SCHWARTZ, J. 2009. A hyperfused mitochondrial state achieved at G1-S regulates cyclin E buildup and entry into S phase. *Proc Natl Acad Sci U S A,* 106**,** 11960-5.

MIYATA, T., TAKIZAWA, S. & VAN YPERSELE DE STRIHOU, C. 2011. Hypoxia. 1. Intracellular sensors for oxygen and oxidative stress: novel therapeutic targets. *Am J Physiol Cell Physiol,* 300**,** C226-31.

MOHANTY, A. & MCBRIDE, H. M. 2013. Emerging roles of mitochondria in the evolution, biogenesis, and function of peroxisomes. *Front Physiol,* 4**,** 268.

MONTAGNOLI, A., TENCA, P., SOLA, F., CARPANI, D., BROTHERTON, D., ALBANESE, C. & SANTOCANALE, C. 2004. Cdc7 inhibition reveals a p53-dependent replication checkpoint that is defective in cancer cells. *Cancer Res,* 64**,** 7110-6.

MORGAN, D. O. 1997. Cyclin-dependent kinases: engines, clocks, and microprocessors. *Annu Rev Cell Dev Biol,* 13**,** 261-91.

MORGAN, D. O. 2006. *The cell cycle : principles of control,* London, New Science Press.

MOSCAT, J. & DIAZ-MECO, M. T. 2012. p62: a versatile multitasker takes on cancer. *Trends Biochem Sci,* 37**,** 230-6.

MUKHERJEE, S. 2010. *The emperor of all maladies : a biography of cancer,* New York, Scribner.

MULVEY, C., TUDZAROVA, S., CRAWFORD, M., WILLIAMS, G. H., STOEBER, K. & GODOVAC-ZIMMERMANN, J. 2010. Quantitative Proteomics Reveals a "Poised Quiescence" Cellular State after Triggering the DNA Replication Origin Activation Checkpoint. *Journal of Proteome Research,* 9**,** 5445-5460.

MULVEY, C. M., TUDZAROVA, S., CRAWFORD, M., WILLIAMS, G. H., STOEBER, K. & GODOVAC-ZIMMERMANN, J. 2013. Subcellular proteomics reveals a role for nucleo-cytoplasmic trafficking at the DNA replication origin activation checkpoint. *J Proteome Res,* 12**,** 1436-53.

MURPHY, M. P. 2012. Mitochondrial thiols in antioxidant protection and redox signaling: distinct roles for glutathionylation and other thiol modifications. *Antioxid Redox Signal,* 16**,** 476-95.

MUSACCHIO, A. & SALMON, E. D. 2007. The spindle-assembly checkpoint in space and time. *Nat Rev Mol Cell Biol,* 8**,** 379-93.

NAIK, E. & DIXIT, V. M. 2011. Mitochondrial reactive oxygen species drive proinflammatory cytokine production. *J Exp Med,* 208**,** 417-20.

NAM, S. Y. & SABAPATHY, K. 2011. p53 promotes cellular survival in a context-dependent manner by directly inducing the expression of haeme-oxygenase-1. *Oncogene,* 30**,** 4476-86.

NARENDRA, D., KANE, L. A., HAUSER, D. N., FEARNLEY, I. M. & YOULE, R. J. 2010. p62/SQSTM1 is required for Parkin-induced mitochondrial clustering but not mitophagy; VDAC1 is dispensable for both. *Autophagy,* 6**,** 1090-106.

NARGUND, A. M., PELLEGRINO, M. W., FIORESE, C. J., BAKER, B. M. & HAYNES, C. M. 2012. Mitochondrial import efficiency of ATFS-1 regulates mitochondrial UPR activation. *Science,* 337**,** 587-90.

NATHAN, C. 2002. Points of control in inflammation. *Nature,* 420**,** 846-52.

NEARY, C. L. & PASTORINO, J. G. 2010. Nucleocytoplasmic shuttling of hexokinase II in a cancer cell. *Biochem Biophys Res Commun,* 394**,** 1075-81.

NEUMANN, C. A., KRAUSE, D. S., CARMAN, C. V., DAS, S., DUBEY, D. P., ABRAHAM, J. L., BRONSON, R. T., FUJIWARA, Y., ORKIN, S. H. & VAN

ETTEN, R. A. 2003. Essential role for the peroxiredoxin Prdx1 in erythrocyte antioxidant defence and tumour suppression. *Nature,* 424**,** 561-5.

NGO, J. K., POMATTO, L. C. & DAVIES, K. J. 2013. Upregulation of the mitochondrial Lon Protease allows adaptation to acute oxidative stress but dysregulation is associated with chronic stress, disease, and aging. *Redox Biol,* 1**,** 258-264.

NGUYEN, T., HUANG, H. C. & PICKETT, C. B. 2000. Transcriptional regulation of the antioxidant response element. Activation by Nrf2 and repression by MafK. *J Biol Chem,* 275**,** 15466-73.

NOGUEIRA, V., PARK, Y., CHEN, C. C., XU, P. Z., CHEN, M. L., TONIC, I., UNTERMAN, T. & HAY, N. 2008. Akt determines replicative senescence and oxidative or oncogenic premature senescence and sensitizes cells to oxidative apoptosis. *Cancer Cell,* 14**,** 458-70.

NUMAZAWA, S., ISHIKAWA, M., YOSHIDA, A., TANAKA, S. & YOSHIDA, T. 2003. Atypical protein kinase C mediates activation of NF-E2-related factor 2 in response to oxidative stress. *Am J Physiol Cell Physiol,* 285**,** C334-42.

O'CALLAGHAN, K. M., AYLLON, V., O'KEEFFE, J., WANG, Y. R., COX, O. T., LOUGHRAN, G., FORGAC, M. & O'CONNOR, R. 2010. Heme-binding Protein HRG-1 Is Induced by Insulin-like Growth Factor I and Associates with the Vacuolar H+-ATPase to Control Endosomal pH and Receptor Trafficking. *Journal of Biological Chemistry,* 285**,** 381-391.

O'FARRELL, P. H. 1975. High resolution two-dimensional electrophoresis of proteins. *J Biol Chem,* 250**,** 4007-21.

OKATSU, K., SAISHO, K., SHIMANUKI, M., NAKADA, K., SHITARA, H., SOU, Y. S., KIMURA, M., SATO, S., HATTORI, N., KOMATSU, M., TANAKA, K. & MATSUDA, N. 2010. p62/SQSTM1 cooperates with Parkin for perinuclear clustering of depolarized mitochondria. *Genes Cells,* 15**,** 887-900.

OLSEN, J. V., DE GODOY, L. M., LI, G., MACEK, B., MORTENSEN, P., PESCH, R., MAKAROV, A., LANGE, O., HORNING, S. & MANN, M. 2005. Parts per million mass accuracy on an Orbitrap mass spectrometer via lock mass injection into a C-trap. *Mol Cell Proteomics,* 4**,** 2010-21.

ONG, S. E., BLAGOEV, B., KRATCHMAROVA, I., KRISTENSEN, D. B., STEEN, H., PANDEY, A. & MANN, M. 2002. Stable isotope labeling by amino acids in cell culture, SILAC, as a simple and accurate approach to expression proteomics. *Molecular & cellular proteomics : MCP,* 1**,** 376-86.

ONG, S. E. & MANN, M. 2005. Mass spectrometry-based proteomics turns quantitative. *Nat Chem Biol,* 1**,** 252-62.

ONG, S. E. & MANN, M. 2006. A practical recipe for stable isotope labeling by amino acids in cell culture (SILAC). *Nature Protocols,* 1**,** 2650-2660.

ORIENT, A., DONKO, A., SZABO, A., LETO, T. L. & GEISZT, M. 2007. Novel sources of reactive oxygen species in the human body. *Nephrol Dial Transplant,* 22**,** 1281-8.

ORZAEZ, M., GORTAT, A., MONDRAGON, L., BACHS, O. & PEREZ-PAYA, E. 2009. ATP-noncompetitive inhibitors of CDK-cyclin complexes. *ChemMedChem,* 4**,** 19-24.

OSBURN, W. O. & KENSLER, T. W. 2008. Nrf2 signaling: an adaptive response pathway for protection against environmental toxic insults. *Mutat Res,* 659**,** 31-9.

PACHER, P., BECKMAN, J. S. & LIAUDET, L. 2007. Nitric oxide and peroxynitrite in health and disease. *Physiol Rev,* 87**,** 315-424.

PANKIV, S., LAMARK, T., BRUUN, J. A., OVERVATN, A., BJORKOY, G. & JOHANSEN, T. 2010. Nucleocytoplasmic shuttling of p62/SQSTM1 and its role in recruitment of nuclear polyubiquitinated proteins to promyelocytic leukemia bodies. *J Biol Chem,* 285**,** 5941-53.

PARK, J., LEE, J. & CHOI, C. 2011. Mitochondrial network determines intracellular ROS dynamics and sensitivity to oxidative stress through switching inter-mitochondrial messengers. *PLoS One,* 6**,** e23211.

PATTI, M. E. & CORVERA, S. 2010. The role of mitochondria in the pathogenesis of type 2 diabetes. *Endocr Rev,* 31**,** 364-95.

PELUSO, J. J., DECERBO, J. & LODDE, V. 2012. Evidence for a genomic mechanism of action for progesterone receptor membrane component-1. *Steroids,* 77**,** 1007-12.

PELUSO, J. J., LIU, X., GAWKOWSKA, A., LODDE, V. & WU, C. A. 2010. Progesterone inhibits apoptosis in part by PGRMC1-regulated gene expression. *Mol Cell Endocrinol,* 320**,** 153-61.

PELUSO, J. J., YUAN, A., LIU, X. & LODDE, V. 2013. Plasminogen activator inhibitor 1 RNA-binding protein interacts with progesterone receptor membrane component 1 to regulate progesterone's ability to maintain the viability of spontaneously immortalized granulosa cells and rat granulosa cells. *Biol Reprod,* 88**,** 20.

PERKINS, D. N., PAPPIN, D. J., CREASY, D. M. & COTTRELL, J. S. 1999. Probability-based protein identification by searching sequence databases using mass spectrometry data. *Electrophoresis,* 20**,** 3551-67.

PERRY, R. H., COOKS, R. G. & NOLL, R. J. 2008. Orbitrap mass spectrometry: instrumentation, ion motion and applications. *Mass Spectrom Rev,* 27**,** 661-99.

PETERSEN, S. L., INTLEKOFER, K. A., MOURA-CONLON, P. J., BREWER, D. N., DEL PINO SANS, J. & LOPEZ, J. A. 2013. Novel progesterone receptors: neural localization and possible functions. *Front Neurosci,* 7**,** 164.

PHANG, J. M., LIU, W., HANCOCK, C. & CHRISTIAN, K. J. 2012. The proline regulatory axis and cancer. *Front Oncol,* 2**,** 60.

PICKERING, A. M., STAAB, T. A., TOWER, J., SIEBURTH, D. & DAVIES, K. J. 2013. A conserved role for the 20S proteasome and Nrf2 transcription factor in oxidative stress adaptation in mammals, Caenorhabditis elegans and Drosophila melanogaster. *J Exp Biol,* 216**,** 543-53.

PINTO, G., ALHAIEK, A. A., AMADI, S., QATTAN, A., CRAWFORD, M., RADULOVIC, M. & GODOVAC-ZIMMERMANN, J. 2014. Systematic Nucleo-Cytoplasmic Trafficking of Proteins Following Exposure of MCF7 Breast Cancer Cells to Estradiol. *J Proteome Res*.

PITT, J. J. 2009. Principles and applications of liquid chromatography-mass spectrometry in clinical biochemistry. *Clin Biochem Rev,* 30**,** 19-34.

PRIEST, R. E. & DAVIES, L. M. 1969. Cellular proliferation and synthesis of collagen. *Lab Invest,* 21**,** 138-42.

QATTAN, A. T., MULVEY, C., CRAWFORD, M., NATALE, D. A. & GODOVAC-ZIMMERMANN, J. 2010. Quantitative organelle proteomics of MCF-7 breast cancer cells reveals multiple subcellular locations for proteins in cellular functional processes. *J Proteome Res,* 9**,** 495-508.

QATTAN, A. T., RADULOVIC, M., CRAWFORD, M. & GODOVAC-ZIMMERMANN, J. 2012. Spatial distribution of cellular function: the partitioning of proteins between mitochondria and the nucleus in MCF7 breast cancer cells. *J Proteome Res,* 11**,** 6080-101.

RAY, P. D., HUANG, B. W. & TSUJI, Y. 2012. Reactive oxygen species (ROS) homeostasis and redox regulation in cellular signaling. *Cell Signal,* 24**,** 981-90.

RHEE, S. G. 2006. Cell signaling. H2O2, a necessary evil for cell signaling. *Science,* 312**,** 1882-3.

RICE, R. H., MEANS, G. E. & BROWN, W. D. 1977. Stabilization of bovine trypsin by reductive methylation. *Biochim Biophys Acta,* 492**,** 316-21.

ROBERTSON, R. P. 2004. Chronic oxidative stress as a central mechanism for glucose toxicity in pancreatic islet beta cells in diabetes. *J Biol Chem,* 279**,** 42351-4.

RODRIGUEZ-ACEBES, S., PROCTOR, I., LODDO, M., WOLLENSCHLAEGER, A., RASHID, M., FALZON, M., PREVOST, A. T., SAINSBURY, R., STOEBER, K. & WILLIAMS, G. H. 2010. Targeting DNA replication before it starts: Cdc7 as a therapeutic target in p53-mutant breast cancers. *Am J Pathol,* 177**,** 2034-45.

ROSENFELD, J., CAPDEVIELLE, J., GUILLEMOT, J. C. & FERRARA, P. 1992. In-gel digestion of proteins for internal sequence analysis after one- or two-dimensional gel electrophoresis. *Anal Biochem,* 203**,** 173-9.

ROSS, P. L., HUANG, Y. N., MARCHESE, J. N., WILLIAMSON, B., PARKER, K., HATTAN, S., KHAINOVSKI, N., PILLAI, S., DEY, S., DANIELS, S., PURKAYASTHA, S., JUHASZ, P., MARTIN, S., BARTLET-JONES, M., HE, F., JACOBSON, A. & PAPPIN, D. J. 2004. Multiplexed protein quantitation in Saccharomyces cerevisiae using amine-reactive isobaric tagging reagents. *Mol Cell Proteomics,* 3**,** 1154-69.

RUSHWORTH, S. A., ZAITSEVA, L., MURRAY, M. Y., SHAH, N. M., BOWLES, K. M. & MACEWAN, D. J. 2012. The high Nrf2 expression in human acute myeloid leukemia is driven by NF-kappaB and underlies its chemo-resistance. *Blood,* 120**,** 5188-98.

RYTER, S. W. & CHOI, A. M. 2013. Autophagy: An Integral Component of the Mammalian Stress Response. *J Biochem Pharmacol Res,* 1**,** 176-188.

SABLINA, A. A., BUDANOV, A. V., ILYINSKAYA, G. V., AGAPOVA, L. S., KRAVCHENKO, J. E. & CHUMAKOV, P. M. 2005. The antioxidant function of the p53 tumor suppressor. *Nat Med,* 11**,** 1306-13.

SAINSBURY, R., PROCTOR, I., RODRIGUEZ, S., LODDO, M., TUDZAROVA, S., STOEBER, K. & WILLIAMS, G. 2010. Targeting DNA replication before it

starts: Cdc7 as a therapeutic target in p53 mutant Her2 and triple negative breast cancer. *Breast Cancer Research,* 12**,** S15-S16.

SAKURAI, S., KITANO, K., YAMAGUCHI, H., HAMADA, K., OKADA, K., FUKUDA, K., UCHIDA, M., OHTSUKA, E., MORIOKA, H. & HAKOSHIMA, T. 2005. Structural basis for recruitment of human flap endonuclease 1 to PCNA. *EMBO J,* 24**,** 683-93.

SARSOUR, E. H., VENKATARAMAN, S., KALEN, A. L., OBERLEY, L. W. & GOSWAMI, P. C. 2008. Manganese superoxide dismutase activity regulates transitions between quiescent and proliferative growth. *Aging Cell,* 7**,** 405-417.

SAWA, M. & MASAI, H. 2009. Drug design with Cdc7 kinase: a potential novel cancer therapy target. *Drug Des Devel Ther,* 2**,** 255-64.

SCHIEBER, M. & CHANDEL, N. S. 2014. ROS function in redox signaling and oxidative stress. *Curr Biol,* 24**,** R453-62.

SCHUMACKER, P. T. 2006. Reactive oxygen species in cancer cells: live by the sword, die by the sword. *Cancer Cell,* 10**,** 175-6.

SCHWARTZ, J. C., SENKO, M. W. & SYKA, J. E. 2002. A two-dimensional quadrupole ion trap mass spectrometer. *J Am Soc Mass Spectrom,* 13**,** 659-69.

SCIARRETTA, S., ZHAI, P., SHAO, D., ZABLOCKI, D., NAGARAJAN, N., TERADA, L. S., VOLPE, M. & SADOSHIMA, J. 2013. Activation of NADPH oxidase 4 in the endoplasmic reticulum promotes cardiomyocyte autophagy and survival during energy stress through the protein kinase RNA-activated-like endoplasmic reticulum kinase/eukaryotic initiation factor 2alpha/activating transcription factor 4 pathway. *Circ Res,* 113**,** 1253-64.

SCIGELOVA, M., HORNSHAW, M., GIANNAKOPULOS, A. & MAKAROV, A. 2011. Fourier transform mass spectrometry. *Mol Cell Proteomics,* 10**,** M111 009431.

SCIGELOVA, M. & MAKAROV, A. 2006. Orbitrap mass analyzer--overview and applications in proteomics. *Proteomics,* 6 Suppl 2**,** 16-21.

SCLAFANI, R. A. & HOLZEN, T. M. 2007. Cell cycle regulation of DNA replication. *Annu Rev Genet,* 41**,** 237-80.

SEDDING, D. G. 2008. FoxO transcription factors in oxidative stress response and ageing--a new fork on the way to longevity? *Biol Chem,* 389**,** 279-83.

SEMENZA, G. L. 2012. Hypoxia-inducible factors in physiology and medicine. *Cell,* 148**,** 399-408.

SENA, L. A. & CHANDEL, N. S. 2012. Physiological roles of mitochondrial reactive oxygen species. *Mol Cell,* 48**,** 158-67.

SHANNON, P., MARKIEL, A., OZIER, O., BALIGA, N. S., WANG, J. T., RAMAGE, D., AMIN, N., SCHWIKOWSKI, B. & IDEKER, T. 2003. Cytoscape: a software environment for integrated models of biomolecular interaction networks. *Genome Res,* 13**,** 2498-504.

SHEN, J., SHENG, X., CHANG, Z., WU, Q., WANG, S., XUAN, Z., LI, D., WU, Y., SHANG, Y., KONG, X., YU, L., LI, L., RUAN, K., HU, H., HUANG, Y., HUI, L., XIE, D., WANG, F. & HU, R. 2014. Iron Metabolism Regulates p53 Signaling through Direct Heme-p53 Interaction and Modulation of p53 Localization, Stability, and Function. *Cell Rep,* 7**,** 180-93.

SHERR, C. J. & ROBERTS, J. M. 1999. CDK inhibitors: positive and negative regulators of G1-phase progression. *Genes Dev,* 13**,** 1501-12.

SHEVCHENKO, A., TOMAS, H., HAVLIS, J., OLSEN, J. V. & MANN, M. 2006. In-gel digestion for mass spectrometric characterization of proteins and proteomes. *Nature protocols,* 1**,** 2856-60.

SHEVCHENKO, A., WILM, M., VORM, O. & MANN, M. 1996. Mass spectrometric sequencing of proteins silver-stained polyacrylamide gels. *Anal Chem,* 68**,** 850-8.

SMOOT, M. E., ONO, K., RUSCHEINSKI, J., WANG, P. L. & IDEKER, T. 2011. Cytoscape 2.8: new features for data integration and network visualization. *Bioinformatics,* 27**,** 431-2.

SOHAL, R. S. 2002. Oxidative stress hypothesis of aging. *Free radical biology & medicine,* 33**,** 573-4.

SOUBANNIER, V., MCLELLAND, G. L., ZUNINO, R., BRASCHI, E., RIPPSTEIN, P., FON, E. A. & MCBRIDE, H. M. 2012. A vesicular transport pathway shuttles cargo from mitochondria to lysosomes. *Curr Biol,* 22**,** 135-41.

SPENCER, N. Y., YAN, Z., BOUDREAU, R. L., ZHANG, Y., LUO, M., LI, Q., TIAN, X., SHAH, A. M., DAVISSON, R. L., DAVIDSON, B., BANFI, B. & ENGELHARDT, J. F. 2011. Control of hepatic nuclear superoxide production by glucose 6-phosphate dehydrogenase and NADPH oxidase-4. *J Biol Chem,* 286**,** 8977-87.

SPORN, M. B. & LIBY, K. T. 2012. NRF2 and cancer: the good, the bad and the importance of context. *Nat Rev Cancer,* 12**,** 564-71.

SUBRAMANI, S. & MALHOTRA, V. 2013. Non-autophagic roles of autophagy-related proteins. *EMBO Rep,* 14**,** 143-51.

SUNDARARAJAN, R., CHEN, G., MUKHERJEE, C. & WHITE, E. 2005. Caspase-dependent processing activates the proapoptotic activity of deleted in breast cancer-1 during tumor necrosis factor-alpha-mediated death signaling. *Oncogene,* 24**,** 4908-20.

SUTLIFF, R. L., HILENSKI, L. L., AMANSO, A. M., PARASTATIDIS, I., DIKALOVA, A. E., HANSEN, L., DATLA, S. R., LONG, J. S., EL-ALI, A. M., JOSEPH, G., GLEASON, R. L., JR., TAYLOR, W. R., HART, C. M.,

GRIENDLING, K. K. & LASSEGUE, B. 2013. Polymerase delta interacting protein 2 sustains vascular structure and function. *Arterioscler Thromb Vasc Biol,* 33**,** 2154-61.

SUZUKI, C. K., REP, M., VANDIJL, J. M., SUDA, K., GRIVELL, L. A. & SCHATZ, G. 1997. ATP-dependent proteases that also chaperone protein biogenesis. *Trends in Biochemical Sciences,* 22**,** 118-123.

SWORDS, R., MAHALINGAM, D., O'DWYER, M., SANTOCANALE, C., KELLY, K., CAREW, J. & GILES, F. 2010. Cdc7 kinase - a new target for drug development. *European journal of cancer,* 46**,** 33-40.

SZATROWSKI, T. P. & NATHAN, C. F. 1991. Production of large amounts of hydrogen peroxide by human tumor cells. *Cancer Res,* 51**,** 794-8.

SZETO, J., KANIUK, N. A., CANADIEN, V., NISMAN, R., MIZUSHIMA, N., YOSHIMORI, T., BAZETT-JONES, D. P. & BRUMELL, J. H. 2006. ALIS are stress-induced protein storage compartments for substrates of the proteasome and autophagy. *Autophagy,* 2**,** 189-99.

SZKLARCZYK, D., FRANCESCHINI, A., KUHN, M., SIMONOVIC, M., ROTH, A., MINGUEZ, P., DOERKS, T., STARK, M., MULLER, J., BORK, P., JENSEN, L. J. & VON MERING, C. 2011. The STRING database in 2011: functional interaction networks of proteins, globally integrated and scored. *Nucleic Acids Res,* 39**,** D561-8.

TAN, M., LI, S., SWAROOP, M., GUAN, K., OBERLEY, L. W. & SUN, Y. 1999. Transcriptional activation of the human glutathione peroxidase promoter by p53. *J Biol Chem,* 274**,** 12061-6.

THOMAS, P., PANG, Y. F. & DONG, J. 2014. Enhancement of Cell Surface Expression and Receptor Functions of Membrane Progestin Receptor alpha (mPR alpha) by Progesterone Receptor Membrane Component 1 (PGRMC1): Evidence for a Role of PGRMC1 as an Adaptor Protein for Steroid Receptors. *Endocrinology,* 155**,** 1107-1119.

THOMPSON, C. B. 2011. Rethinking the regulation of cellular metabolism. *Cold Spring Harb Symp Quant Biol,* 76**,** 23-9.

TISSIER, A., JANEL-BINTZ, R., COULON, S., KLAILE, E., KANNOUCHE, P., FUCHS, R. P. & CORDONNIER, A. M. 2010. Crosstalk between replicative and translesional DNA polymerases: PDIP38 interacts directly with Pol eta. *DNA Repair,* 9**,** 922-928.

TONDERA, D., GRANDEMANGE, S., JOURDAIN, A., KARBOWSKI, M., MATTENBERGER, Y., HERZIG, S., DA CRUZ, S., CLERC, P., RASCHKE, I., MERKWIRTH, C., EHSES, S., KRAUSE, F., CHAN, D. C., ALEXANDER, C., BAUER, C., YOULE, R., LANGER, T. & MARTINOU, J. C. 2009. SLP-2 is required for stress-induced mitochondrial hyperfusion. *EMBO J,* 28**,** 1589-600.

TONKS, N. K. 2006. Protein tyrosine phosphatases: from genes, to function, to disease. *Nat Rev Mol Cell Biol,* 7**,** 833-46.

TRACHOOTHAM, D., ZHOU, Y., ZHANG, H., DEMIZU, Y., CHEN, Z., PELICANO, H., CHIAO, P. J., ACHANTA, G., ARLINGHAUS, R. B., LIU, J. & HUANG, P. 2006. Selective killing of oncogenically transformed cells through a ROS-mediated mechanism by beta-phenylethyl isothiocyanate. *Cancer Cell,* 10**,** 241-52.

TRAUERNICHT, A. M., KIM, S. J., KIM, N. H. & BOYER, T. G. 2007. Modulation of estrogen receptor alpha protein level and survival function by DBC-1. *Molecular Endocrinology,* 21**,** 1526-1536.

TUDZAROVA, S., TROTTER, M. W. B., WOLLENSCHLAEGER, A., MULVEY, C., GODOVAC-ZIMMERMANN, J., WILLIAMS, G. H. & STOEBER, K. 2010. Molecular architecture of the DNA replication origin activation checkpoint. *Embo Journal,* 29**,** 3381-3394.

TWIG, G. & SHIRIHAI, O. S. 2011. The Interplay Between Mitochondrial Dynamics and Mitophagy. *Antioxidants & Redox Signaling,* 14**,** 1939-1951.

VALKO, M., MORRIS, H. & CRONIN, M. T. 2005. Metals, toxicity and oxidative stress. *Curr Med Chem,* 12**,** 1161-208.

VAN BUUL, J. D., FERNANDEZ-BORJA, M., ANTHONY, E. C. & HORDIJK, P. L. 2005. Expression and localization of NOX2 and NOX4 in primary human endothelial cells. *Antioxid Redox Signal,* 7**,** 308-17.

VANDER HEIDEN, M. G., CANTLEY, L. C. & THOMPSON, C. B. 2009. Understanding the Warburg effect: the metabolic requirements of cell proliferation. *Science,* 324**,** 1029-33.

VAUGHN, A. E. & DESHMUKH, M. 2008. Glucose metabolism inhibits apoptosis in neurons and cancer cells by redox inactivation of cytochrome c. *Nat Cell Biol,* 10**,** 1477-83.

VOGEL, C., SILVA, G. M. & MARCOTTE, E. M. 2011. Protein expression regulation under oxidative stress. *Molecular & cellular proteomics : MCP,* 10**,** M111 009217.

WALLACE, D. C. 2012. Mitochondria and cancer. *Nat Rev Cancer,* 12**,** 685-98.

WALTHER, T. C. & MANN, M. 2010. Mass spectrometry-based proteomics in cell biology. *The Journal of cell biology,* 190**,** 491-500.

WANG, L., CHEN, Y., STERNBERG, P. & CAI, J. 2008a. Essential roles of the PI3 kinase/Akt pathway in regulating Nrf2-dependent antioxidant functions in the RPE. *Invest Ophthalmol Vis Sci,* 49**,** 1671-8.

WANG, W., FANG, H., GROOM, L., CHENG, A., ZHANG, W., LIU, J., WANG, X., LI, K., HAN, P., ZHENG, M., YIN, J., WANG, W., MATTSON, M. P., KAO, J. P., LAKATTA, E. G., SHEU, S. S., OUYANG, K., CHEN, J., DIRKSEN, R.

T. & CHENG, H. 2008b. Superoxide flashes in single mitochondria. *Cell,* 134**,** 279-90.

WANG, Y., NARTISS, Y., STEIPE, B., MCQUIBBAN, G. A. & KIM, P. K. 2012. ROS-induced mitochondrial depolarization initiates PARK2/PARKIN-dependent mitochondrial degradation by autophagy. *Autophagy,* 8**,** 1462-76.

WEHR, T. 2006. Top-down versus bottom-up approaches in proteomics. *Lc Gc North America,* 24**,** 1004-1014.

WHEATON, W. W. & CHANDEL, N. S. 2011. Hypoxia. 2. Hypoxia regulates cellular metabolism. *Am J Physiol Cell Physiol,* 300**,** C385-93.

WILKINS, M. R., SANCHEZ, J. C., GOOLEY, A. A., APPEL, R. D., HUMPHERYSMITH, I., HOCHSTRASSER, D. F. & WILLIAMS, K. L. 1996. Progress with proteome projects: Why all proteins expressed by a genome should be identified and how to do it. *Biotechnology and Genetic Engineering Reviews, Vol 13,* 13**,** 19-50.

WILLIAMS, G. H. & STOEBER, K. 2012. The cell cycle and cancer. *The Journal of pathology,* 226**,** 352-64.

WILSON, J. E. 2003. Isozymes of mammalian hexokinase: structure, subcellular localization and metabolic function. *J Exp Biol,* 206**,** 2049-57.

WINTERBOURN, C. C. & HAMPTON, M. B. 2008. Thiol chemistry and specificity in redox signaling. *Free Radic Biol Med,* 45**,** 549-61.

WONG, A., ZHANG, S. F., MORDUE, D., WU, J. M., ZHANG, Z. T., DARZYNKIEWICZ, Z., LEE, E. Y. C. & LEE, M. Y. W. T. 2013. PDIP38 is translocated to the spliceosomes/nuclear speckles in response to UV-induced DNA damage and is required for UV-induced alternative splicing of MDM2. *Cell Cycle,* 12**,** 3184-3193.

WOO, H. A., YIM, S. H., SHIN, D. H., KANG, D., YU, D. Y. & RHEE, S. G. 2010. Inactivation of peroxiredoxin I by phosphorylation allows localized H(2)O(2) accumulation for cell signaling. *Cell,* 140**,** 517-28.

XIE, B., LI, H., WANG, Q., XIE, S. Q., RAHMEH, A., DAI, W. & LEE, M. Y. W. T. 2005. Further characterization of human DNA polymerase delta interacting protein 38. *Journal of Biological Chemistry,* 280**,** 22375-22384.

XU, J. B., ZENG, C. B., CHU, W. H., PAN, F. H., ROTHFUSS, J. M., ZHANG, F. J., TU, Z. D., ZHOU, D., ZENG, D. X., VANGVERAVONG, S., JOHNSTON, F., SPITZER, D., CHANG, K. C., HOTCHKISS, R. S., HAWKINS, W. G., WHEELER, K. T. & MACH, R. H. 2011. Identification of the PGRMC1 protein complex as the putative sigma-2 receptor binding site. *Nature Communications,* 2.

XU, J. M., HAO, Z. M., GOU, X. B., TIAN, W., JIN, Y. L., CUI, S. X., GUO, J., SUN, Y. J., WANG, Y. & XU, Z. L. 2013. Imaging of reactive oxygen species burst from mitochondria using laser scanning confocal microscopy. *Microscopy Research and Technique,* 76**,** 612-617.

YATES, J. R., 3RD 2004. Mass spectral analysis in proteomics. *Annu Rev Biophys Biomol Struct,* 33**,** 297-316.

YEKEZARE, M., GOMEZ-GONZALEZ, B. & DIFFLEY, J. F. 2013. Controlling DNA replication origins in response to DNA damage - inhibit globally, activate locally. *J Cell Sci,* 126**,** 1297-306.

YEOP HAN, C., KARGI, A. Y., OMER, M., CHAN, C. K., WABITSCH, M., O'BRIEN, K. D., WIGHT, T. N. & CHAIT, A. 2010. Differential effect of saturated and unsaturated free fatty acids on the generation of monocyte adhesion and chemotactic factors by adipocytes: dissociation of adipocyte hypertrophy from inflammation. *Diabetes,* 59**,** 386-96.

YOON, K. A., NAKAMURA, Y. & ARAKAWA, H. 2004. Identification of ALDH4 as a p53-inducible gene and its protective role in cellular stresses. *Journal of Human Genetics,* 49**,** 134-140.

ZHANG, D. D. & HANNINK, M. 2003. Distinct cysteine residues in Keap1 are required for Keap1-dependent ubiquitination of Nrf2 and for stabilization of Nrf2 by chemopreventive agents and oxidative stress. *Mol Cell Biol,* 23**,** 8137-51.

ZHOU, H., RANISH, J. A., WATTS, J. D. & AEBERSOLD, R. 2002. Quantitative proteome analysis by solid-phase isotope tagging and mass spectrometry. *Nat Biotechnol,* 20**,** 512-5.

ZHU, H., JIA, Z., ZHANG, L., YAMAMOTO, M., MISRA, H. P., TRUSH, M. A. & LI, Y. 2008. Antioxidants and phase 2 enzymes in macrophages: regulation by Nrf2 signaling and protection against oxidative and electrophilic stress. *Exp Biol Med (Maywood),* 233**,** 463-74.

ZONCU, R., BAR-PELED, L., EFEYAN, A., WANG, S. Y., SANCAK, Y. & SABATINI, D. M. 2011. mTORC1 Senses Lysosomal Amino Acids Through an Inside-Out Mechanism That Requires the Vacuolar H+-ATPase. *Science,* 334**,** 678-683.